The Erosion-Corrosion Behaviour of Copper-Nickel Alloys.

By

George E. Vassiliou

Vol. II

A Thesis submitted to

The Department of Mechanical Engineering

University of Glasgow

UNIVERSITY
of
GLASGOW

in fulfilment of the requirement for

The Degree of Doctor of Philosophy

November 2001

Chapter 7

Results related to the effect of other parameters on erosion-corrosion of Cu-10%Ni and Marinel.

7.1. Effect of impingement angle on erosion-corrosion processes.

This section incorporates aspects such as the effect of impingement angle on weight loss and the subsequent erosion mechanisms and the corrosion rate. The results of this part of the work are described in the following sections, 7.1.1. (for Cu-10%Ni), and 7.1.2. (for Marinel).

7.1.1. Effect of impingement angle on erosion-corrosion of Cu-10%Ni.

A series of experiments at the impinging velocity of 17m/s, were carried out to determine the effect of the impingement angle on the total weight loss under free erosion-corrosion conditions, under cathodic protection and in anodic polarisation tests. The corrosion monitoring includes linear polarisation to assess the time dependency of the corrosion rates.

7.1.1.1. <u>Total Weight Loss.</u>

Table 7.1. shows the total weight loss/impingement angle data. It is quite clear that for impact angles of 30° and 90° after exposures of 8 hours, the Cu-10%Ni alloy exhibited similar weight losses which were higher than when impinging at 17m/s, at 45° and 60°. Same weight losses were also observed for the other group of impact angles, (45° and 60°).

Impingement angle	Total Weight Loss (mg)	Total Weight Loss (mg) – Average	Rate of Total Weight Loss (mg/h)
30°	2.0 , 2.1	2.05	0.26
45°	1.5 , 1.7	1.60	0.20
60°	1.5 , 1.7	1.60	0.20
90°	2.0 , 2.2	2.10	0.26

Table 7.1. Total weight loss/impingement angles data.

7.1.1.2. Weight Loss due to the Pure Erosion component.

Experiments at impingement angles of 30° and 90°, in which the specimen was subjected to cathodic protection for 8 hours, obtained the contribution of the pure erosive component to the total weight damage. These results are presented in Table 7.2., and show the weight losses with slightly higher losses at 90°.

Impingement angle	Pure Erosion Weight Loss (mg)	Pure Erosion Weight Loss (mg) – Average	Rate of Pure Erosion Weight Loss (mg/h)
30°	0.2 , 0.3	0.25	0.03
90°	0.4 , 0.4	0.40	0.05

Table 7.2. Weight loss values due to the erosion component.

7.1.1.3. Weight Loss due to the Direct Corrosion component.

Figure 7.1a-b and Figure 7.2a-b show the typical anodic and cathodic polarisation curves respectively, generated from tests after 8 hours in 3.5% NaCl solution at impact angles of 30° and 90°.

The detailed trends in the polarisation curves will be discussed in Chapter 9; for the moment their use is to facilitate determination of corrosion rates via the Tafel extrapolation method. The instantaneous corrosion rates expressed in mg/h as calculated by the Tafel extrapolation method are shown in Table 7.3. Clearly the weight loss due to the direct corrosion component was much higher at 30°.

Impingement angle	Direct corrosion current density, ($\mu A/cm^2$)	Direct corrosion current density, ($\mu A/cm^2$) – Average	Instantaneous Direct corrosion weight loss (mg/h)
30^0	23.3 , 27.7	25.50	0.12
90°	8.5 , 7.8	8.15	0.04

Table 7.3. Weight loss values due to the direct corrosion component.

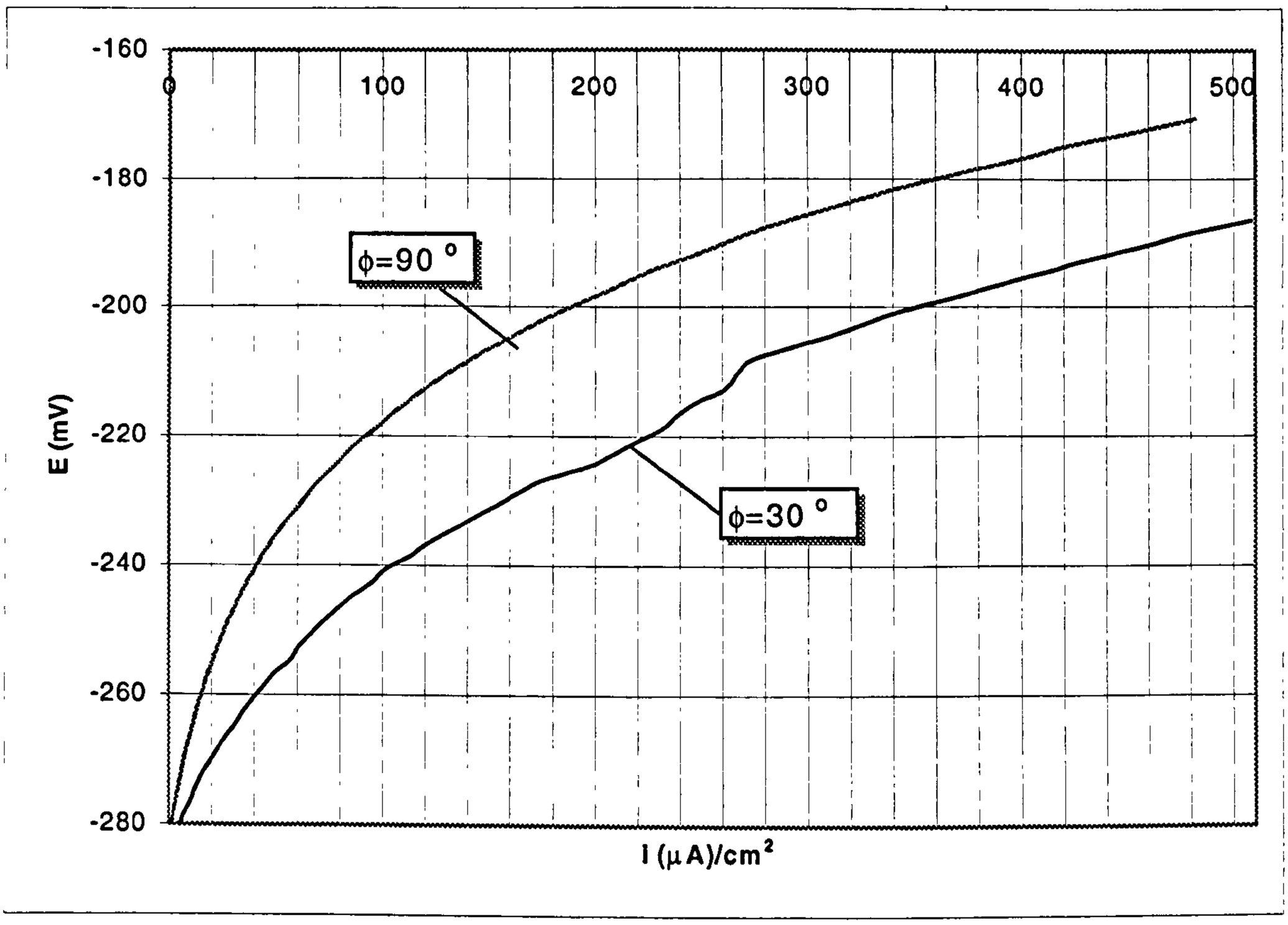

Figure 7.1a. Anodic polarisation tests of Cu-10%Ni upon an initial exposure of 8 hours under the impinging jet. The impact angles are 90° and 30°.

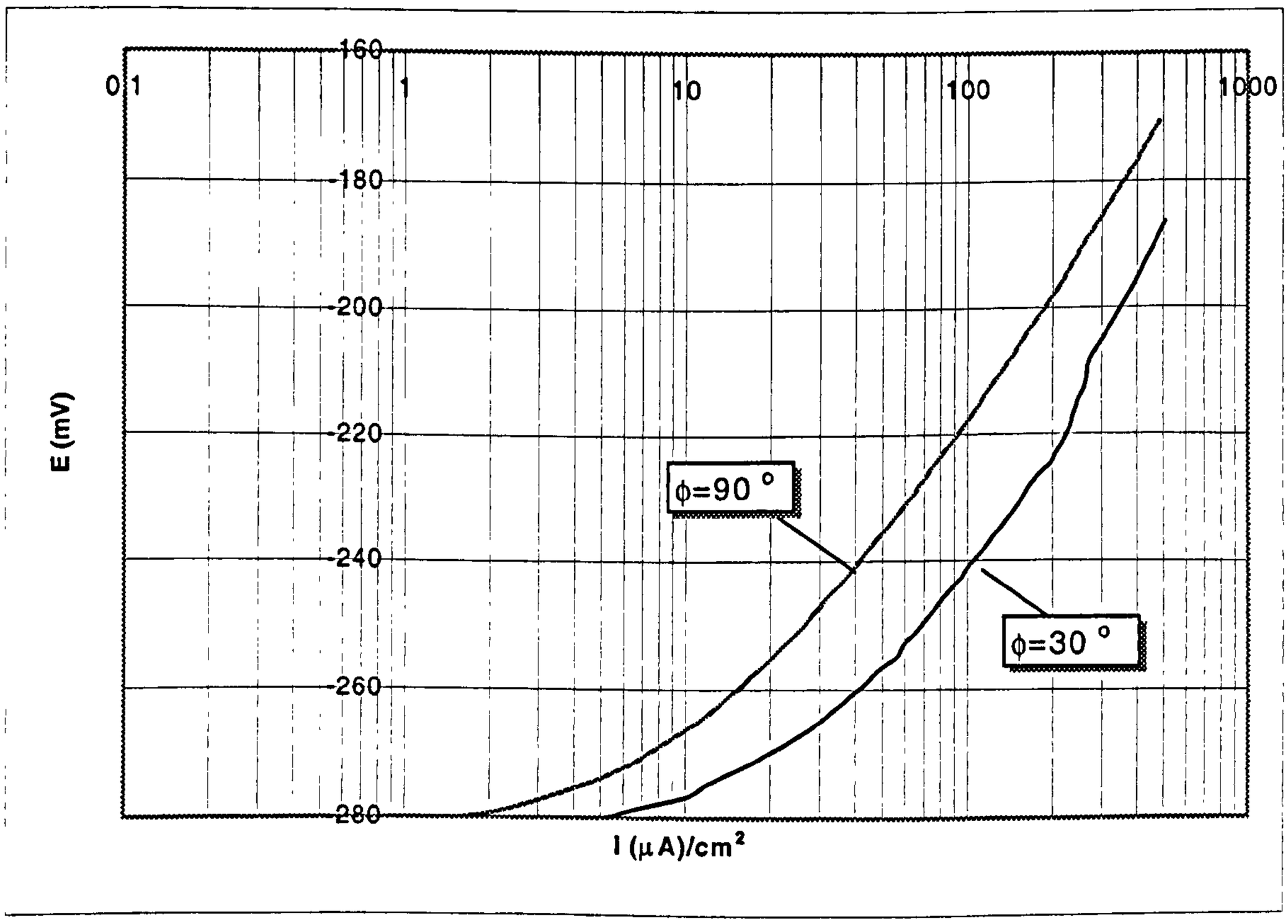

Figure 7.1b. Anodic polarisation tests of Cu-10%Ni upon an initial exposure of 8 hours under the impinging jet. The impact angles are 90° and 30°.

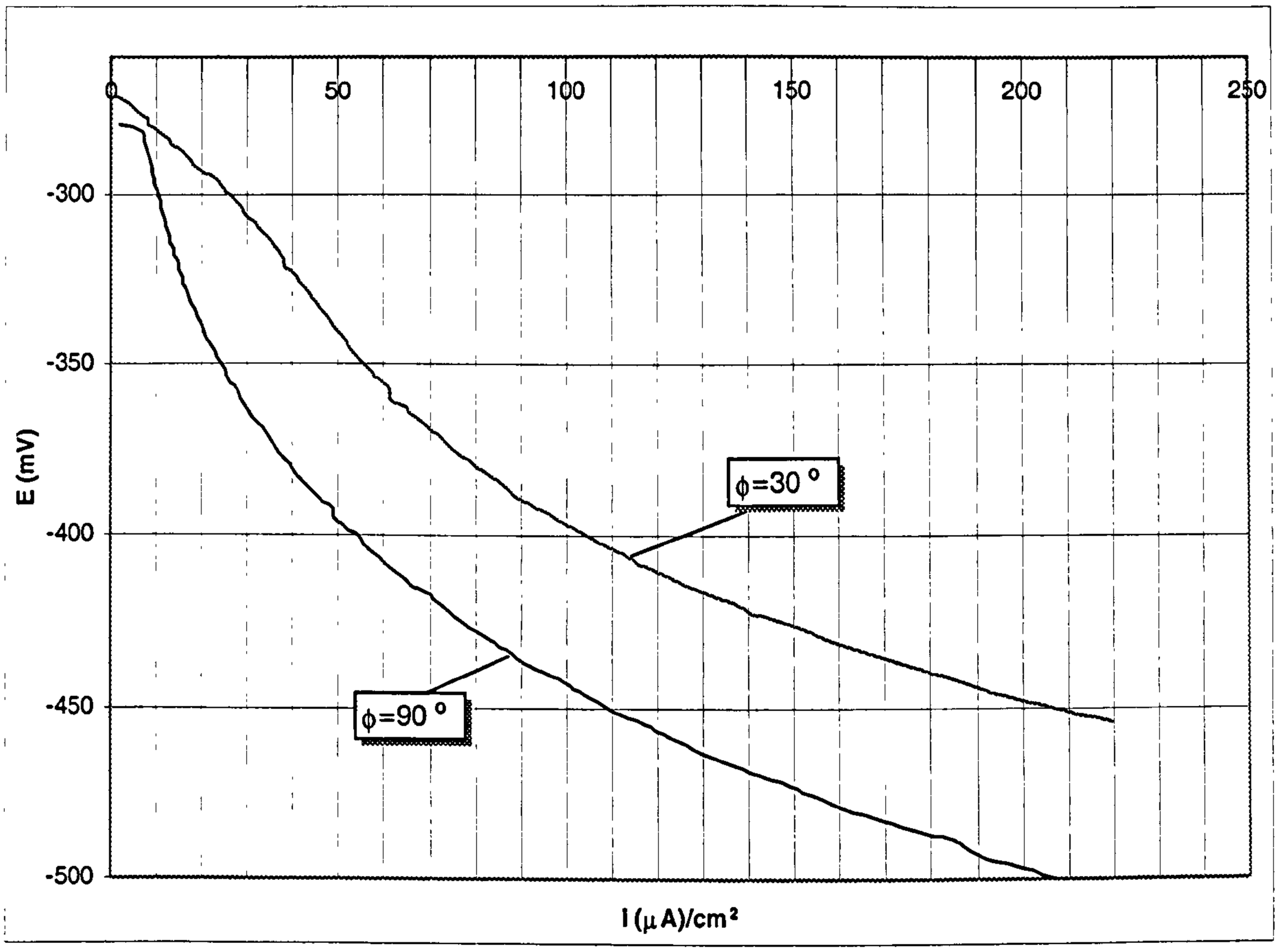

Figure 7.2a. Cathodic polarisation tests of Cu-10%Ni upon an initial exposure of 8 hours under the impinging jet. The impact angles are 90° and 30°.

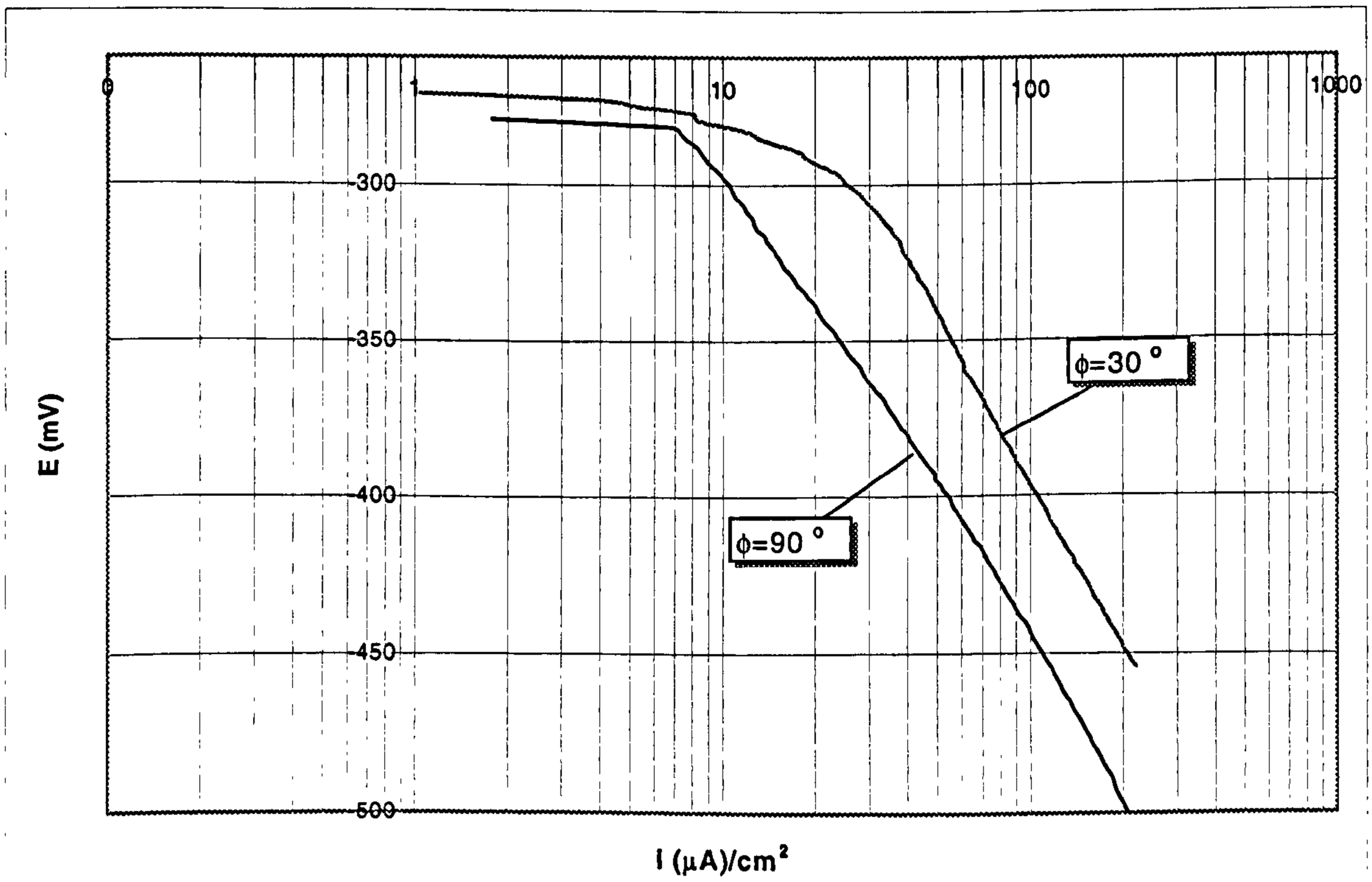

Figure 7.2b. Cathodic polarisation tests of Cu-10%Ni upon an initial exposure of 8 hours under the impinging jet. The impact angles are 90° and 30°.

7.1.1.4. Remarks on the effect of impingement angle on erosion-corrosion for 8 hours at 17m/s.

Table 7.4. shows the weight loss values due to erosion, corrosion and indirect corrosion, (i.e. synergy) for impact angles of 30° and 90°, at 17m/s after 8 hours of exposure. Even if the total weight loss is the same for 30° and 90°, the detailed mechanistic studies revealed that at 30°, the contribution due to the pure erosion and due to the synergy decreases, while the contribution due to the direct corrosion increases.

Impingement angle	Rate of Total Weight Loss (mg/h)	Rate of Pure Erosion Weight Loss (mg/h)	Instantaneous Direct Corrosion Weight Loss (mg/h)	Rate of Synergy (mg/h)
30°	0.26	0.03	0.12	0.11
%		12	46	42
90°	0.26	0.05	0.04	0.17
%		19	15	66

Table 7.4. Weight loss values due to erosion, corrosion and indirect corrosion (i.e. synergy effect).

Clearly this is a complex situation in terms of the impinging angle influence. The rate of the total weight losses shows maximum values at 30° and 90°, while the rate of pure erosion weight losses appears to be higher at 90° than at 30°, with the converse situation to appear for the instantaneous direct corrosion losses. This shows how complex the erosion corrosion behaviour is, emphasising the futility to simply transferring angular relationships obtained from dry erosion, through to aqueous erosion-corrosion.

The higher corrosion rate at 30° than at 90°, may be explained by a larger area influenced by the hydrodynamics effects at 30°; this will be discussed in Chapter 9.

7.1.1.5. Linear polarisation type tests.

With the objective of obtaining an indication of the effect of time on the direct corrosion rate at 30° impingement angle, an experiment was run with an increase by 22mV to the value of E_{corr}, at 30 mins, 4 and 8 hours.

Figure 7.3a-b. shows the resulting anodic polarisation curves generated from duplicate tests at constant velocity of 17m/s, at an impingement angle of 30°. Evidently the contribution due to direct corrosion increases with time.

Table 7.5. shows the average values of E_{corr}, R_p' and $1/R_p'$ for Cu-10%Ni , impinging at 30° at different time exposures. According to the results the value of E_{corr} shifts continuously in the positive direction. Figure 7.4. presents the $1/R_p'$ values versus time plots for 30° and 90°, with clearly higher values for the 30° tests.

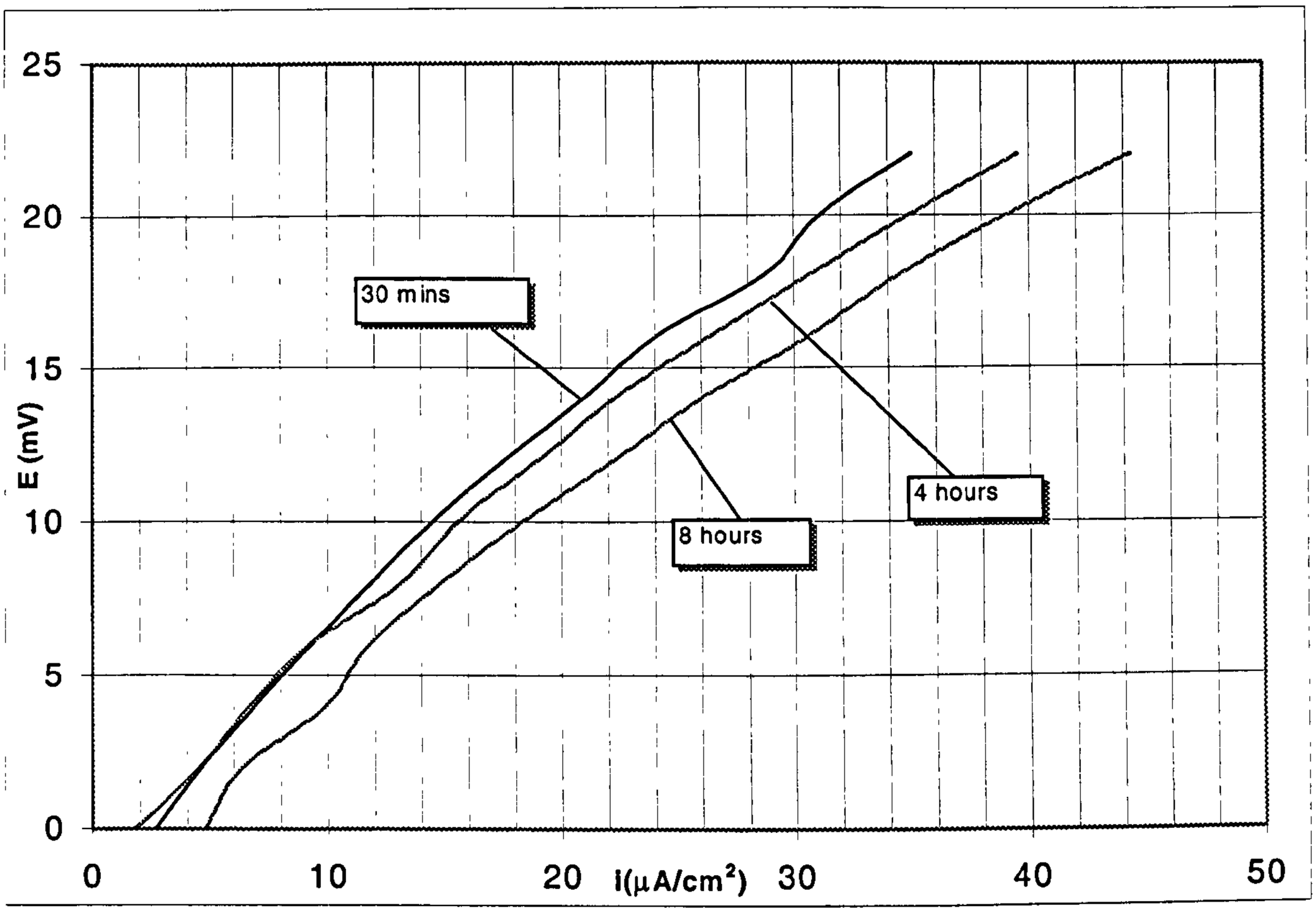

Figure 7.3a. Anodic polarisation curves of Cu-10%Ni for an increase by 22mV to the value of E_{corr}, upon exposures of 30mins, 4 and 8 hours, at 30° impingement angle.

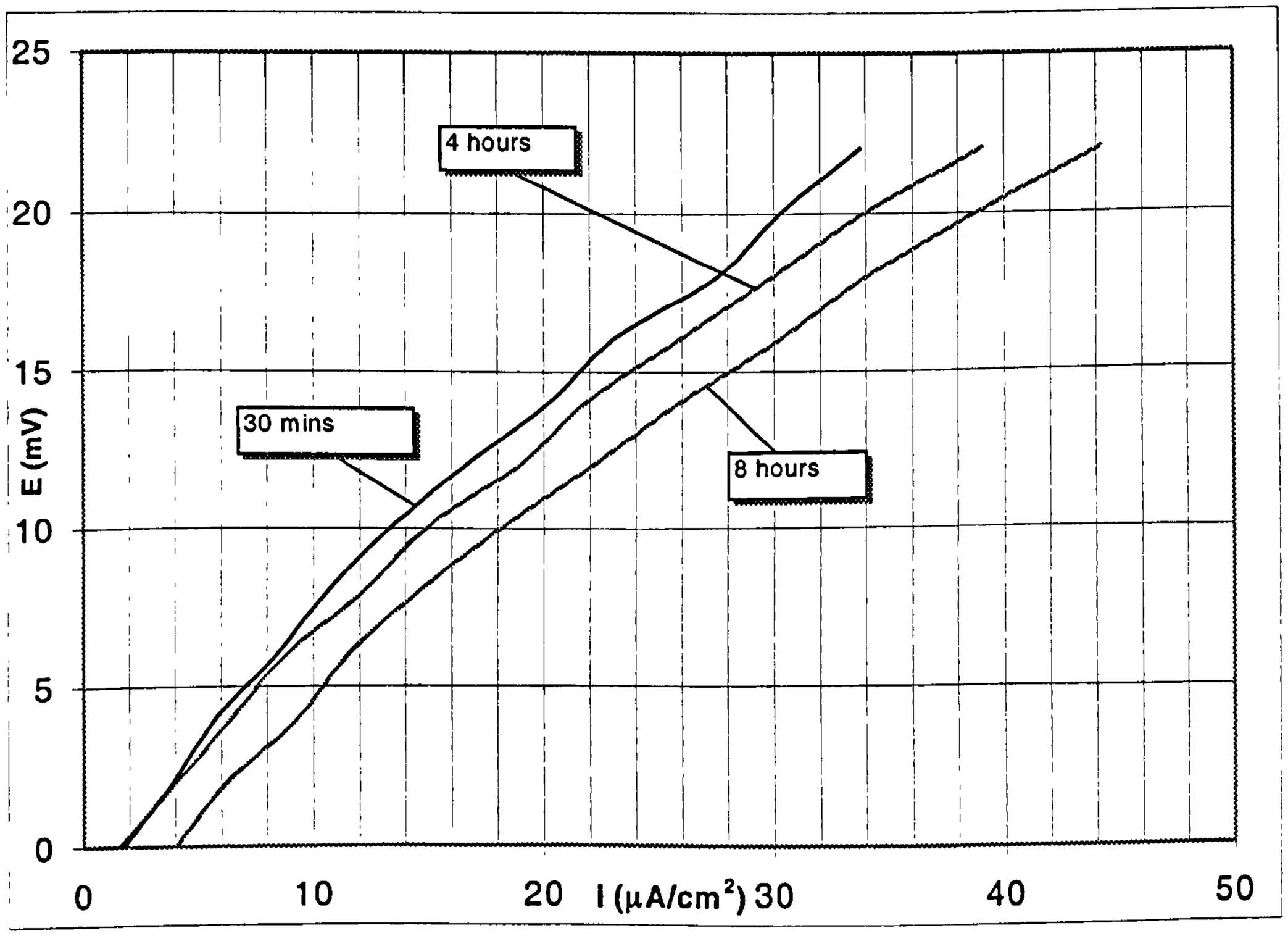

Figure 7.3b. Anodic polarisation curves of Cu-10%Ni for an increase by 22mV to the value of E_{corr}, upon exposures of 30mins, 4 and 8 hours, at 30° impingement angle.

Time (hours)	Average E_{corr} (mV)	Average $R_p^{'}$ *(KOhm*cm²)*	Average $1/R_p^{'}$ *(1/(KOhm*cm²))*
½	-289.323	0.667	1.500
4	-286.569	0.582	1.718
8	-280.755	0.546	1.831

Table 7.5. The average values of E_{corr}, $R_p^{'}$, $1/R_p^{'}$ for Cu-10%Ni at different time exposures, for an increase by 22mV to the value of E_{corr}.

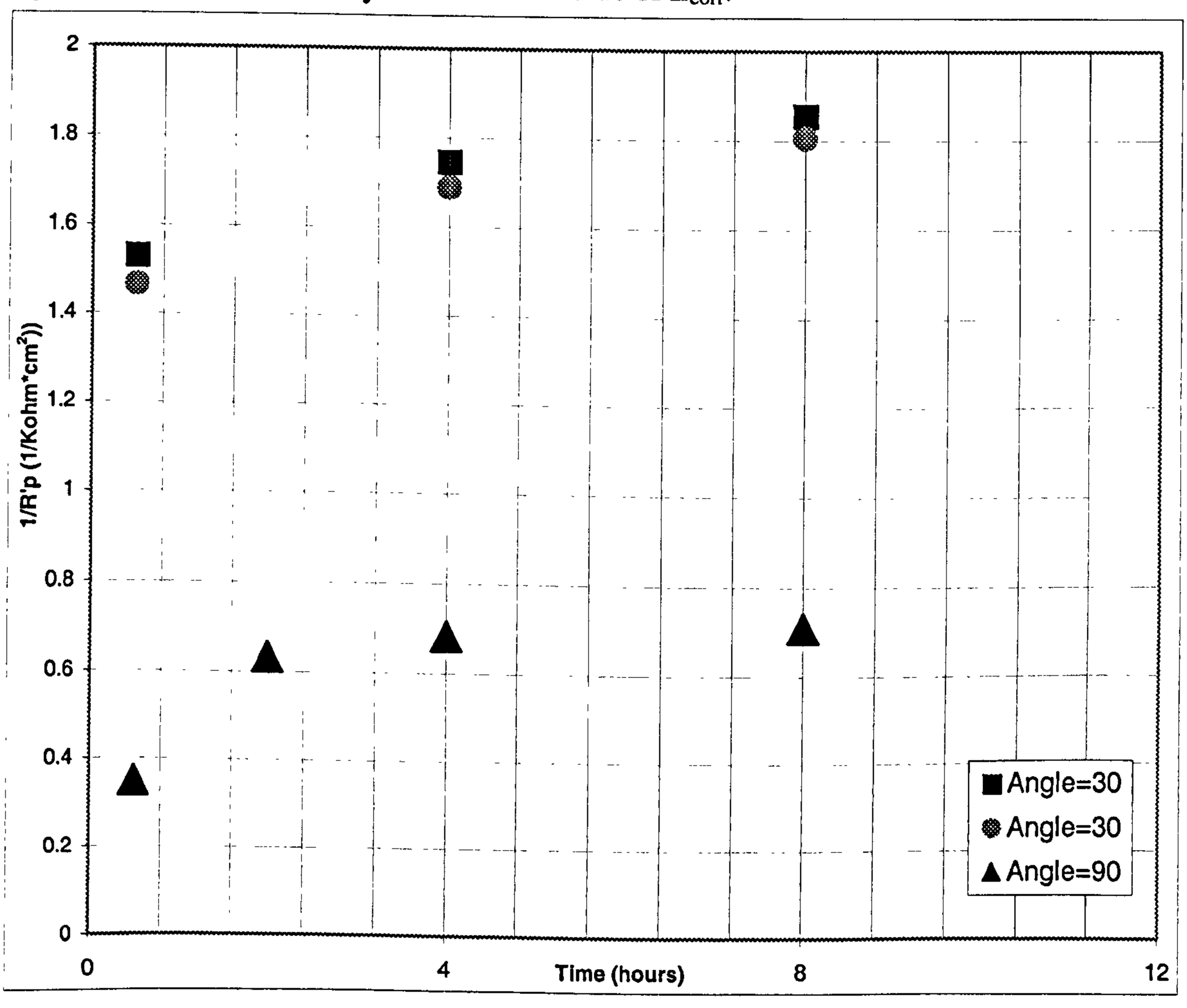

Figure 7.4. $1/R_p^{'}$ values vs. Time curve for the specimen of Cu-10%Ni under impingement velocity of 17 m/s at 30° and 90° tests.

7.1.2. Effect of impingement angle on erosion-corrosion of Marinel.

These tests involved exposure of the specimens for 8 hours under impingement conditions at 30°.

7.1.2.1. Total Weight Loss.

Table 7.6. shows the total weight loss/impingement angle data. It is apparent that the impingement angle dependence of total weight loss rate is complex as is indicated by the results.

Impingement angle	Total Weight Loss (mg)	Total Weight Loss (mg) – Average	Rate of Total Weight Loss (mg/h)
30	1.1 , 1.0	1.05	0.13
45	0.6 , 0.7	0.65	0.08
60	1.1 , 1.2	1.15	0.14
90	0.8 , 0.8	0.80	0.10

Table 7.6. Total weight loss/impingement angles data.

7.2. Effect of salinity on erosion-corrosion processes.

This section involves aspects such as the effect of the concentration of the NaCl in the solution, on the erosion-corrosion rate. The results of this part of the work are described in the 7.2.1 section for Cu-10%Ni.

7.2.1. Effect of salinity on erosion corrosion of Cu-10%Ni.

Figure 7.5a-b. show the typical anodic polarisation curves generated from 72 hours tests in 3.5% NaCl and 1.75% NaCl, impinging at 17m/s. The direct corrosion rate clearly remains the same with salinity variations.

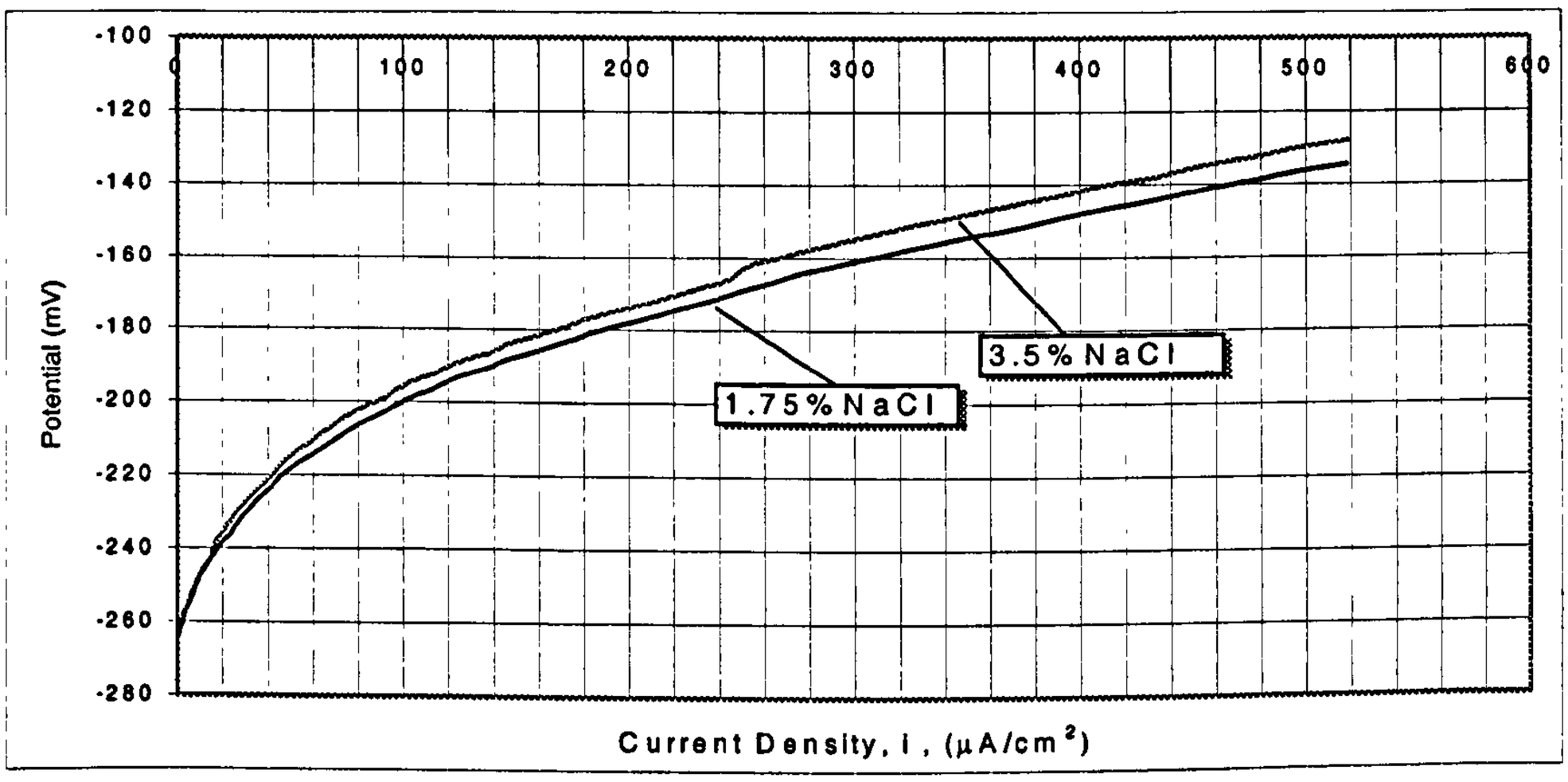

Figure 7.5a. Anodic polarisation curves from 72 hours tests impinging at 17m/s.

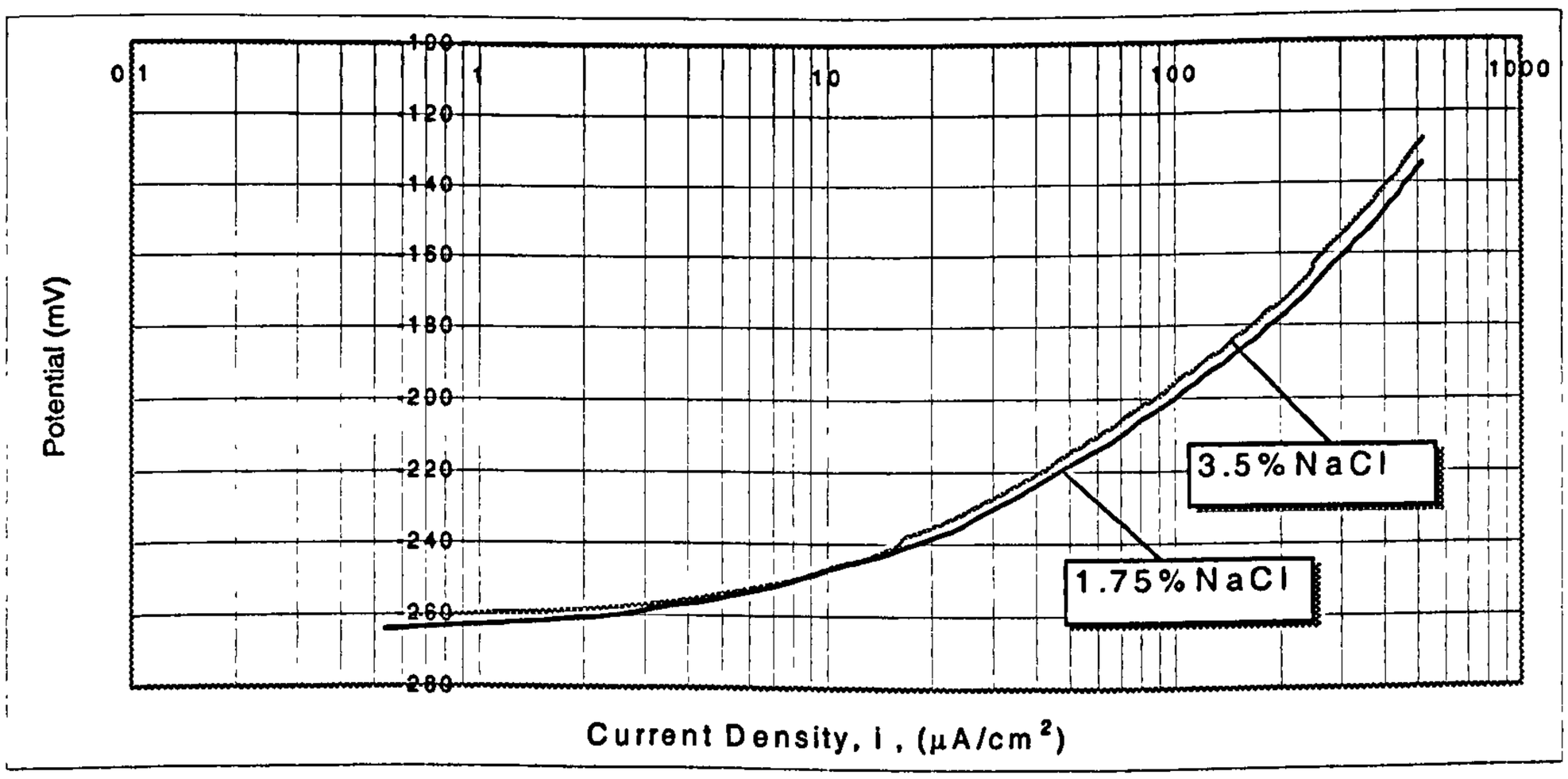

Figure 7.5b. Anodic polarisation curves from 72 hours tests impinging at 17m/s.

7.3. Effect of temperature on erosion-corrosion processes.

In contrast to the initial electrochemical studies at 19±2°C, a series of tests at 35±1°C were carried out to determine the effect of the temperature on the erosion-corrosion processes. The results are presented in the following sections, 7.3.1. (for Cu-10%Ni), and 7.3.2. (for Marinel).

7.3.1. Effect of temperature on the erosion-corrosion of Cu-10%Ni.

These tests involved exposure of the specimens for 48 hours at 35°C, impinging at 17m/s; mainly focusing to the effect of temperature on the total weight loss of Cu-10%Ni.

7.3.1.1. Total Weight Loss.

The total weight loss/temperature data for the two temperatures, (ambient-19°C as shown previously in Table 6.12, and 35°C), are compared directly in Table 7.7. The results demonstrate a clear trend of increasing weight loss with increasing temperature.

Temperature (°C)	Total Weight Loss (mg)	Average Total Weight Loss (mg)
19	8.5 , 9.1	8.80
35	10.5 , 11.3	10.9

Table 7.7. Total weight loss/temperature data for Cu-10%Ni, at the two temperatures after 48 hours exposure time, impinging at 17m/s.

7.3.2. Effect of temperature on the erosion-corrosion of Marinel.

Each test, (anodic and cathodic polarisation, total weight loss and cathodic protection), includes at least one replication. The corrosion monitoring includes linear polarisation to assess the time dependency of the corrosion rates. Further more a group of tests were contacted for specimens with small diameter, placed direct under the impinging jet.

7.3.2.1. Total Weight Loss.

Table 7.8. shows the total weight loss of Marinel after 48 hours under an impinging velocity of 17m/s, at 35° C, in comparison with the results, (shown previously in Table 6.25.) at same impinging velocity, at 19° C. Although there is more scatter in the results at 35°C, it is evident that the total weight loss decreases with increased temperatures. Even the highest value of the total weight loss at 35° C, is less than the lowest value of total weight loss at 19° C.

Temperature (°C)	Total Weight Loss (mg)	Total Weight Loss Average - (mg)
19	2.0 , 2.0	2.00
35	1.0 , 1.1 , 1.3 , 1.6	1.25

Table 7.8. Total weight losses of Marinel after 48 hours at 19°C and 35° C.

7.3.2.2. Weight Loss due to the Erosion component.

The pure erosive component of damage was obtained by experiments in which the specimen was cathodically protected and the weight loss was measured. These results in comparison with the results at 19 °C, (from Table 6.25.), are presented in Table 7.9.

Evidently the temperature does not affect the very small weight loss due to the erosion component.

Temperature (°C)	Pure Erosion Weight Loss (mg)	Average Pure Weight Loss (mg)
19	0.2 , 0.2	0.20
35	0.2 , 0.2	0.20

Table 7.9. Weight losses of Marinel due to the erosion component.

7.3.2.3. Weight loss due to the Direct Corrosion component.

Figure 7.6a-b show the typical anodic polarisation curves generated from tests in 3.5% NaCl solution, under a 1mm impinging jet at 17m/s, at temperature of 35°C. Evidently the temperature increase did not significantly affect the E_{corr} value, (in the range –282mV to –308mV at 35° C).

The anodic polarisation curves indicate the gradual establishment of a passive film on Marinel at 35° C. The current passing through the specimens reached very low values while the shift in the potential from E_{corr} and this trend was accentuated with the passage of time.

Table 7.10, shows the current densities at 4, 8 and 48 hours, as calculated by Tafel extrapolations, and the average instantaneous corrosion rates calculated using Faraday's law.

It is quite clear that instantaneous corrosion rates decreased dramatically from 4 to 48 hours, as is shown also on Figure 7.7., which shows the instantaneous corrosion rates plotted from the data in Table 7.10.

The integrated total direct corrosion rates at 35°C, (estimated from the area under the curve in Figure 7.7.), in comparison with that at 19°C, for an exposure period of 48 hours, (from Table 6.25.), are presented in Table 7.11.

Table 7.10 and Table 7.11 clearly demonstrate that over the entire exposure of 48 hours at 35°C, the Marinel is remarkably more passive than at 19°C.

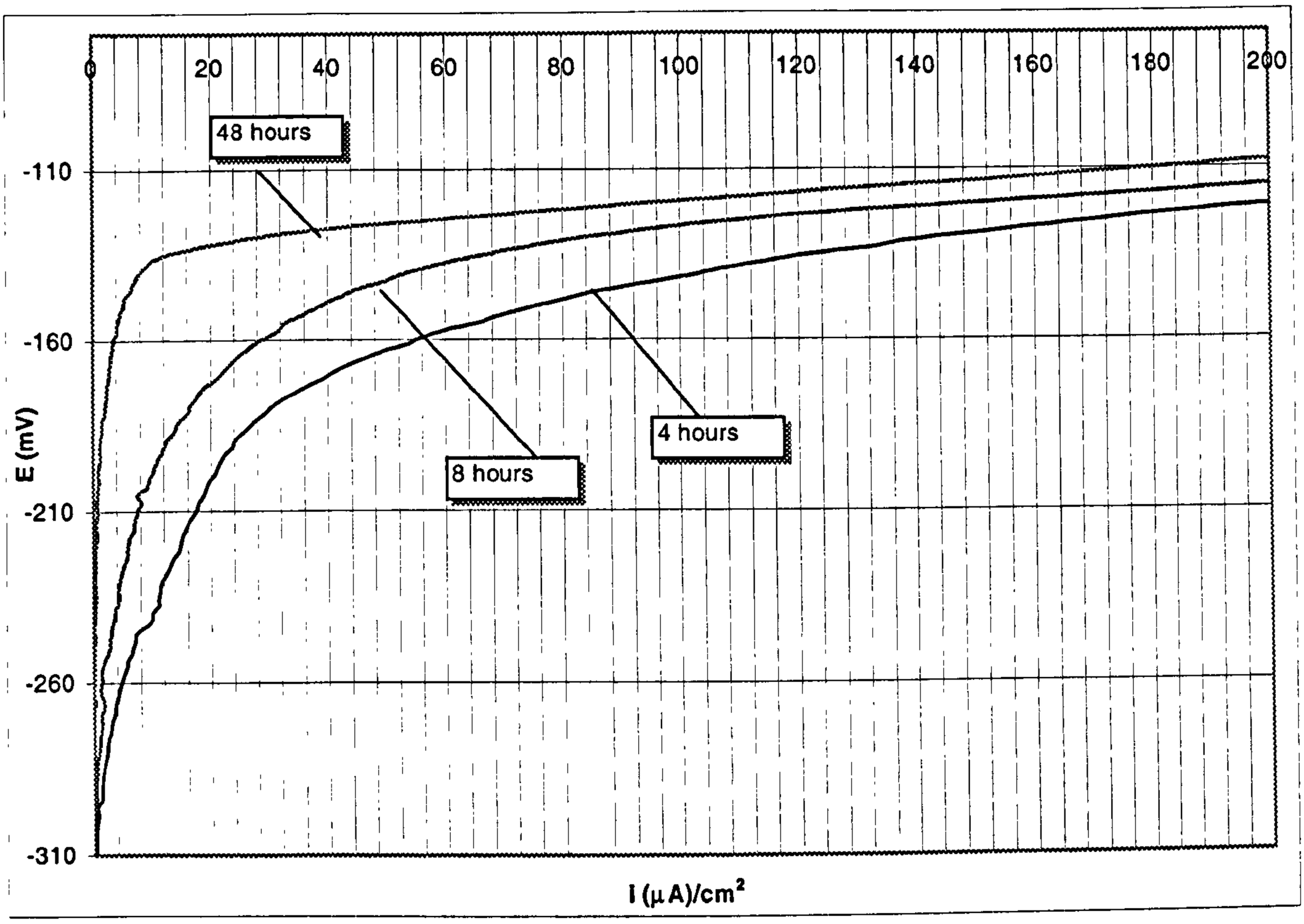

Figure 7.6a. Anodic polarisation curves of Marinel at exposures of 4, 8 and 48 hours, under the impinging jet, at 17m/s and 35°C.

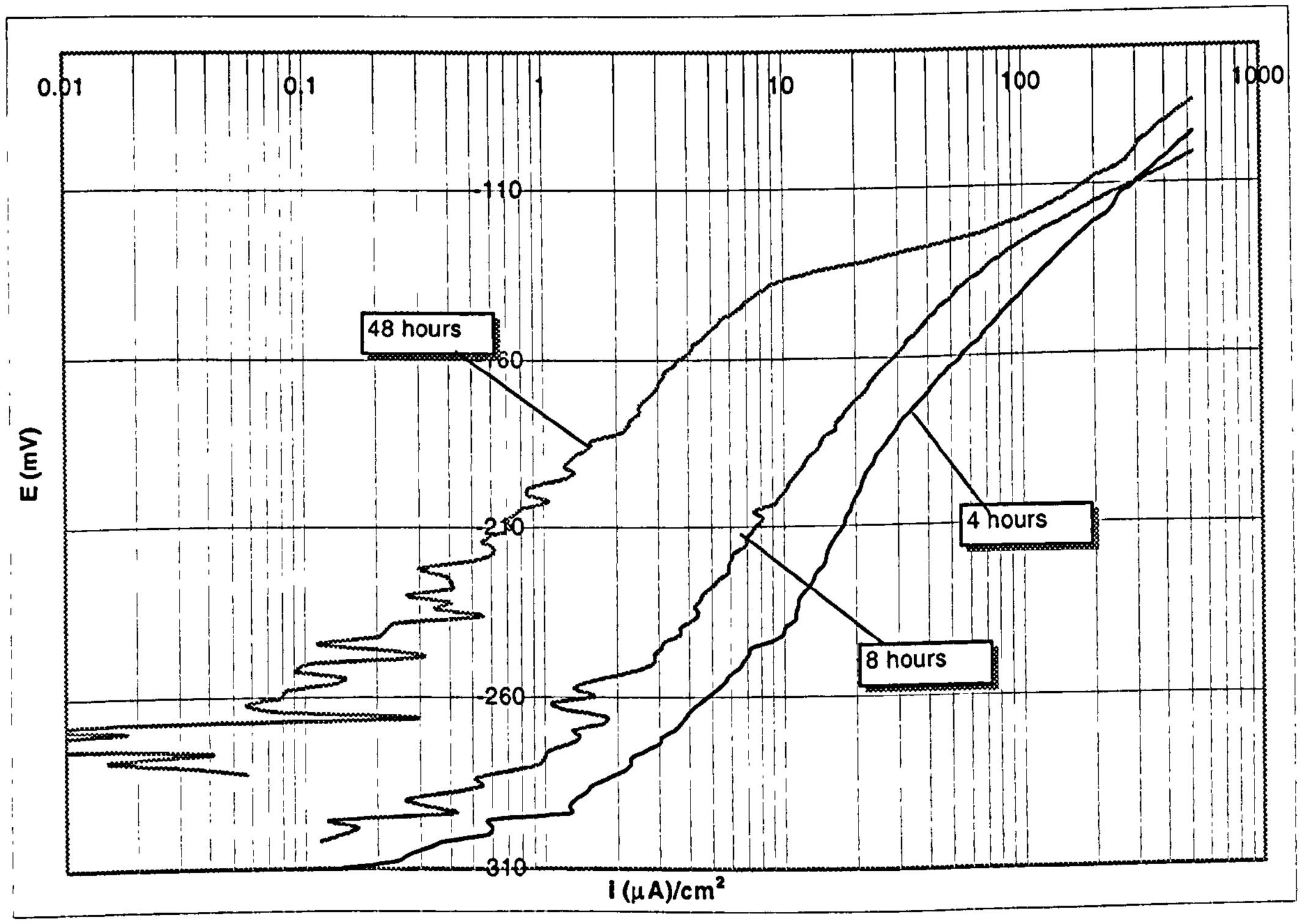

Figure 7.6b. Anodic polarisation curves of Marinel at exposures of 4, 8 and 48 hours, under the impinging jet, at 17m/s and 35°C.

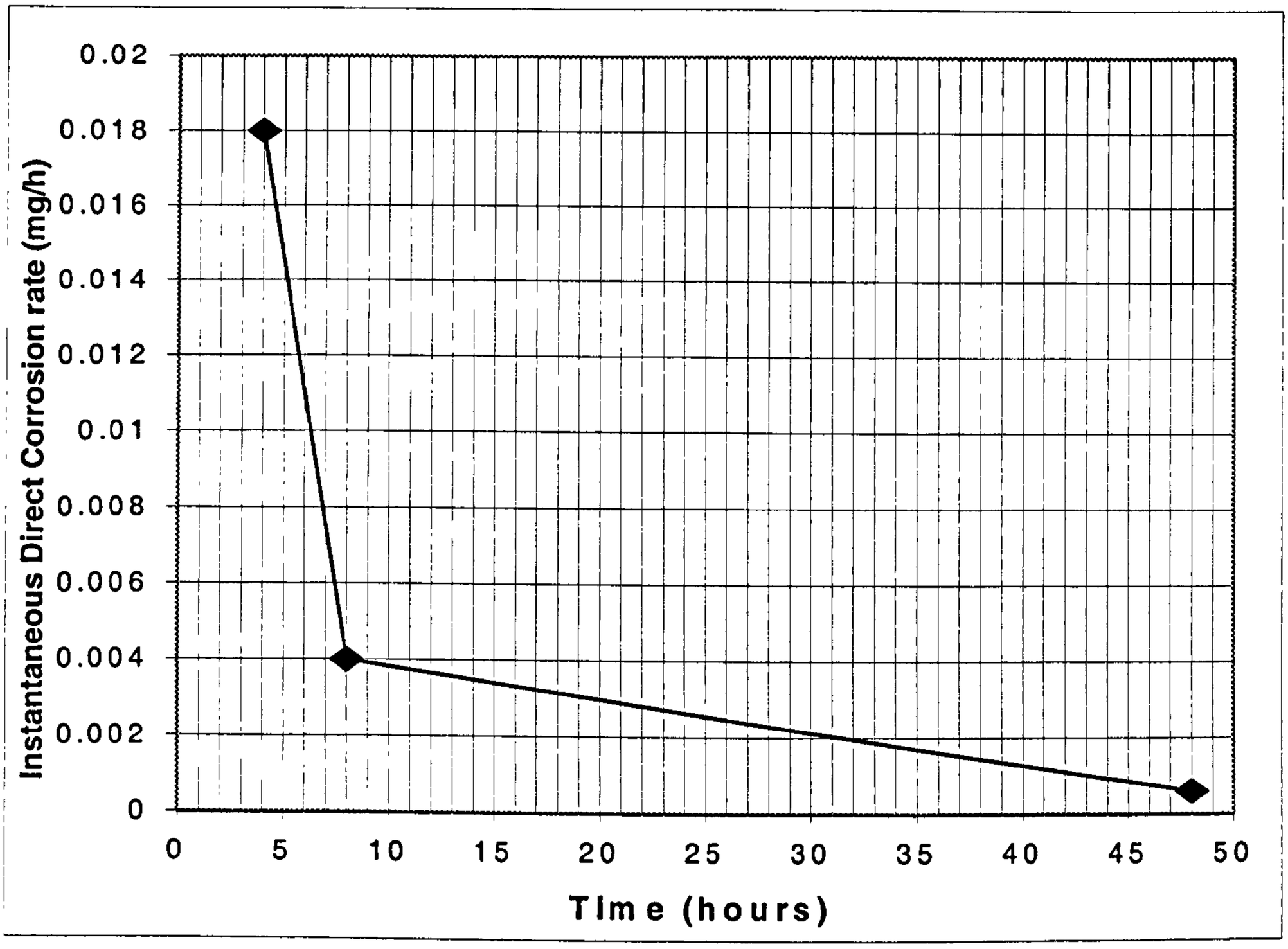

Figure 7.7. Instantaneous direct corrosion rate vs. time graph for Marinel at 17m/s and 35 °C.

Time (hours)	Current density ($\mu A/cm^2$) – 35°C	Instantaneous Direct Corrosion Weight Loss (mg/h) – 35°C	Instantaneous Direct Corrosion Weight Loss (mg/h) – *Average* – *35 °C*	Instantaneous Direct Corrosion Weight Loss (mg/h) – *Average* – *19 °C*
4	3.2 , 3.3	0.0179, 0.0183	0.018	0.090
8	0.76 , 0.8	0.0043 , 0.0044	0.004	0.039
48	0.1 , 0.1	0.0006 , 0.0006	0.0006	0.033

Table 7.10. Average instantaneous direct corrosion weight losses at 4, 8 and 48 hours, and current densities as calculated by Tafel extrapolations for 35°C and 19°C.

Temperature °C	Direct Corrosion Weight Loss (mg)
19	1.740
35	0.181

Table 7.11. Integrated total direct corrosion weight losses for a time period of 48 hours at 19°C and 35°C, for Marinel, at an impinging velocity of 17m/s.

7.3.2.4. Remarks on the effect of temperature on erosion-corrosion for 48 hours.

Table 7.12. shows the weight loss values due to erosion, corrosion and indirect corrosion (synergy) for 19°C and 35°C. An apparently large proportion due to synergy is indicated at the higher temperatures.

Temperature (°C)	Average Total Weight Loss (mg)	Average Pure Erosion Weight Loss (mg)	Average Direct Corrosion Weight Loss (mg)	Synergy *Average* - (mg)
19	2.00	0.20	1.74	0.06
%		10	87	3
35	1.25	0.20	0.18	0.87
%		16	14	70

Table 7.12. Weight losses due to Pure Erosion, Corrosion, and indirect corrosion (Synergy) effect, at 19°C and 35°C.

On account of the very large synergetic percentage at 35°C relative to 19°C, it was decided to run another experiment at 35°C for 4 hours. The idea of this was to assess whether a large proportion of the total weight loss occurred in the initial few hours and hence whether this affect the proportions of components such as the Synergy.

The results of this 4-hour test at 35°C were total weight losses of 0.40 mg and 0.40 mg in duplicate specimens. This does in fact show that at 35°C not only was the direct corrosion rate falling with time, but so was the total erosion-corrosion rate.

7.3.2.5. Linear polarisation type tests.

In order to obtain more data to assist in the evaluation of the effect of temperature in the corrosion rate with time, one experiment was carried out at 35°C impinging at 17m/s, and another one at 35°C at static conditions. In both of them a series of linear polarisation type monitoring exercises was undertaken at times of 2, 4, 8, 16, 24, 32, 40, 48 hours. Typical plots of polarisation/current density in this series of tests are shown in Figure 7.8a-b., in which (to facilitate comparison) the actual E_{corr} values are adjusted to zero on the y-axis. Table 7.13a-b., shows the calculated values of $R_p^{'}$ and $1/R_p^{'}$ for the various exposures times, on the reasonable basis of a direct between $1/R_p^{'}$ and corrosion rate. The plots of $1/R_p^{'}$ against time (Figures 7.9a-b-c.) provide more-detailed evidence that the corrosion rate decreased dramatically, from relatively high initial values, in the first 4-8 hours supporting the notion of a rapid development of a protective film on the surface even in the severe 17m/s impingement velocity.

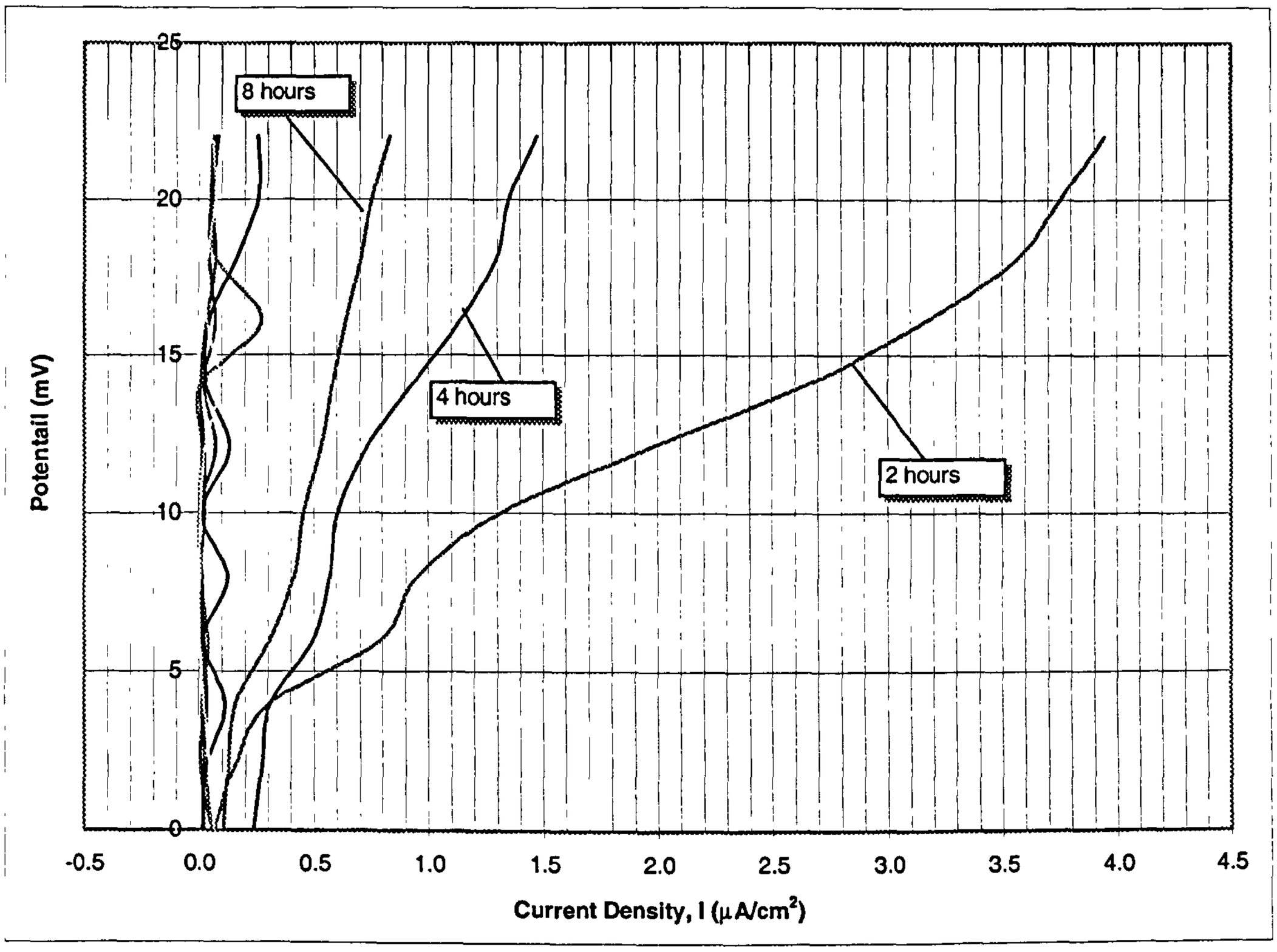

Figure 7.8a. Typical anodic polarisation curves of a specimen of Marinel at 35°C, for an increase by 22mV to the value of E_{corr}, impinging at 17m/s.

Time (hours)	Average E_{corr} (mV)	Average $R_p^{'}$ (KOhm*cm^2)	Average $1/R_p^{'}$ (1/(Kohm*cm^2))
2	-316.742	4.835	0.206
4	-310.792	16.116	0.062
8	-307.602	28.594	0.035
16	-303.234	56.156	0.017
24	-299.942	71.09	0.011
32	-290.346	149.7	0.006
40	-286.437	185.36	0.005
48	-282.309	235.12	0.004

Table 7.13a. The average values of E_{corr}, $R_p^{'}$, $1/R_p^{'}$ for Marinel at different time exposures for an increase by 22mV to the value of E_{corr}, at 17m/s.

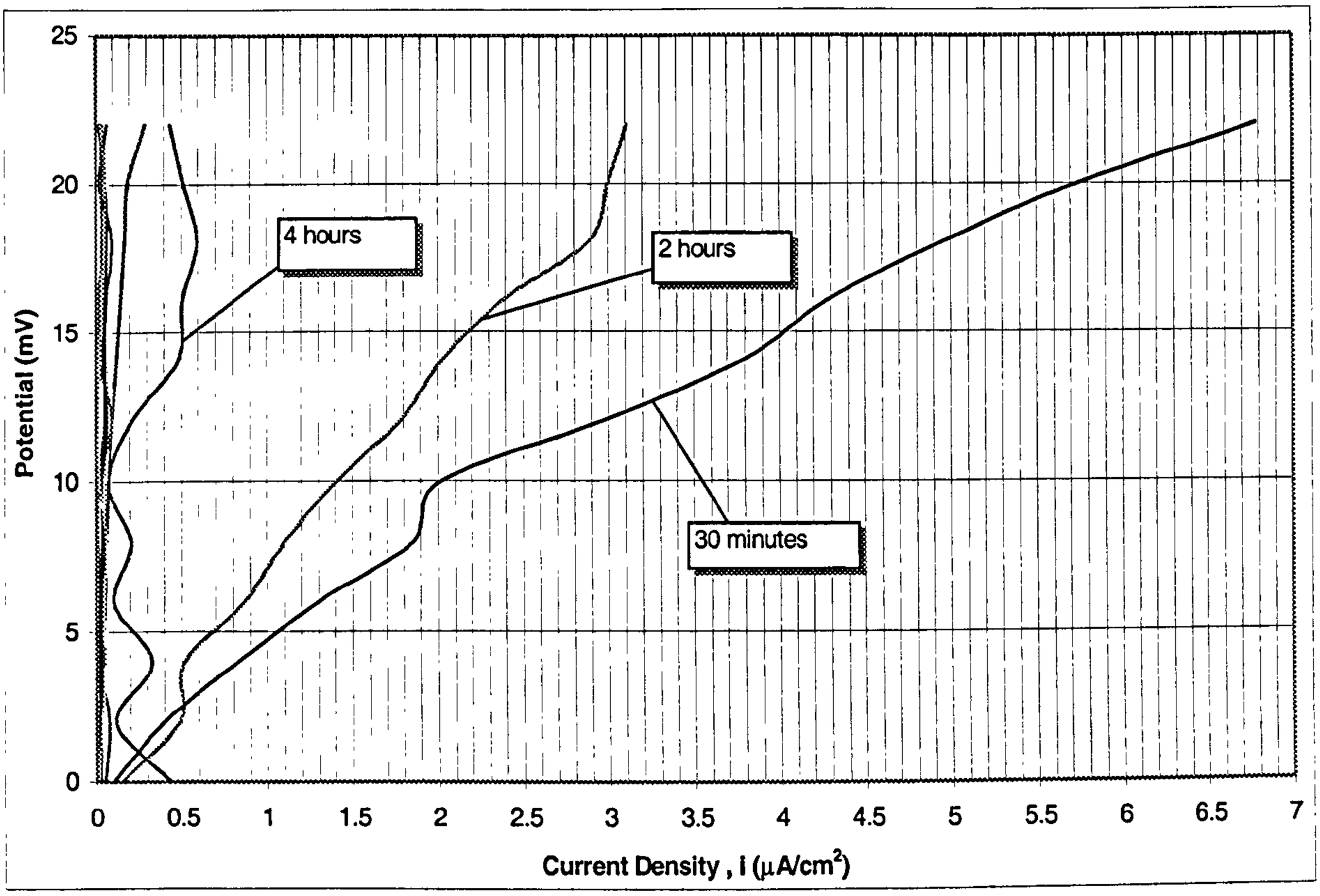

Figure 7.8b. Typical anodic polarisation curves of a specimen of Marinel at 35°C, for an increase by 22mV to the value of E_{corr}, at static conditions.

Time (hours)	Average E_{corr} (mV)	Average $R_p^{'}$ (KOhm*cm^2)	Average $1/R_p^{'}$ (1/(Kohm*cm^2))
0.5	-325.873	3.262	0.306
2	-314.531	6.876	0.145
4	-302.831	23.352	0.043
8	-287.623	86.36	0.012
24	-303.861	123.72	0.008
32	-298.796	145.621	0.007
40	-288.348	186.15	0.005
48	-295.891	226.5	0.004

Table 7.13b. The average values of E_{corr}, $R_p^{'}$, $1/R_p^{'}$ for Marinel at different time exposures for an increase by 22mV to the value of E_{corr}, at static conditions.

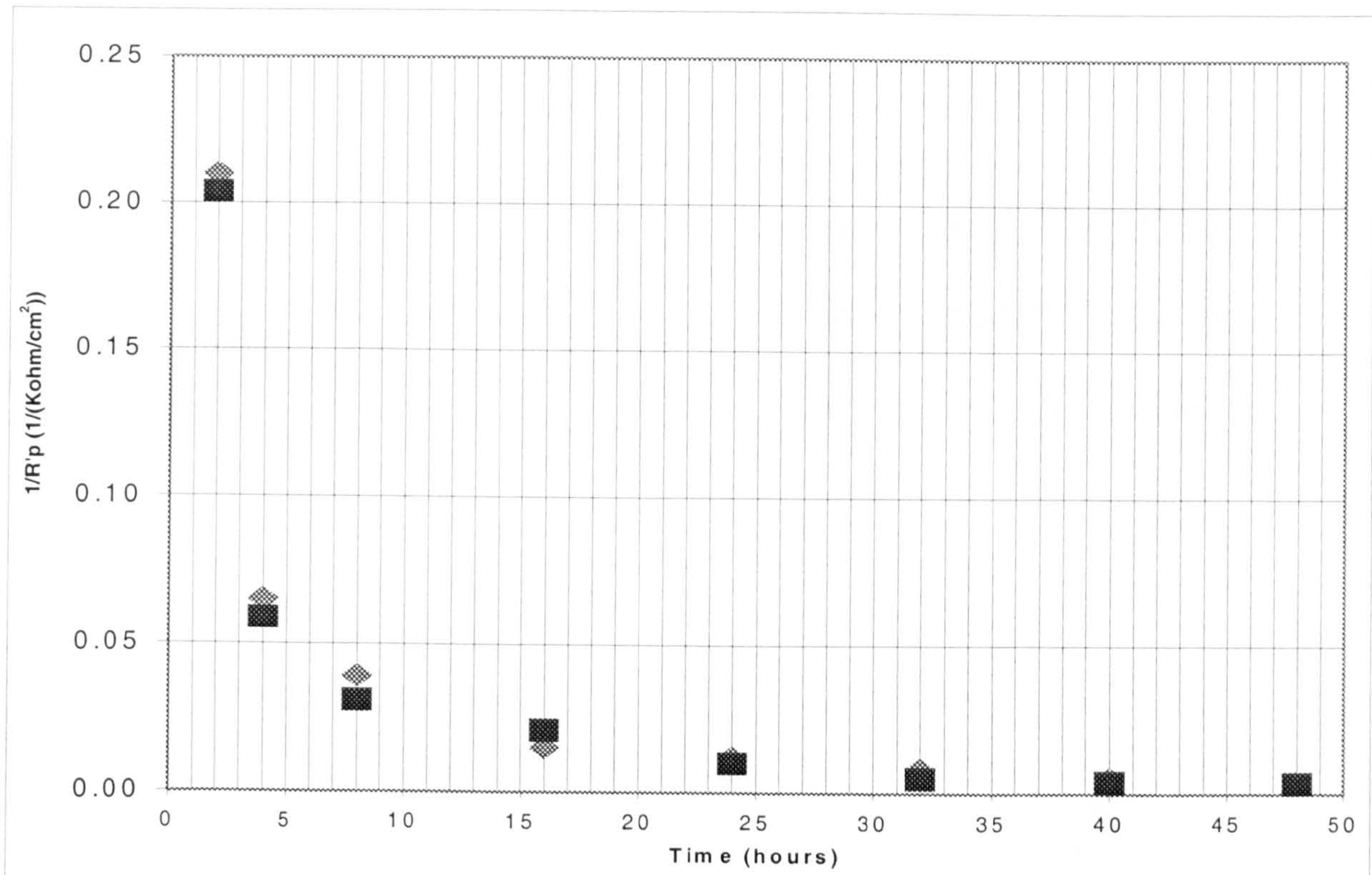

Figure 7.9a. $1/R_p'$ vs. Time curve of Marinel, for an increase by 22mV from the value of E_{corr}, at 35°C, impinging at 17m/s.

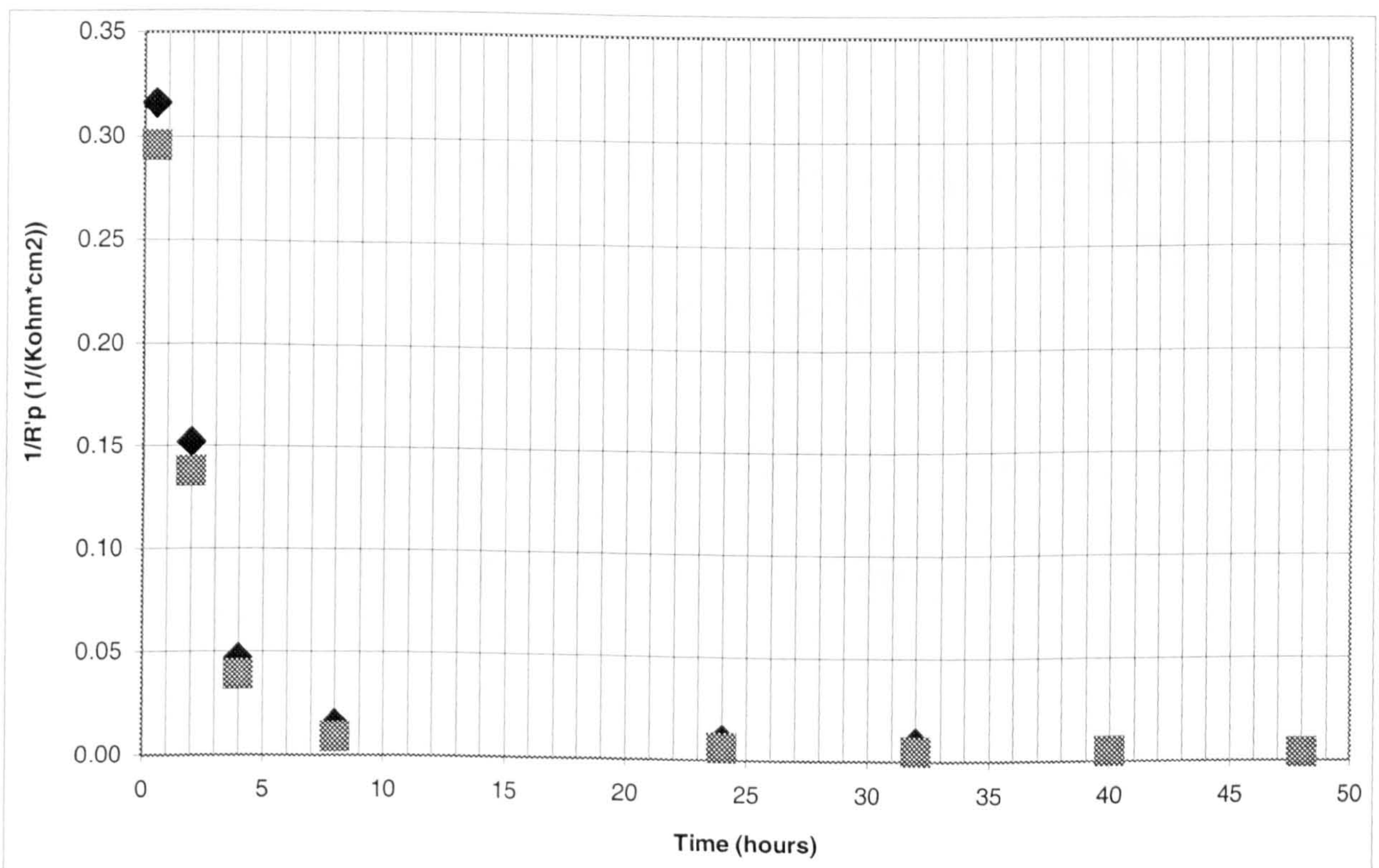

Figure 7.9b. $1/R_p'$ vs. Time curve of Marinel, for an increase by 22mV from the value of E_{corr}, at 35°C, at static conditions.

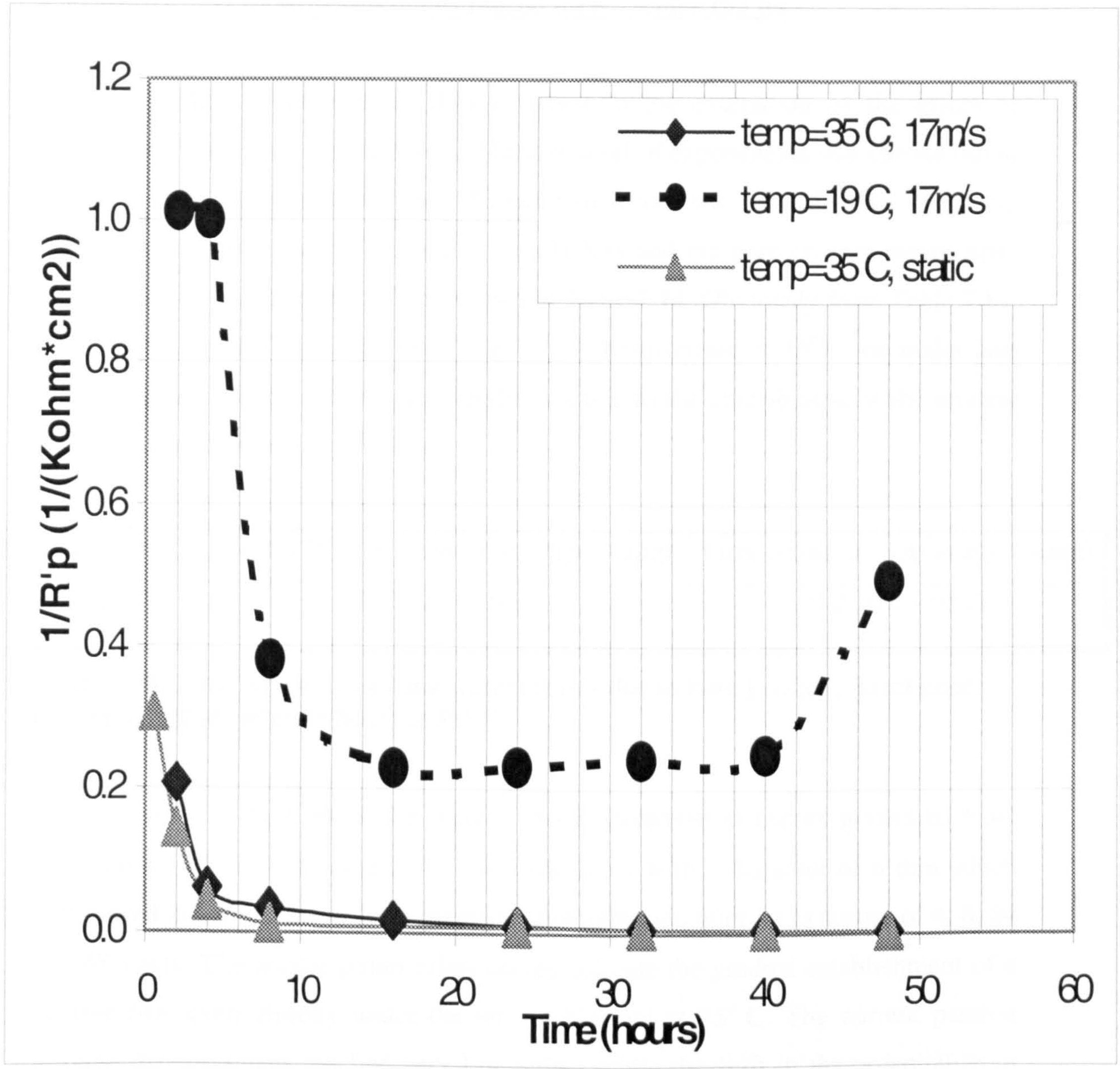

Figure 7.9c. Average $1/R_p'$ vs. Time curve of Marinel, for an increase by 22mV from the value of E_{corr}, at temperatures of 35°C and 19°C impinging at 17m/s, and at 35°C at static conditions.

7.3.2.6. Tests with specimens placed direct under the jet.

In order to obtain more data to assist in the evaluation of the effect of temperature in the total weight loss of Marinel, a set of experiments was carried out at 17m/s, in which a specimen with a diameter of 6 mm was placed direct under the 1mm diameter impinging jet. The total weight loss and the pure erosion results after an exposure of 48 hours at 35°C are shown in Table 7.14. Obviously from Table 7.14. in comparison with Table 7.8. and Table 7.9., at temperature of 35° C the major part of the total weight loss and all the weight loss due to the contribution of the erosion factor, take place direct under the jet.

Temperature °C	Total Weight Loss - (Average) -(mg)	Pure Erosion – (Average) –(mg)
35	0.8 , 0.9 – (0.85)	0.2 , 0.2 – (0.2)

Table 7.14. Total weight losses and weight losses due to Pure Erosion, direct under the impinging jet, after 48 hours at 35° C.

Figure 7.10a-b. show the typical anodic polarisation curves generated from tests carried out at 17m/s and 35°C, for a specimen with a diameter of 6 mm which was placed direct under the 1mm diameter impinging jet, after an exposure of 4, 8, 24 and 48 hours. The anodic polarisation curves indicate the gradual establishment of a passive film even directly under the jet, on Marinel at 35° C. The current passing through the specimens reached very low values while the shift in the potential from E_{corr} and this trend was accentuated with the passage of time.

Table 7.15., shows the current densities at 4, 8, 24 and 48 hours, as calculated by Tafel extrapolations on Figure 7.10b., and the average instantaneous corrosion rates calculated using Faraday's law for the area of 6mm. It is quite clear that corrosion rate decreased dramatically even under the jet from 4 to 48 hours, as is shows also on Figure 7.11., which shows the instantaneous corrosion rates plotted from the data in Table 7.15.

The integrated total direct corrosion rates at 35°C after 48 hours, (estimated from the area under the curve in Figure 7.11.), are presented in Table 7.16., which also includes the total metal loss and the pure erosion, (from Table 7.14.), and the synergy calculated from T.W.L = C + E + S.

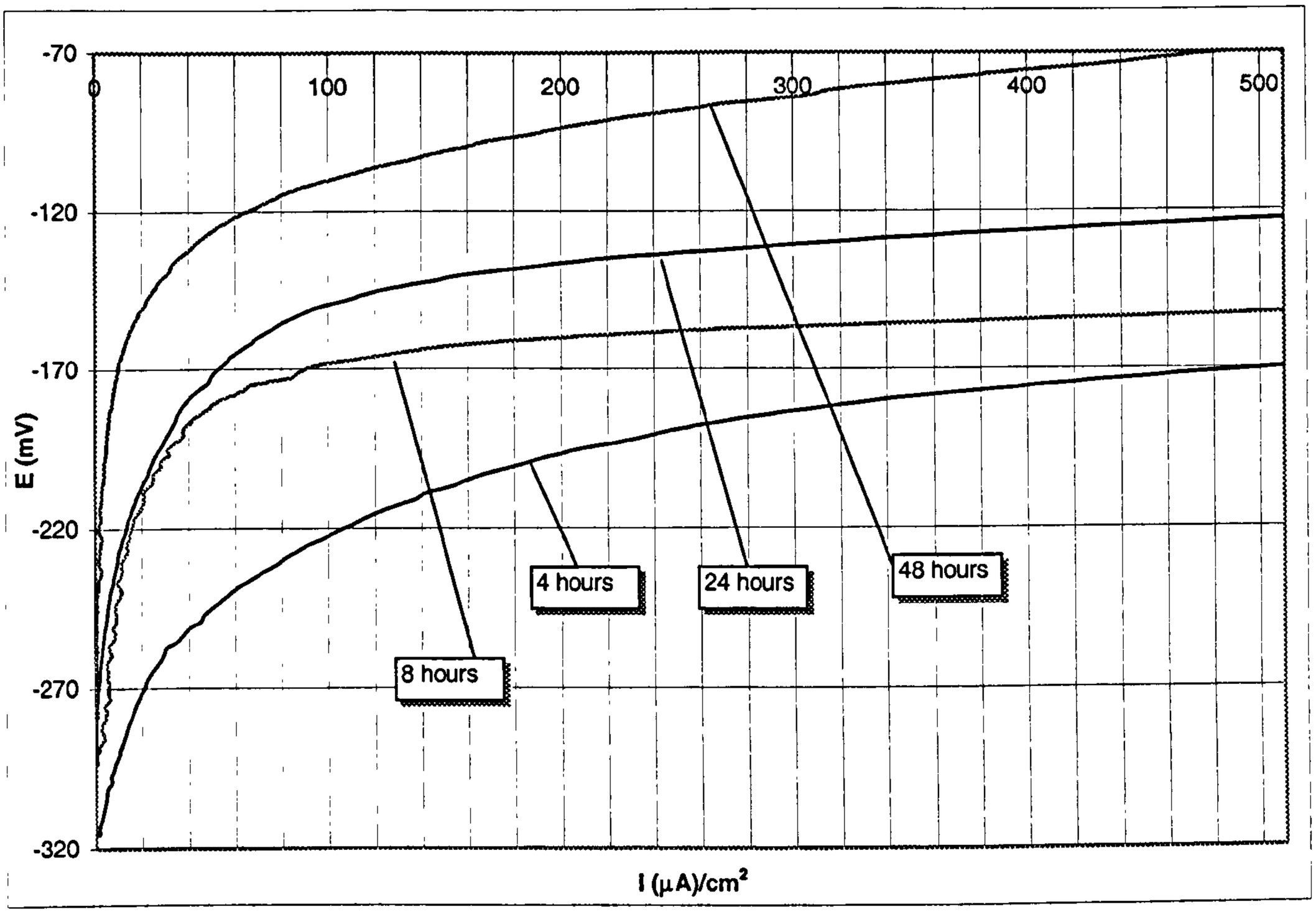

Figure 7.10a. Anodic polarisation curves of Marinel at exposures of 4, 8, 24 and 48 hours direct under the impinging jet, at 17 m/s and 35°C.

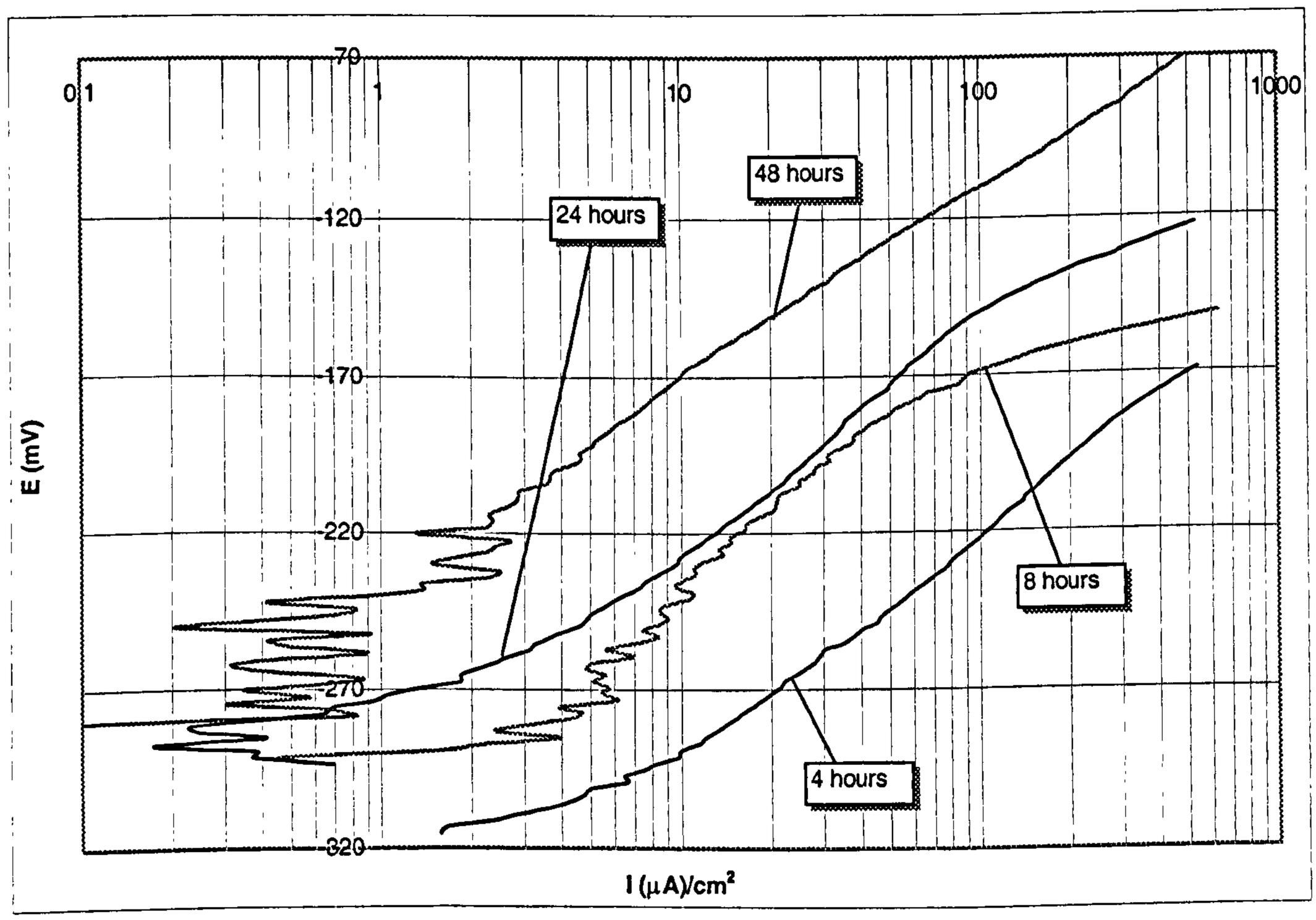

Figure 7.10b. Anodic polarisation curves of Marinel at exposures of 4, 8, 24 and 48 hours direct under the impinging jet, at 17 m/s and 35°C.

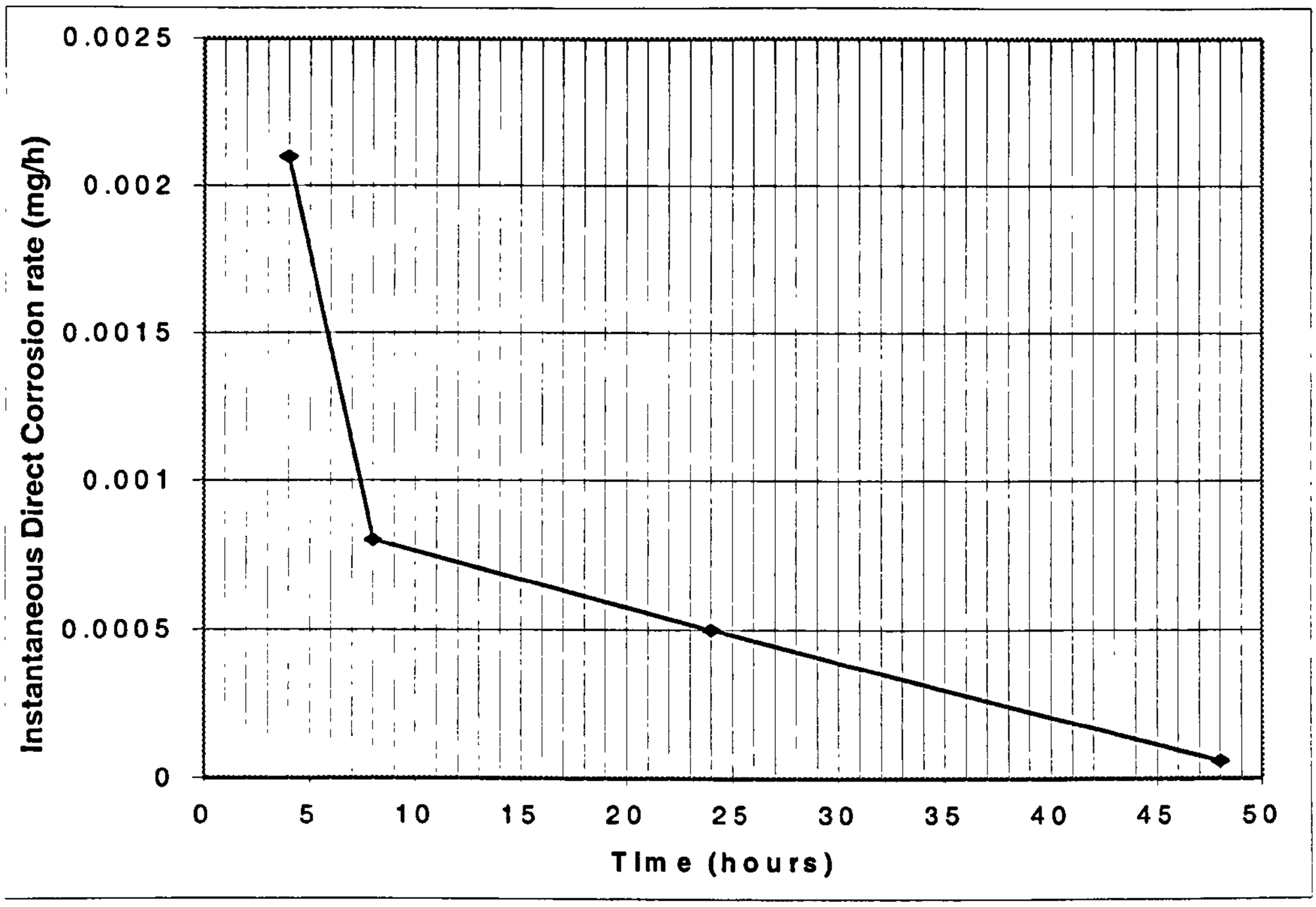

Figure 7.11. Instantaneous direct corrosion rate vs. time graph for Marinel at 17m/s and 35°C, direct under the impinging jet.

Time (hours)	Current density ($\mu A/cm^2$) – 35±1°C	Instantaneous Direct Corrosion Weight Losses (mg/h) – 35±1°C	Instantaneous Direct Corrosion Weight Losses (mg/h) – *Average* – 35±1 °C
4	6 , 7	0.0019 , 0.0023	0.0021
8	2.5 , 2.5	0.0008 , 0.0008	0.0008
24	1.5 , 1.5	0.0005 , 0.0005	0.0005
48	0.17 , 0.19	0.00006 , 0.00006	0.00006

Table 7.15. Average instantaneous corrosion rates at 4, 8, 24 and 48 hours, and current densities as calculated by Tafel extrapolations for 35°C, for the area direct under the jet.

Temperature °C	Total Weight Loss - (Average) -(mg)	Pure Erosion – (Average) –(mg)	Total Direct Corrosion – Average –(mg)	Synergy *Average* - (mg)
35	0.8 , 0.9 – (0.85)	0.2 , 0.2 – (0.2)	0.03	0.62

Table 7.16. Total weight losses, Pure Erosion, Total Direct Corrosion and Synergy losses, directly under the impinging jet, after 48 hours at 35° C.

Evidently the results state that the corrosion current density, in $\mu A/cm^2$, is rather higher in the centre than on the entire surface of the specimen; but the weight losses due to the direct corrosion component for the centre are much less than that on the entire specimen, (this is in contrast to the total weight loss and the erosion values for which a large proportion is on the centre).

7.4. Microscopical examination.

The results of the microscopical examination on the specimens after the tests, focused on the influence of the impingement angle and the temperature on the mechanisms of attack, are presented in the following sections, 7.4.1. for Cu-10%Ni and 7.4.2. for Marinel.

7.4.1. Cu-10%Ni.

7.4.1.1. Impingement angle effect.

The Cu-10%Ni alloy at different impingement angles showed the same surface features as after the same exposure time at the same velocity, (i.e. 17m/s, 8 hours), at $\phi=90^{o}$. Mainly the etched structure is evident implying uniform attack on the metal, (Figure 7.12, Figure 7.13). The only detectable difference on the oblique angles was the tendency for a thicker surface film away from the directly impinged zone, Figure 7.14.

7.4.1.2. Temperature effect.

The entire surface of the Cu-10%Ni specimen after the end of the test, (Figure 7.15.), was covered by a fairly discontinuous yellowish film, with no evidence of hydrodynamic effects. Figures 7.16 shows the patchy film which covered the whole surface. At high magnification the variations in film structure and thickness were evident as shown at Figure 7.17 and Figure 7.18, with some areas where the film was relatively thick and others where it appeared as darkish structural patches, Figure 7.17. The metal grain structure was faintly evident in unfilmed areas and indeed in many areas the film appears decorating the grain boundaries of the underlying metal.

7.4.2. Marinel.

7.4.2.1. Impingement angle effect.

The Marinel alloy at all impingement angles, (i.e. ϕ=30°, ϕ=45°, ϕ=60°), under the directly impinged zone was covered by the discontinuous, acicular, needle-like, film, Figure 7.19. This behaviour is identical to what we have seen for the central region at ϕ=90°, Figure 6.17. A clear difference between the behaviour at ϕ=90° and the other angles is that the more discontinuous dark film which is also evident in the outer regions after perpendicular impingement, (see Figure 6.17.), is absent at the other angles. The acicular film at these oblique angles was of yellow colour and clearly thinner than the dark acicular film at 90°. The outer regions at ϕ=30°, ϕ=45° and ϕ=60°, showed an etched structure together with the precipitate particles, but with an evidence of a lack of sharpness on the images, implying that a thin film is forming, Figure 7.20.

7.4.2.2. Temperature effect.

When the specimen was removed from the rig was clearly covered by a more substantial film over the entire surface, than was the case for the same experiment at ambient temperature, i.e. 19°C. Moreover the film formed at 35°C was more difficult to be removed. Under the microscope the discontinuous film that remained on the surface was less abundant at the centre than at the outer areas of the specimen, Figure 7.21. Another important observation was that the examination of the surface in between the patches of the film, revealed only a faint evidence of the etched structure. Again evident were white, clearly unattacked Ni/Nb particles.

The cathodically protected specimen after removal from the experimental rig, appeared substantially different than the specimen exposed to erosion-corrosion conditions without any electrochemical intervention, i.e. T.W.L. In particular there was no presence of the very thick film that was apparent on the ordinary test.

The appearance of the specimen subjected to erosion-corrosion for 48 hours at 35°C with final anodic polarisation, was essentially identical to the specimen without the anodic polarisation.

Figure 7.12. Cu-10%Ni, V=17m/s, 8 hours, ϕ=45°, T.W.L.
The etched structure evident on the whole surface.

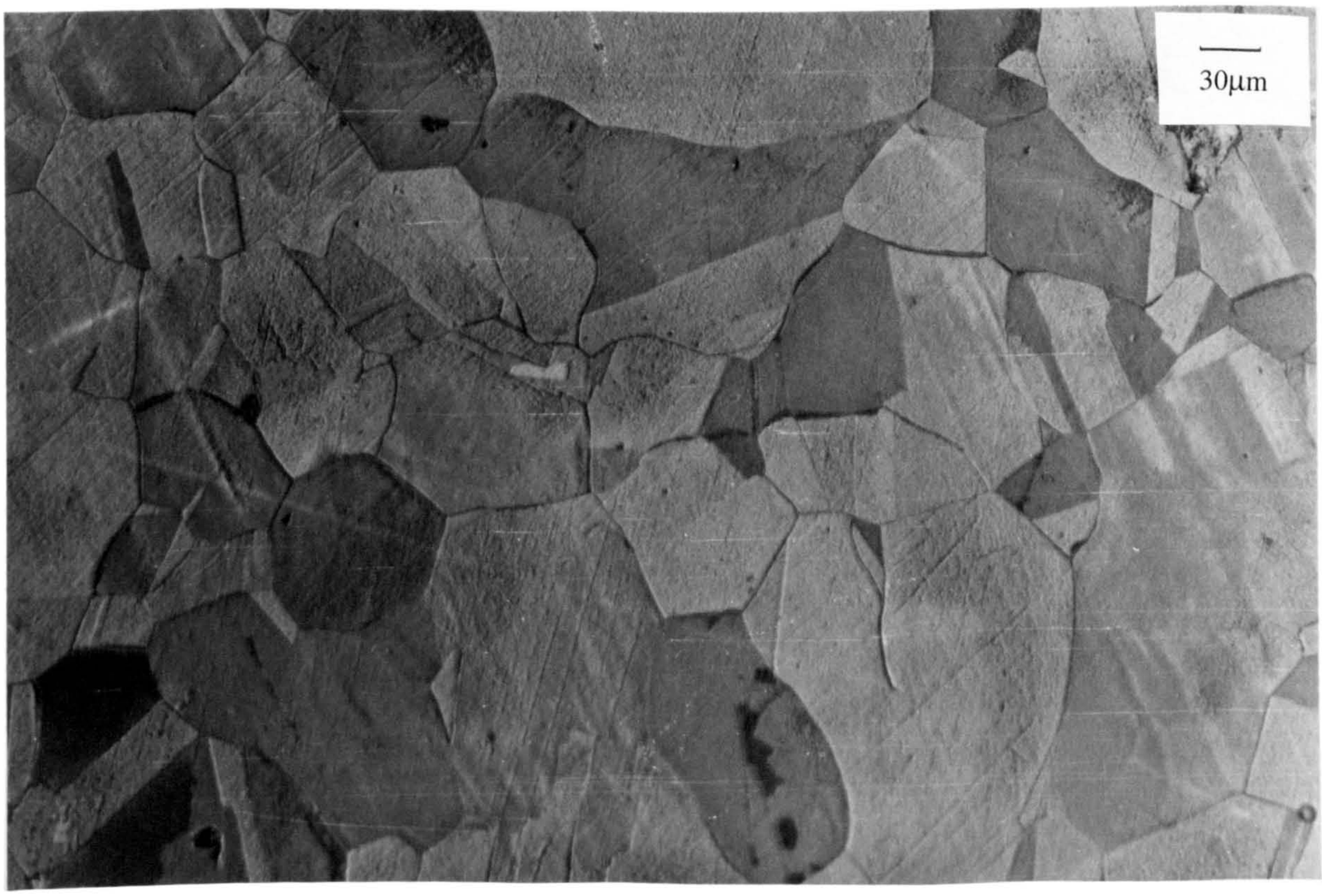

Figure 7.13. Cu-10%Ni, V=17m/s, 8 hours, ϕ=30°, T.W.L.
The etched structure – uniform attack on the metal.

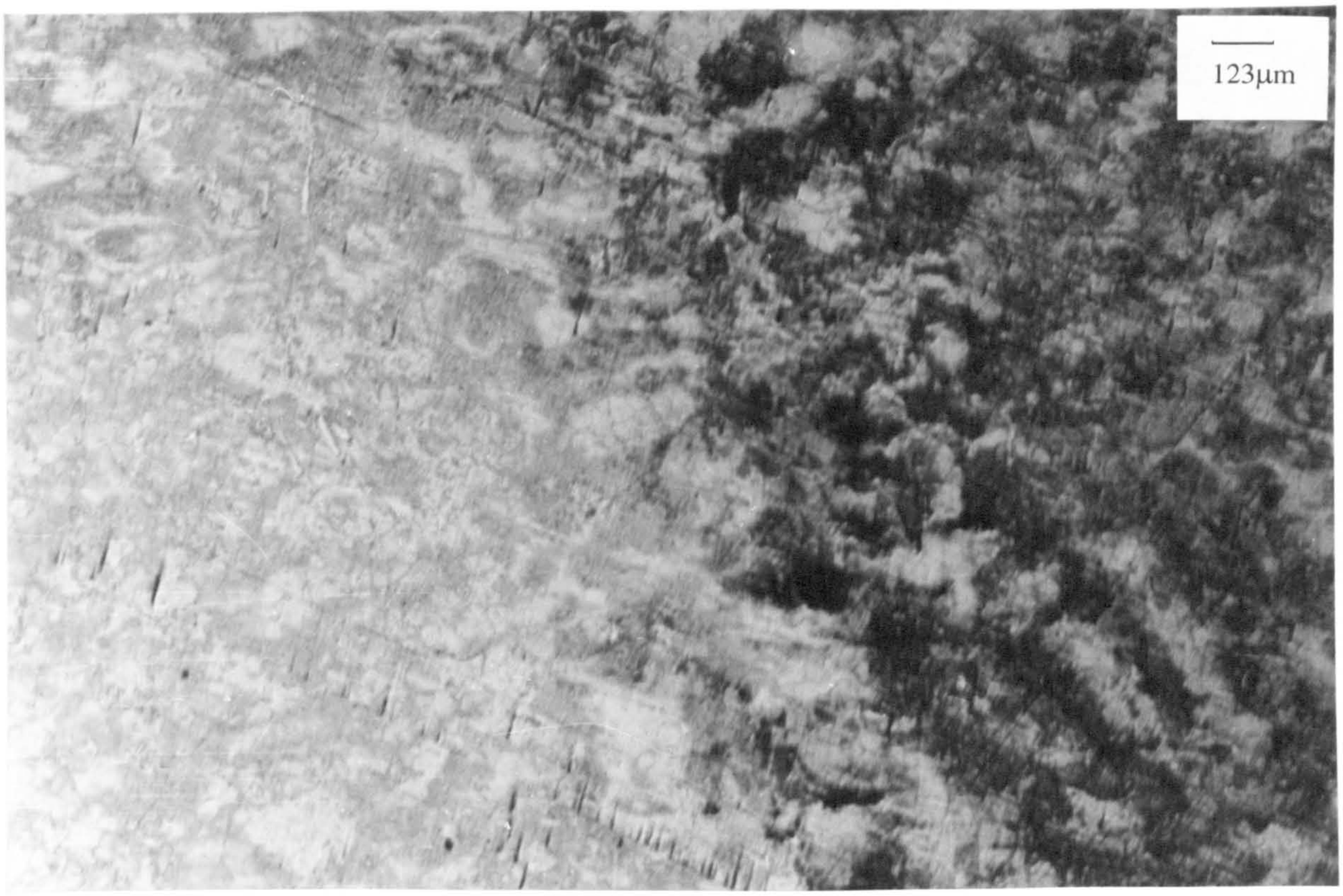

Figure 7.14. Cu-10%Ni, V=17m/s, 8 hours, ϕ=30°, T.W.L.
The thicker film away from the directly impinged zone.

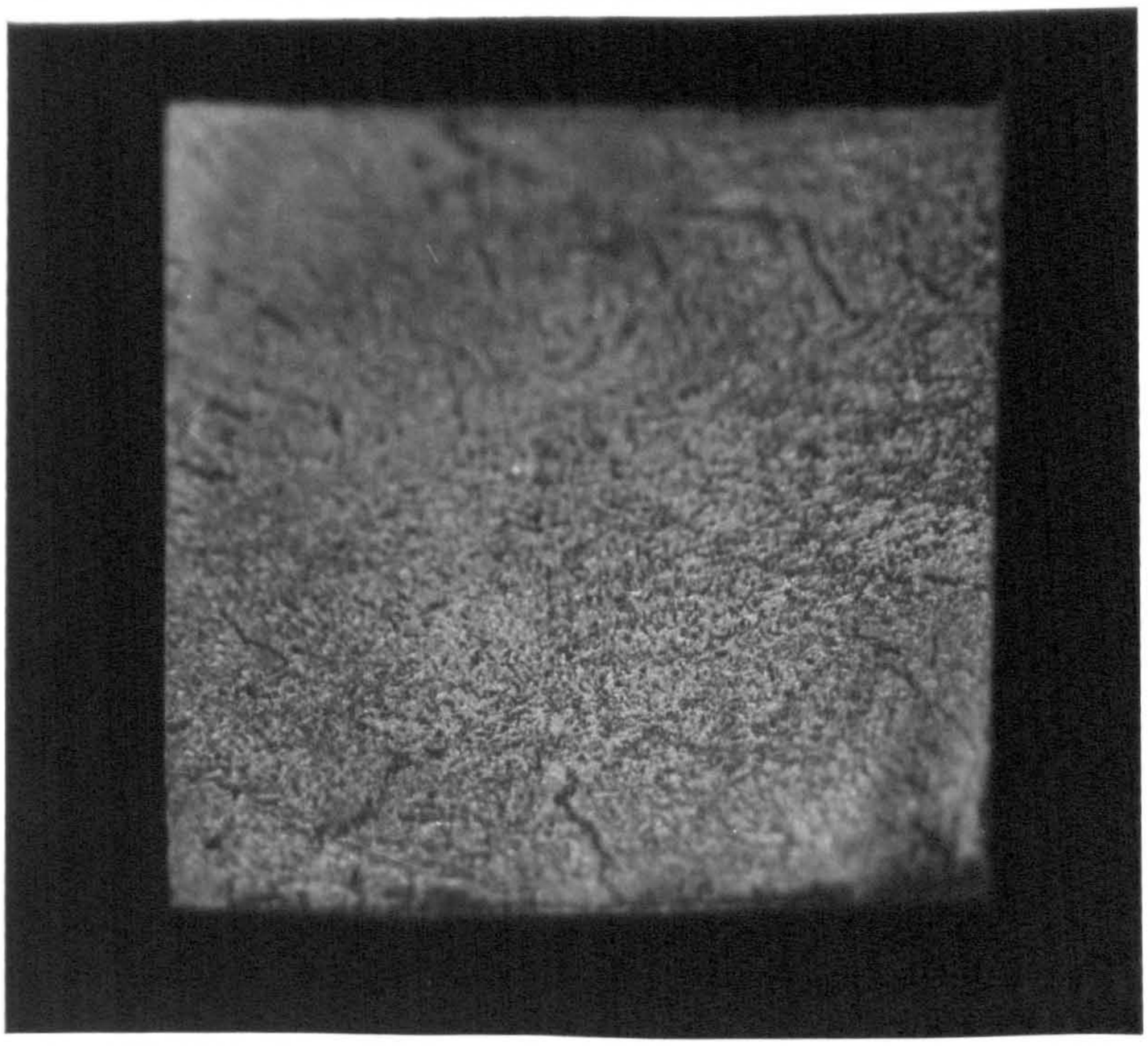

Figure 7.15. Cu-10%Ni, V=17m/s, 48 hours, T=35°C, T.W.L.
The specimen after the test.

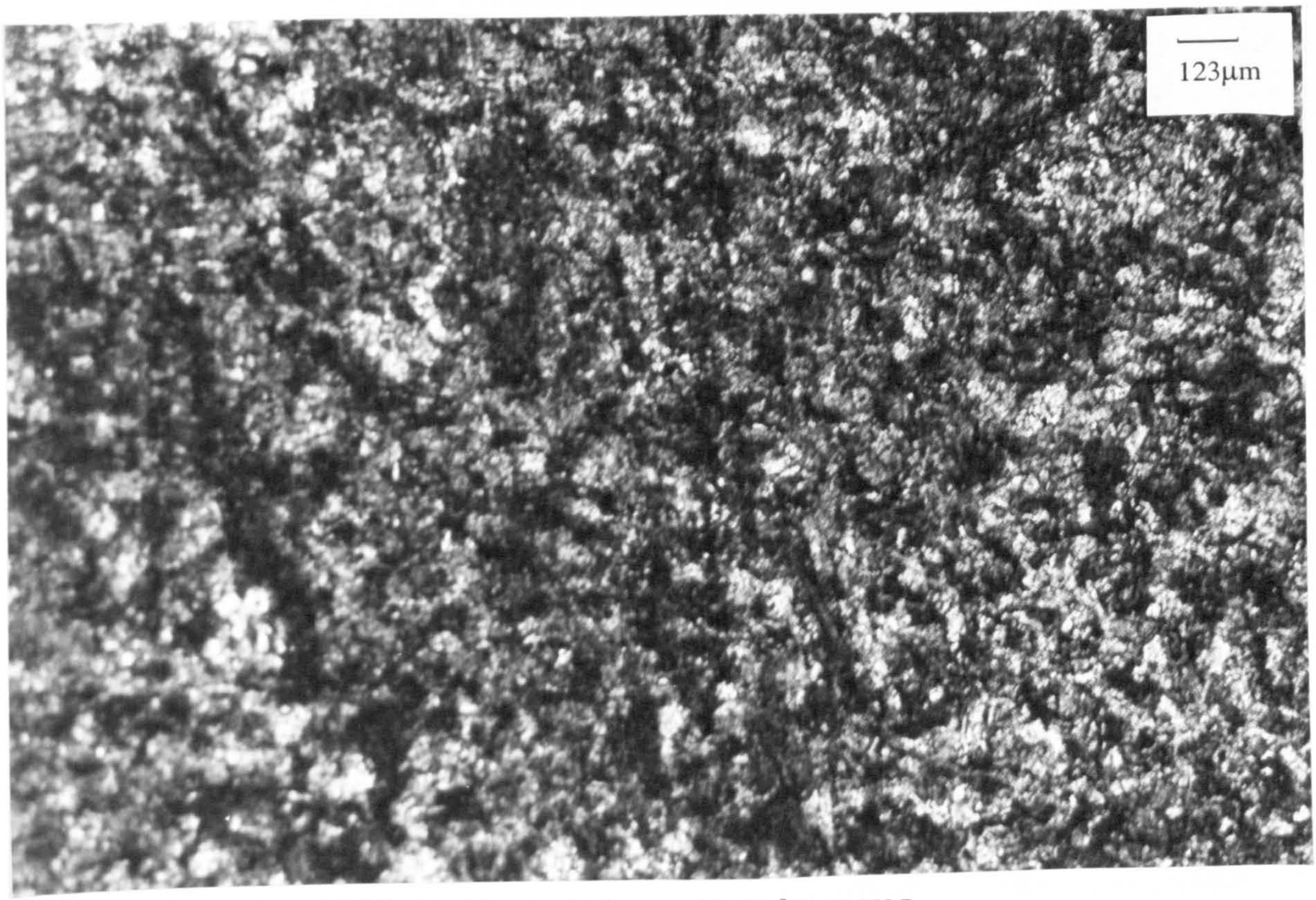

Figure 7.16. Cu-10%Ni, V=17m/s, 48 hours, T=35°C, T.W.L.
The patchy film which covered the whole surface.

Figure 7.17. Cu-10%Ni, V=17m/s, 48 hours, T=35°C, T.W.L.
The variations in film structure and thickness.

Figure 7.18. Cu-10%Ni, V=17m/s, 48 hours, T=35°C, T.W.L.
The variations in film structure and thickness.

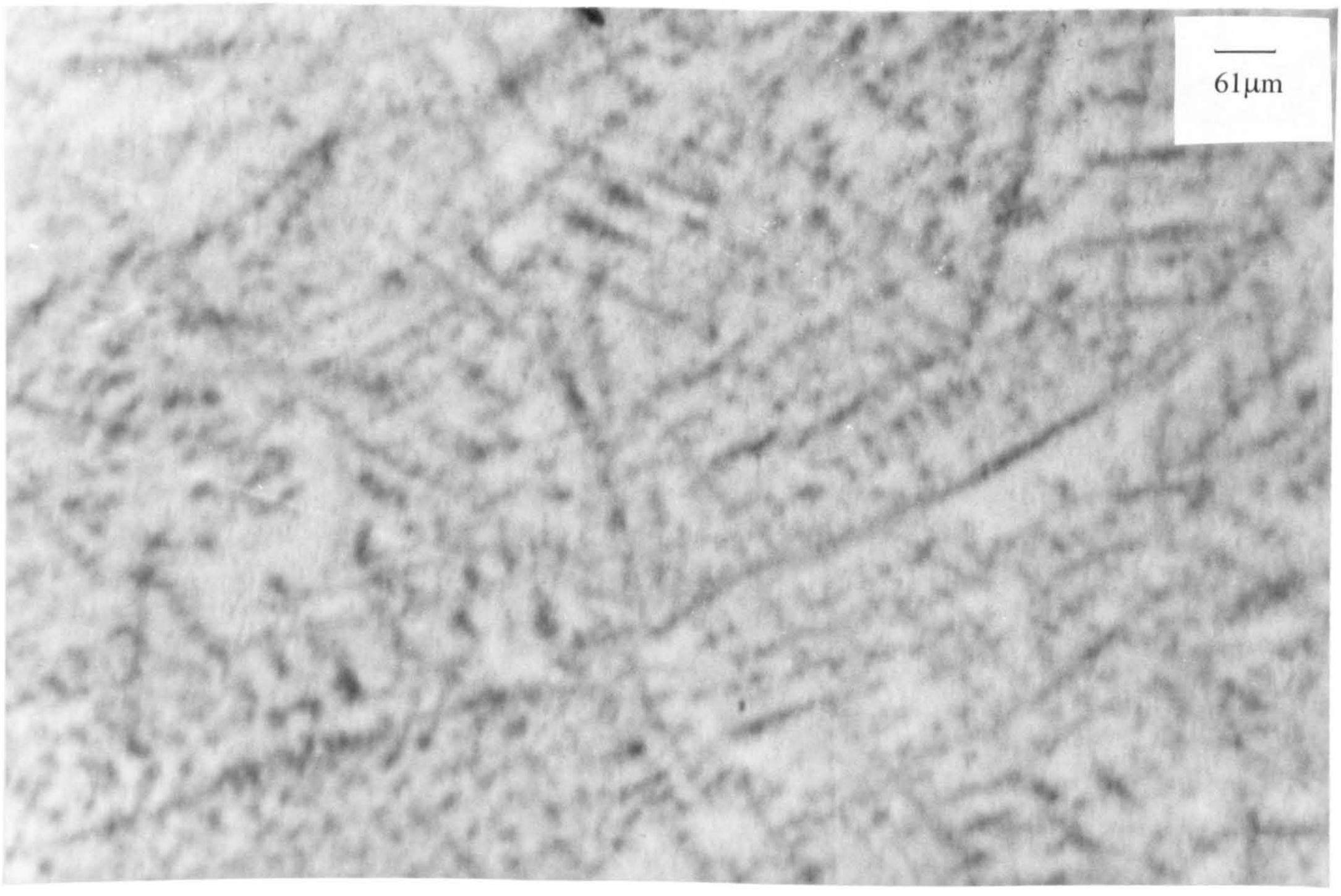

Figure 7.19. Marinel, V=17m/s, 8 hours, ϕ=30°, T.W.L.
The discontinuous, acicular film under the directly impinged-zone.

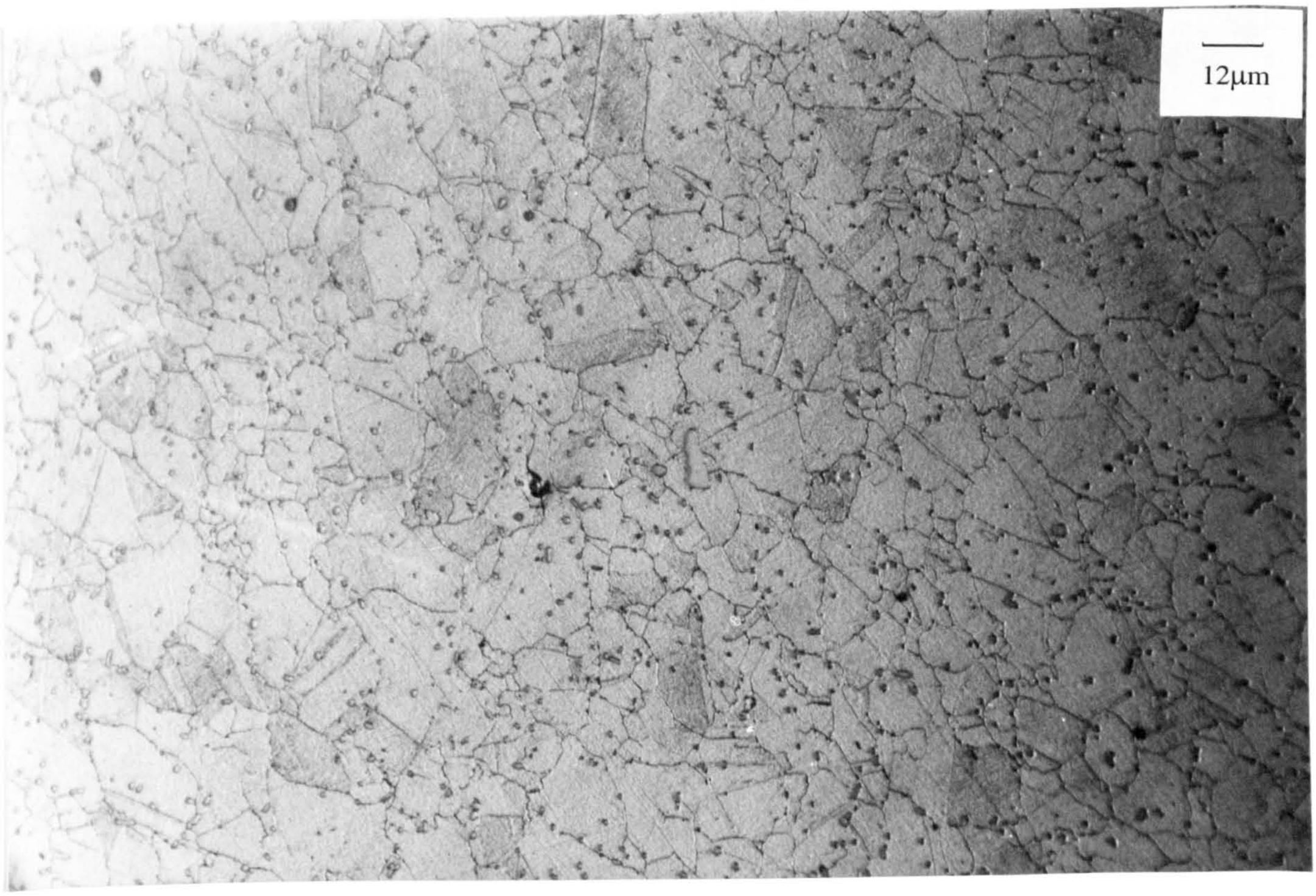

Figure 7.20. Marinel, V=17m/s, 8 hours, ϕ=45°, T.W.L.
The etched structure at the outer regions.

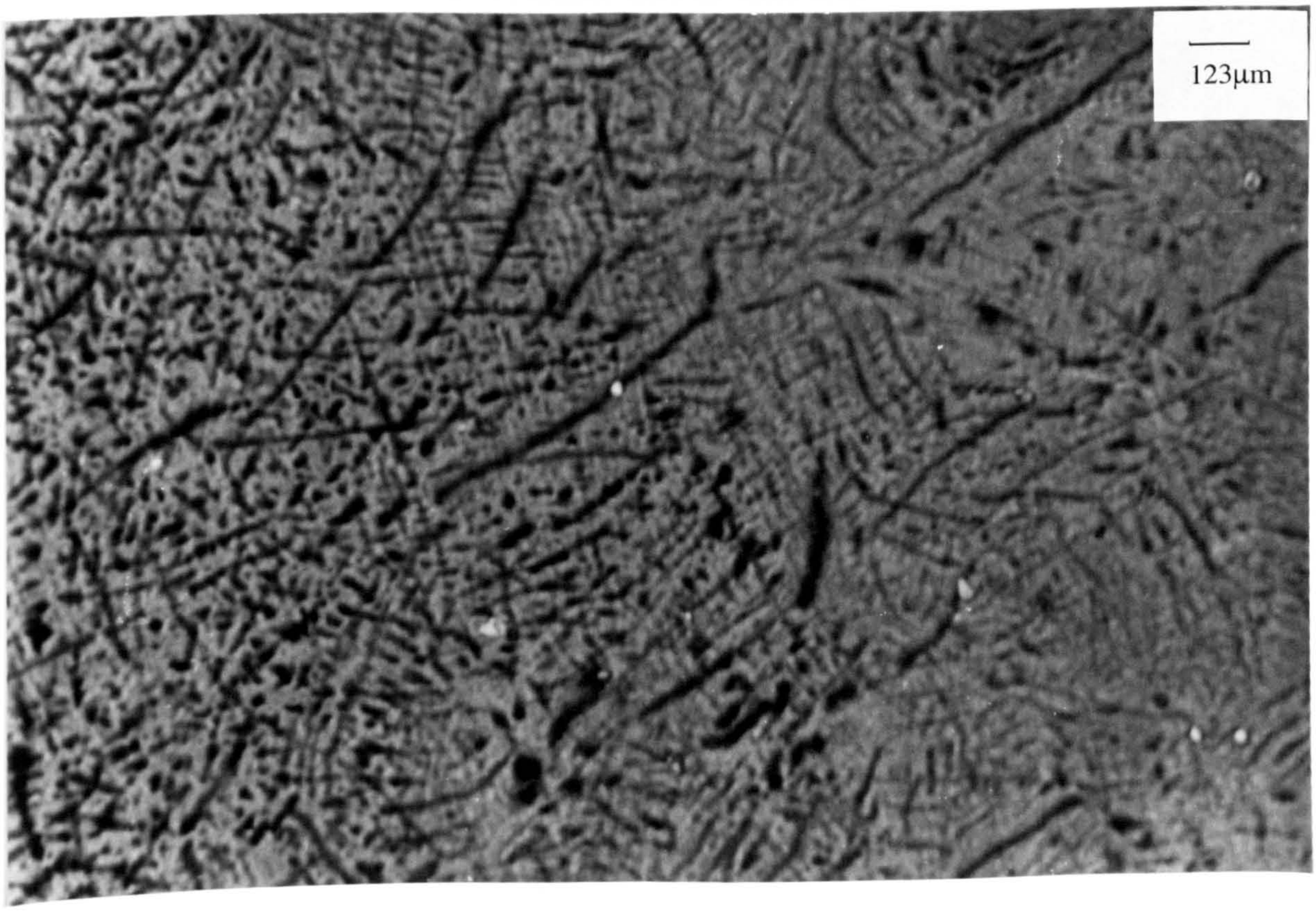

Figure 7.21. Marinel, V=17m/s, 48 hours, T=35°C, T.W.L.
The discontinuous film was less abundant at the centre, (right side of the photograph), than at the outer areas of the specimen, (left side).

Chapter 8

Results related to Concentric Specimens.

8.1 Effect of time and temperature on erosion-corrosion processes for concentric specimens.

The previous sections, (6, 7), presented results focused on composite specimens. This section presents the results obtained from concentric specimens, as described in section 5.2., which were subjected to liquid impingement at 17m/s, using the 1mm nozzle, at ambient temperature $19^{o}\pm2$C, where the jet was incident on the central specimen. A series of linear polarisation tests were conducted during the course of the experiment on both the inner and outer parts to the specimen. Galvanic currents were measured at time intervals during the course of the linear polarisation tests as well as measurement of the change in the free corrosion potential. Full anodic polarisation scans after 48 and 72 hours were also conducted.

Furthermore a series of tests at $35^{o}\pm1$C are also presented for the concentric specimens of Marinel.

The results of this part of the work are described in the following sections, 8.1.1. (for Cu-10%Ni), and 8.1.2. (for Marinel).

8.1.1. Effect of time on erosion-corrosion processes for concentric specimens of Cu-10%Ni.

8.1.1.1. Linear polarisation type tests.

As shown in section 5.2. these experiments involved two separate specimens; one 4mm diameter directly under the jet and the other a square plate with size 20x20mm with a centred 6mm internal diameter. The respective areas were 0.126cm^2 and 3.72cm^2.

They were subjected to a jet, using a nozzle diameter of 1mm at a velocity of 17m/s. One set of experiments involved a linear polarisation-type monitoring exercise, employing an increase in potential by 22mV from E_{corr} after exposures of 30mins, 2, 4, 8, 16, 24, 32, 48 and 72 hours under the impinging jet.

Figure 8.1a-b and Figure 8.2a-b show the resulting anodic polarisation curves for the central and the outer specimen respectively.

Table 8.1. and Table 8.2. show the average values of $R_p^{'}$ and $1/R_p^{'}$ calculated from the gradient of the graphs on Figure 8.1a-b. and Figure 8.2a-b. The tables also include the analogous values for the composite specimen, (from Table 6.16.) for comparison purposes.

Figure 8.3a. and Figure 8.3b. present the $1/R_p^{'}$ versus time plots for the concentric samples and Figure 8.4. presents the $1/R_p^{'}$ average values versus time plots for the concentric samples. The time dependence of corrosion rate appears to be rather complex.

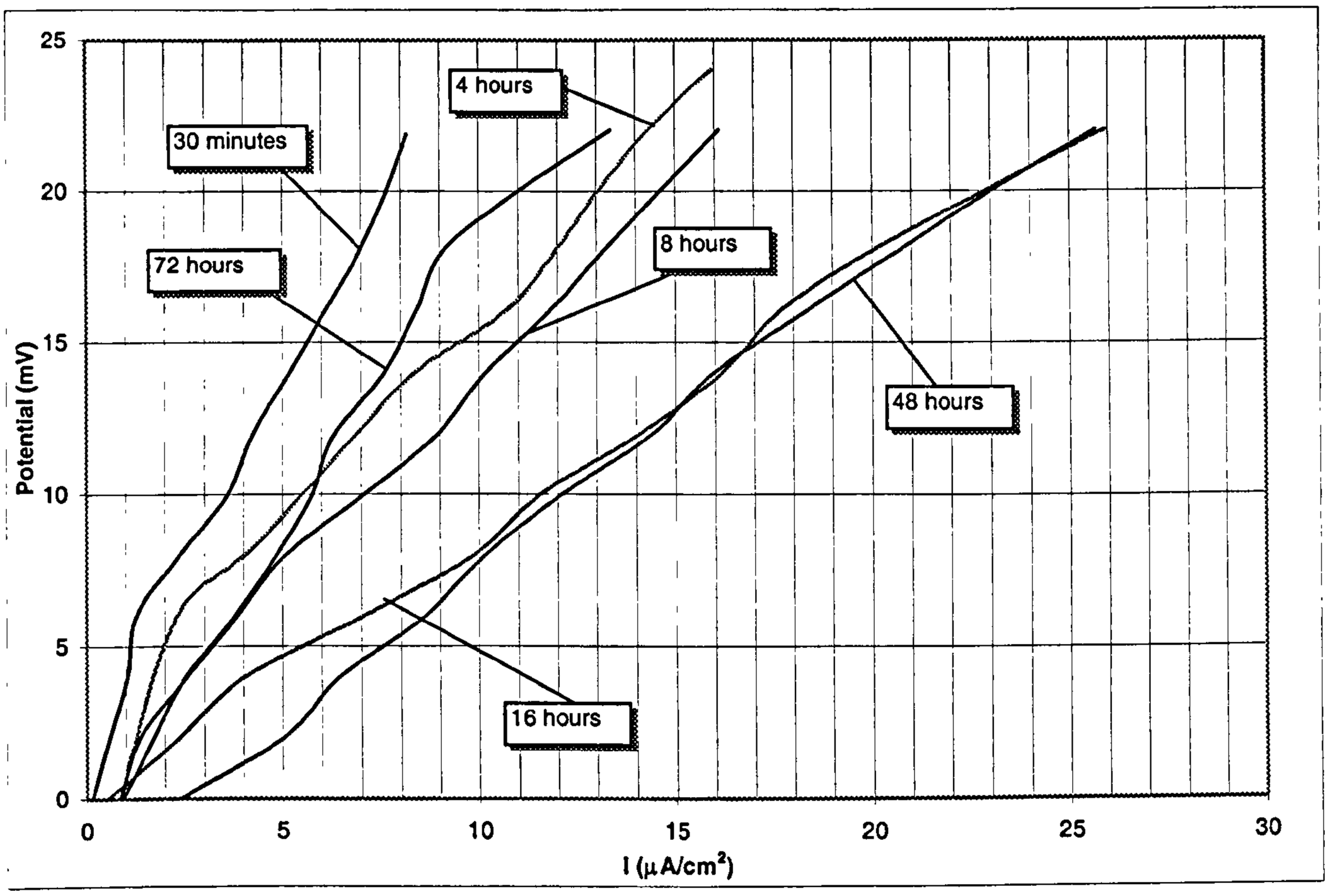

Figure 8.1a. Anodic polarisation curves of the *central* region of a concentric specimen of Cu-10%Ni, for an increase by 22mV to the value of E_{corr}, upon exposures of 30mins, 4, 8, 16, 48 and 72 hours under impingement velocity of 17 m/s.

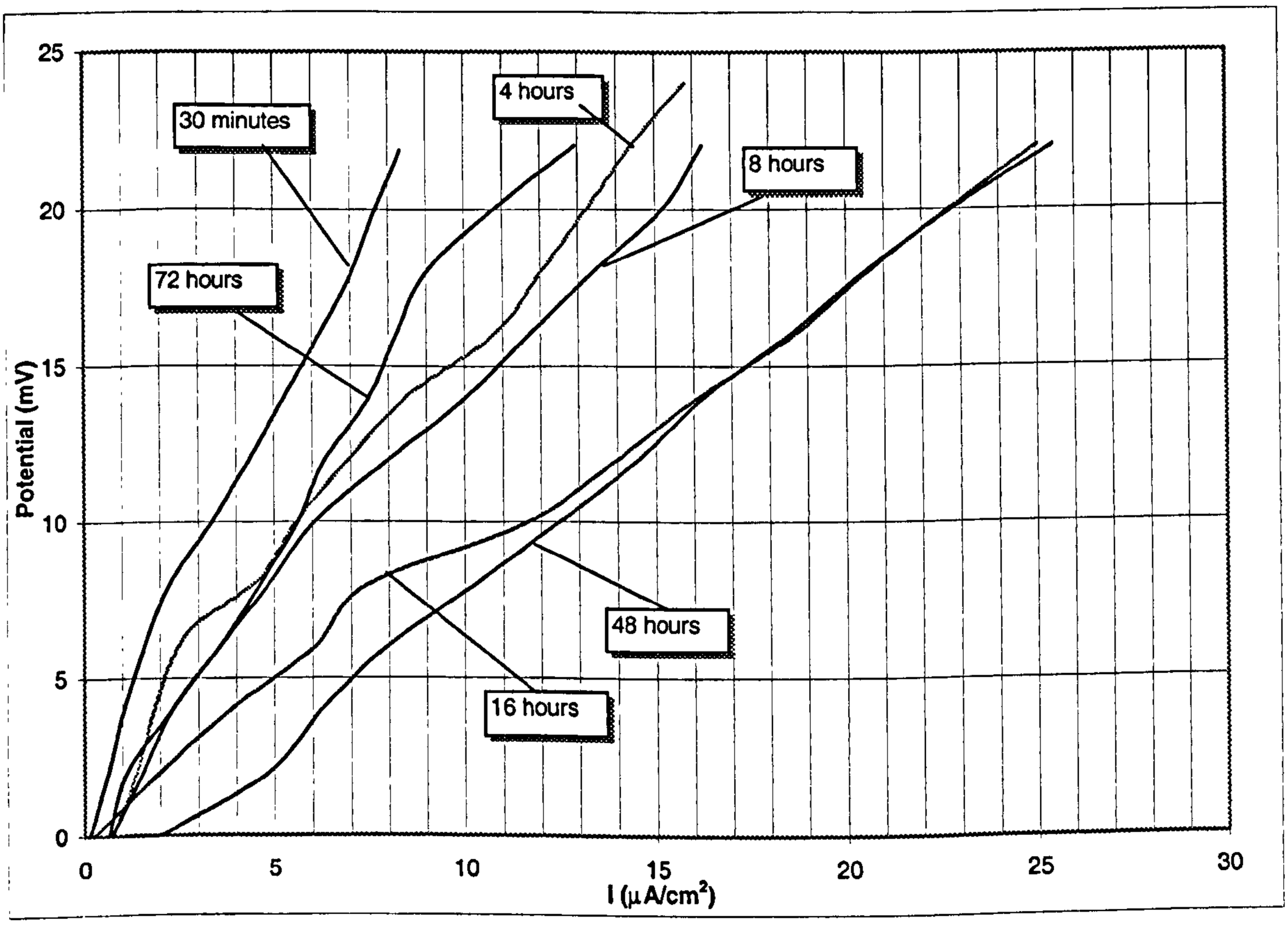

Figure 8.1b. Anodic polarisation curves of the *central* region of a concentric specimen of Cu-10%Ni, for an increase by 22mV to the value of E_{corr}, upon exposures of 30mins, 4, 8, 16, 48 and 72 hours under impingement velocity of 17 m/s.

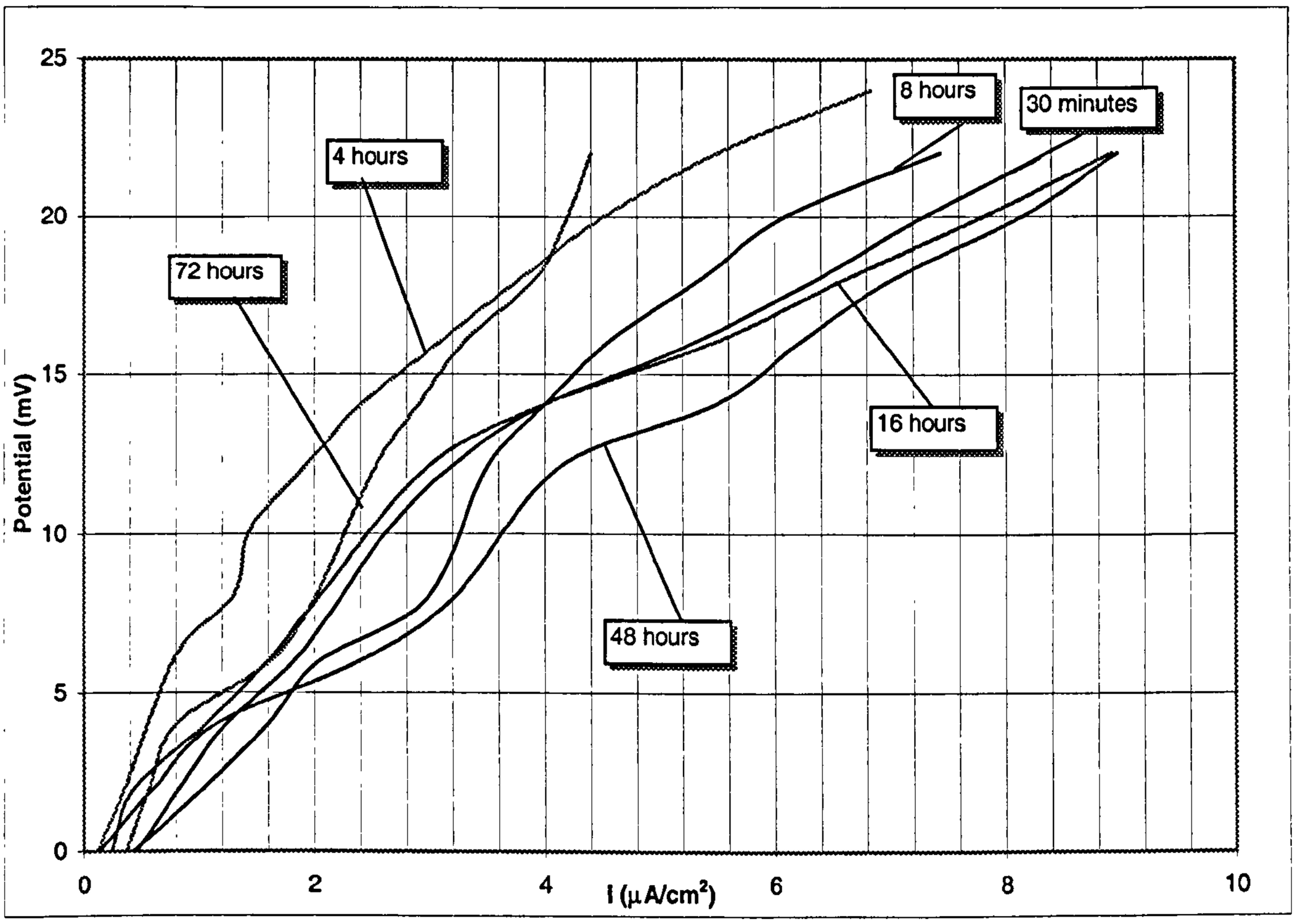

Figure 8.2a. Anodic polarisation curves of the *outside* region of a concentric specimen of Cu-10%Ni, for an increase by 22mV to the value of E_{corr}, upon exposures of 30mins, 4, 8, 16, 24, 32, 48 and 72 hours under impingement velocity of 17 m/s.

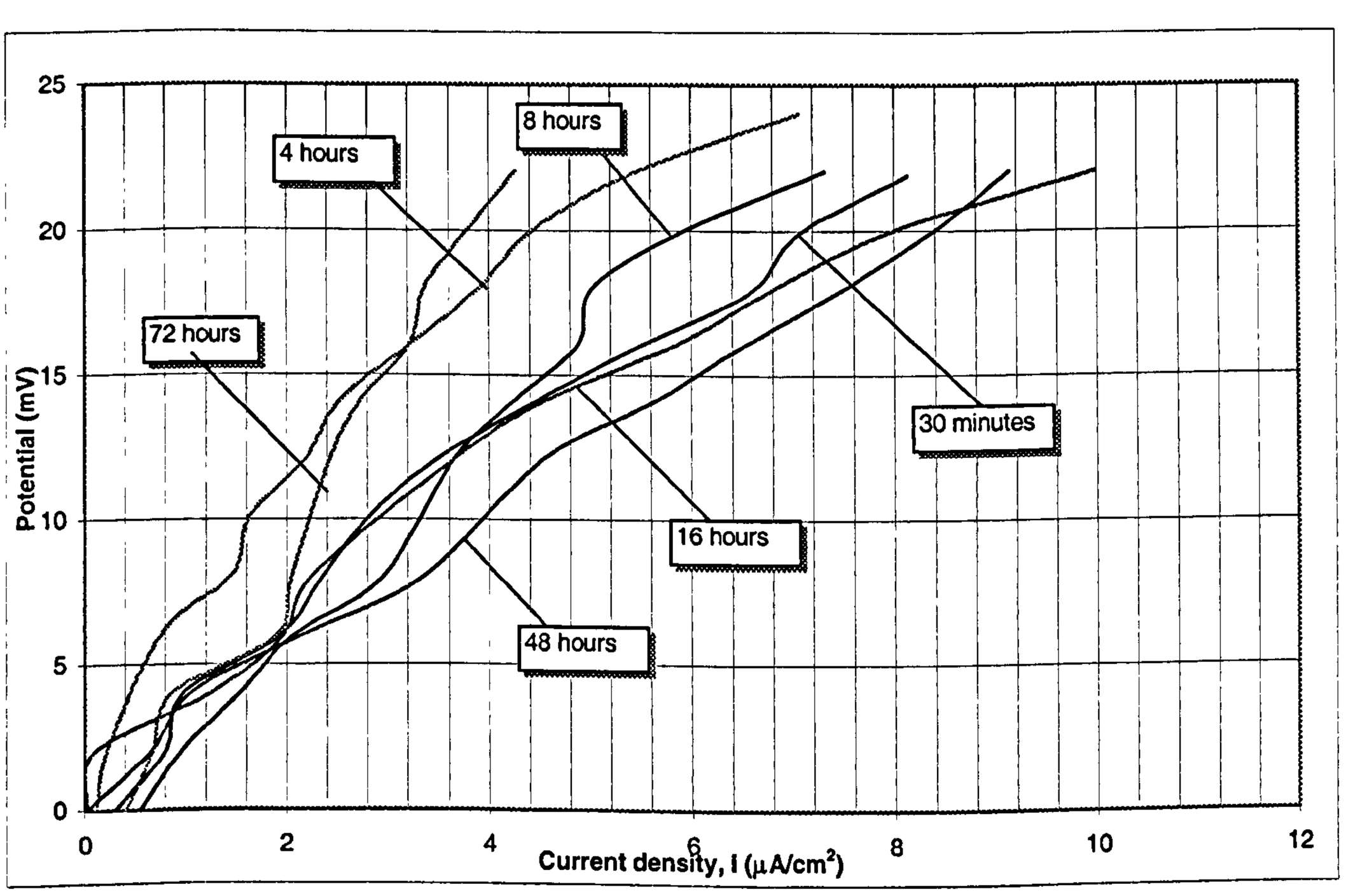

Figure 8.2b. Anodic polarisation curves of the *outside* region of a concentric specimen of Cu-10%Ni, for an increase by 22mV to the value of E_{corr}, upon exposures of 30mins, 4, 8, 16, 48 and 72 hours under impingement velocity of 17 m/s.

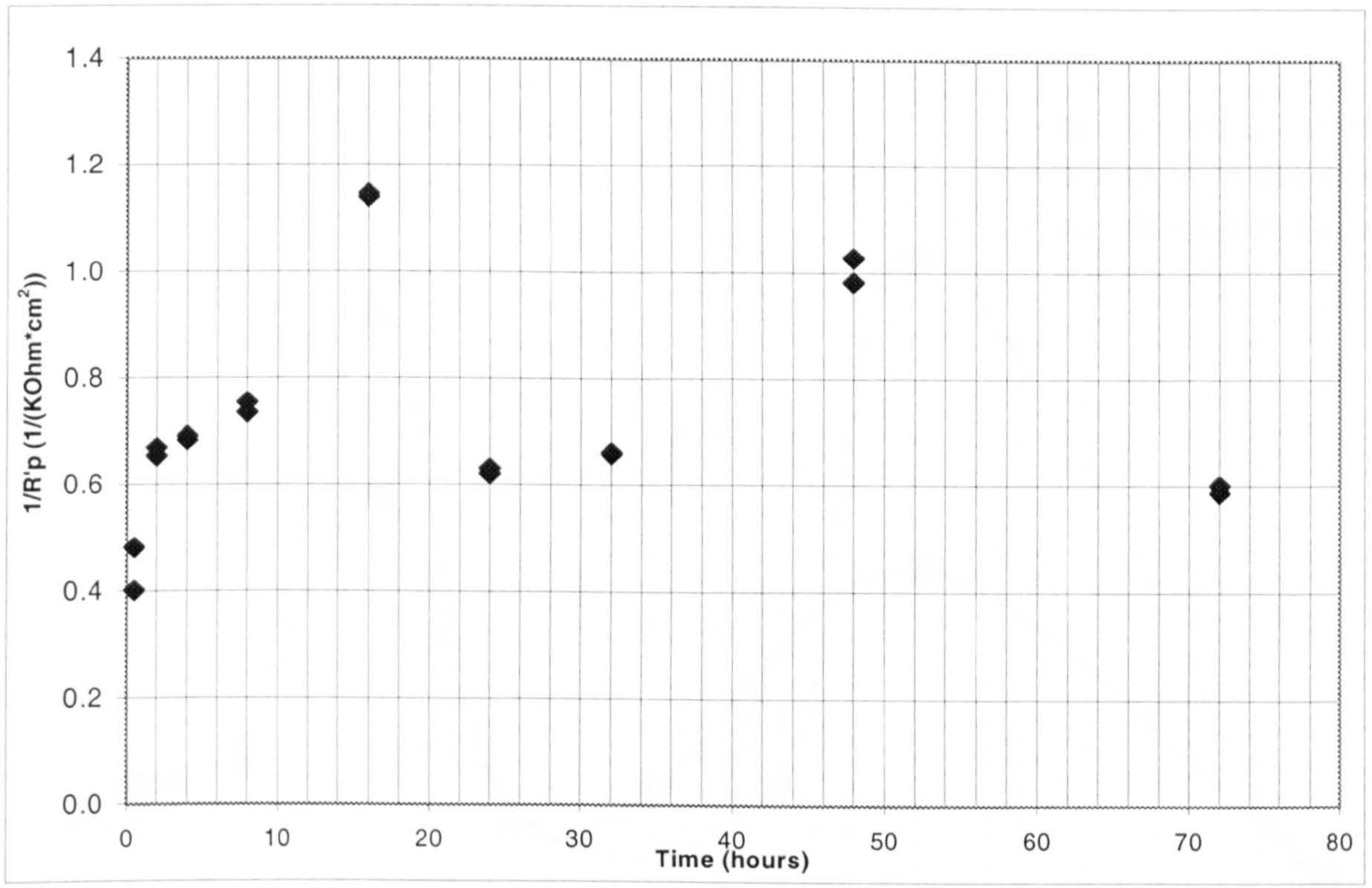

Figure 8.3a. $1/R_p'$ values vs. Time curve for the *central* region of a concentric specimen of Cu-10%Ni under impingement velocity of 17 m/s.

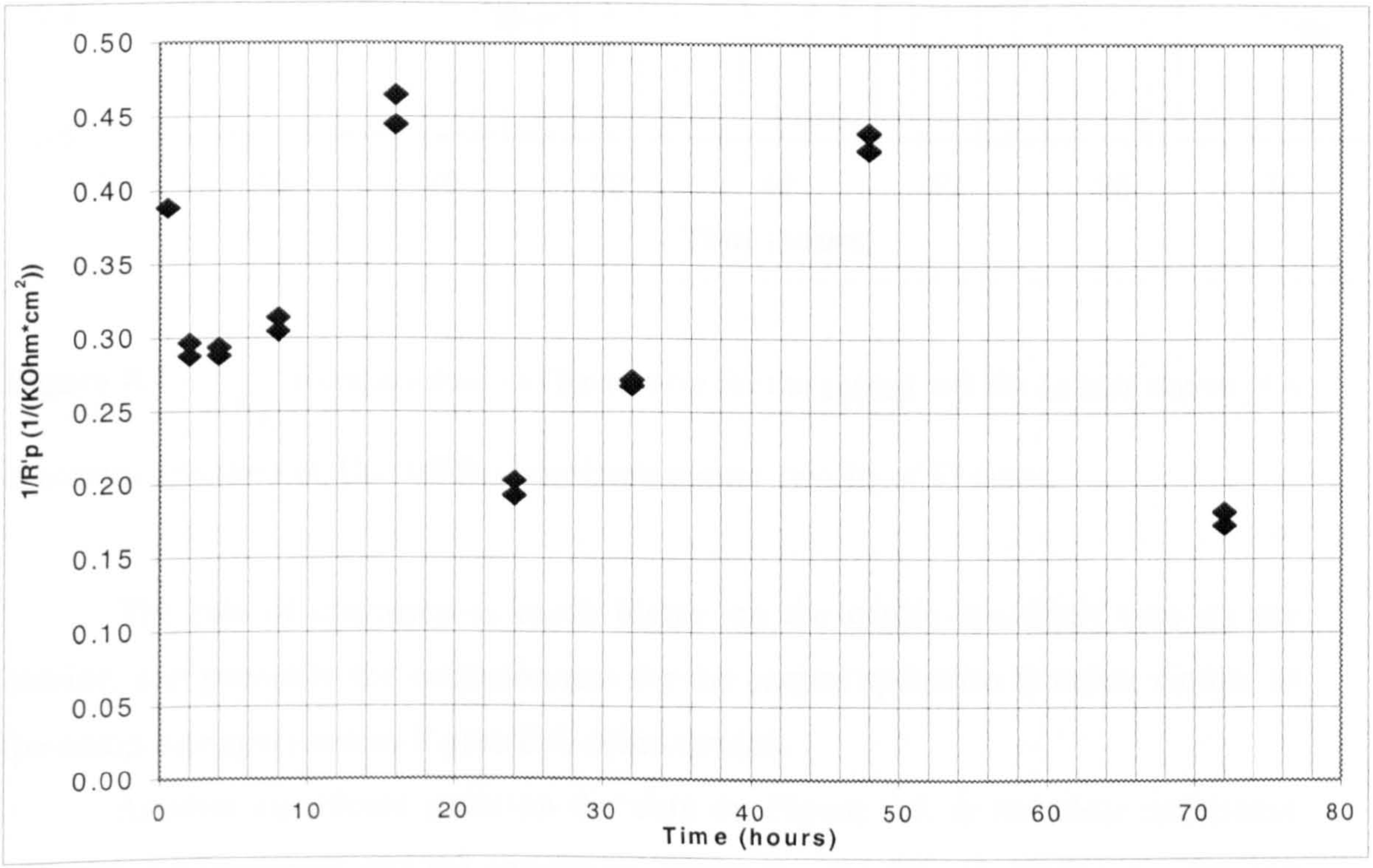

Figure 8.3b. $1/R_p'$ values vs. Time curve for the *outside* region of a concentric specimen of Cu-10%Ni under impingement velocity of 17 m/s.

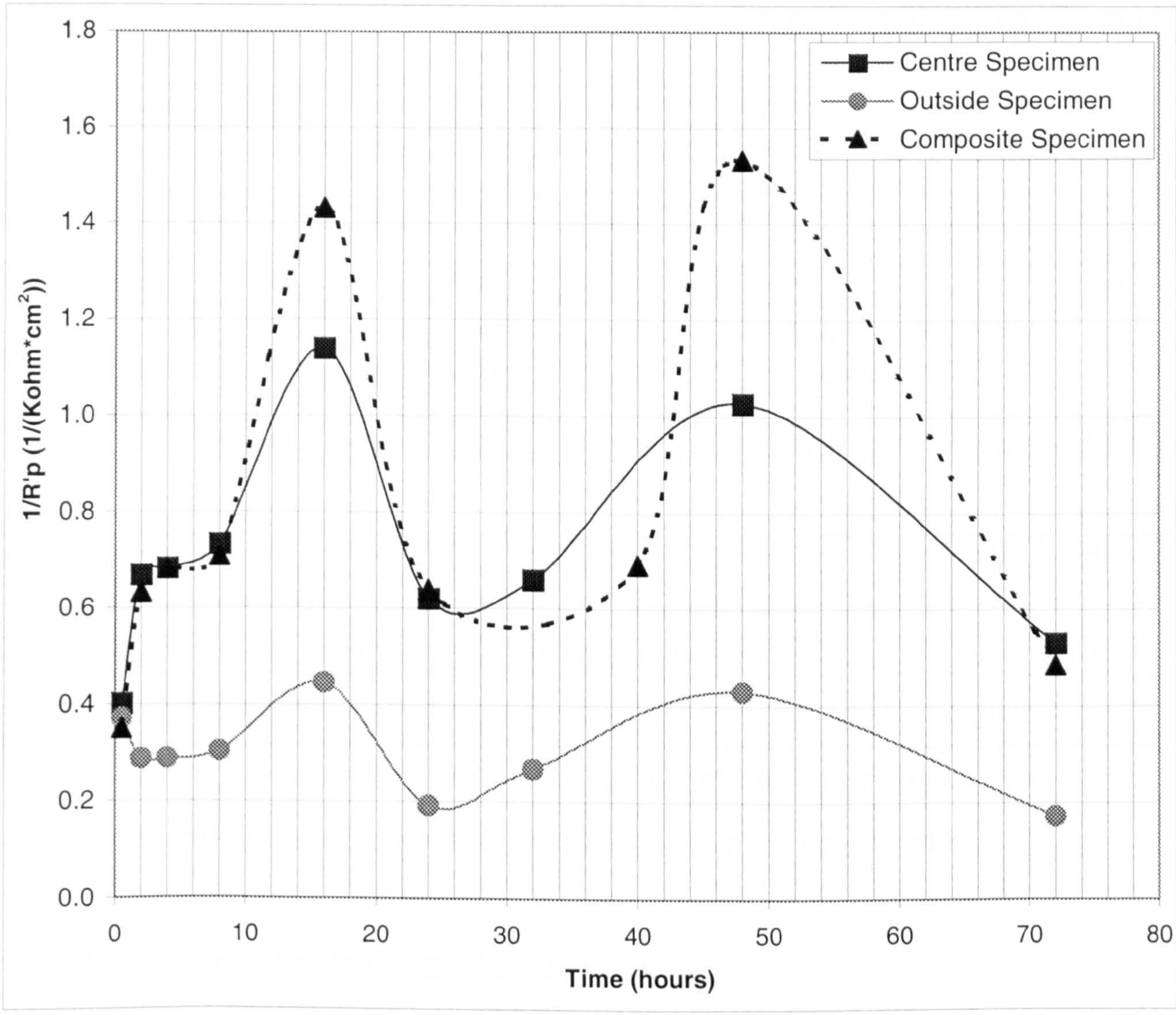

Figure 8.4. $1/R_p'$ average values vs. Time curve for the *central* and the *outside* region of a concentric specimen of Cu-10%Ni under impingement velocity of 17 m/sec.

The rate of corrosion is much higher on the centre specimen than on the outside, and generally the corrosion rate for the central specimen is rather similar to the composite specimen as Figure 8.4. demonstrates.

Another significant point on the data on Figure 8.4. is the clear agreement between the concentric and the composite specimen, (the data of which was obtained at an earlier stage in the experimental programme), in terms of the complex time dependencies.

Time	*30 mins*	*2 hours*	*4 hours*	*8 hours*	*16 hours*	*24 hours*	*32 hours*	*48 hours*	*72 hours*
$R_p^{'}$ *(Kohm*cm²)*									
Composite specimen – Average	2.849	1.576	1.460	1.410	0.698	1.563		0.652	2.059
Centre – Average	2.489	1.494	1.464	1.361	0.878	1.611	1.514	0.974	1.883
Outside – Average	2.696	3.477	3.472	3.280	2.248	5.189	3.738	2.334	5.794

Table 8.1. $R_p^{'}$ average values for both the *central* and the *outside* region of Cu-10%Ni, for different time exposures, for an increase by 22mV to the value of E_{corr}.

Time	*30 mins*	*2 hours*	*4 hours*	*8 hours*	*16 hours*	*24 hours*	*32 hours*	*48 hours*	*72 hours*
$1/R_p^{'}$ *(1/(Kohm*cm²))*									
Composite specimen – Average	0.351	0.634	0.684	0.709	1.432	0.639		1.533	0.485
Centre – Average	0.402	0.669	0.683	0.735	1.139	0.621	0.661	1.027	0.531
Outside – Average	0.371	0.288	0.288	0.305	0.445	0.193	0.268	0.428	0.173

Table 8.2. $1/R_p^{'}$ average values for both the *central* and the *outside* region of Cu-10%Ni, for different time exposures, for an increase by 22mV to the value of E_{corr}.

8.1.1.2. Full Anodic Polarisation scans.

In addition to the "linear polarisation-type" tests, separate experiments were performed, again using the 1mm nozzle and 17m/s, in which full anodic polarisation scans were undertaking after 48 and 72 hours.

Figure 8.5a-b. show the resulting typical anodic polarisation curves for the central and the outer specimens, respectively. The corrosion rates exhibited a decrease at 72 hours compared to 48 hours and this is in agreement with the trend for 48 and 72 hours shown by the linear polarisation-type tests. Moreover, (and again in agreement with the linear polarisation type tests), the values of i_{corr}, (Table 8.3.), are greater for the central specimen.

Table 8.3. also shows that the instantaneous direct corrosion rates, calculated applying the Faraday's Law to the i_{corr} values, decrease by exposure time, for the central, the outside region and the composite specimen, (from Table 6.14).

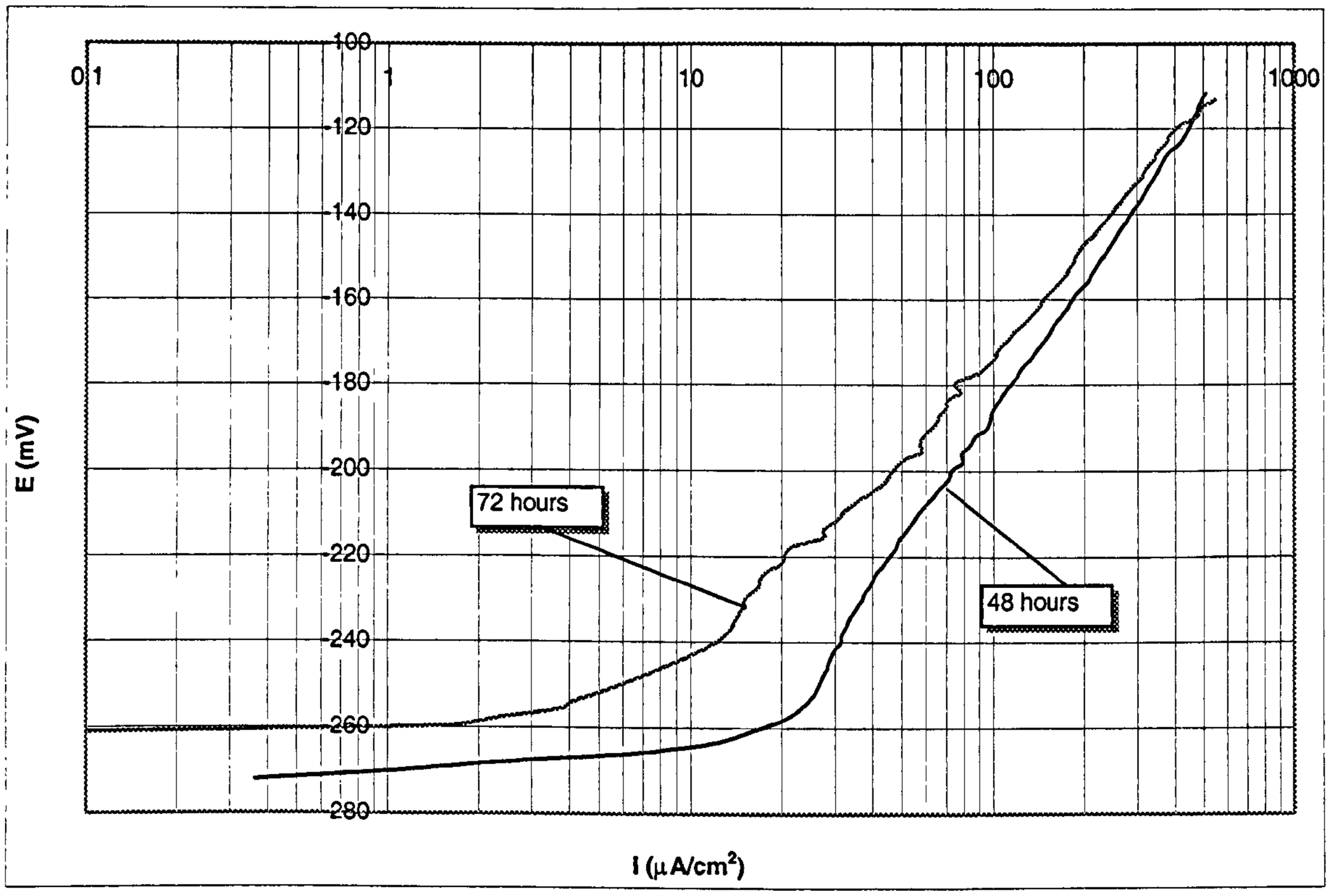

Figure 8.5a. Anodic polarisation curves of the *central* region of a concentric specimen Cu-10%Ni upon exposures of 48 and 72 hours under impingement velocity of 17m/s.

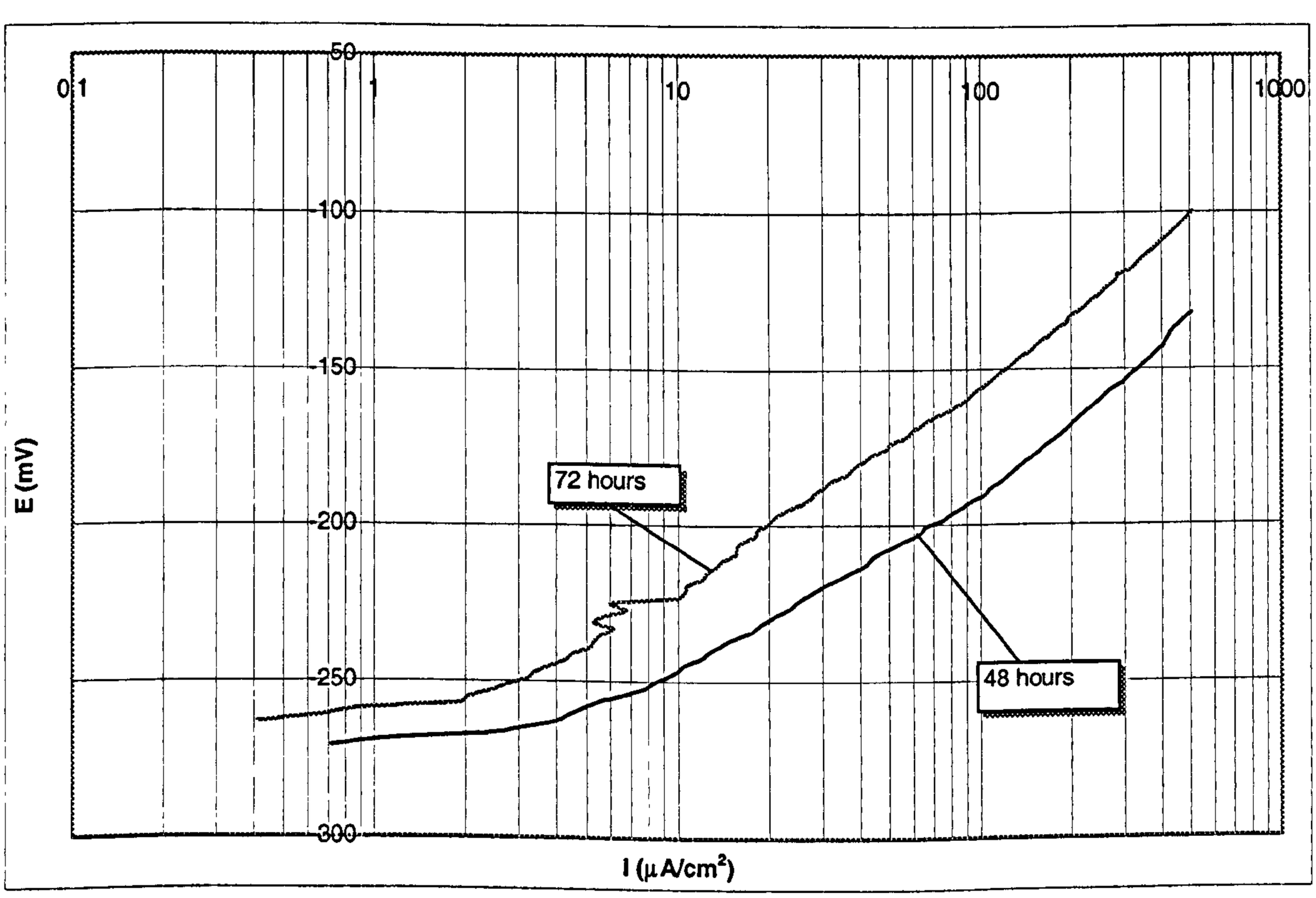

Figure 8.5b. Anodic polarisation curves of the *outside* region of a concentric specimen Cu-10%Ni upon exposures of 48 and 72 hours under impingement velocity of 17m/s.

Exposure time	*48 hours*			*72 hours*		
Specimen	*Centre*	*Outside*	*Composite*	Centre	Outside	*Composite*
Corrosion Current Density ($\mu A/cm^2$)	16 , 17	9 , 11	16 , 19	13 , 14	5 , 7	14.5 , 13.5
Corrosion Current Density – Average ($\mu A/cm^2$)	16.5	10	17.5	13.5	6	14
Instantaneous Direct Corrosion Weight Losses – Average (mg/h)	0.004	0.047	0.082	0.003	0.023	0.066

Table 8.3. Instantaneous weight loss values due to the direct corrosion component for the central, the outside and the composite specimen of Cu-10%Ni.

8.1.1.3. Galvanic Measurements.

In another set of experiments, the galvanic interactions between the outer and the central specimens were investigated. This involved measuring the electrode potentials, (with the same reference electrode), of the separate specimens at various times followed by making a temporary electrical connection between the two specimens and measuring the galvanic current flow between them. Table 8.4. shows which area of the concentric specimen was more electronegative, (i.e. the anode), the potential difference between the two areas, and the measured galvanic current passing from the anode to the cathode.

Evidently the area which acts as anode was the outside area, and through the whole process very small galvanic effects are measured. It is clear that there is a very small driving force of a few mV for galvanic corrosion. The galvanic currents displayed a generally increasing trend with time, for the first 16 hours, as did the $1/R_p$ values of the centre specimens. After this time period, the galvanic corrosion exhibited a gradual decline to extremely low values for the rest of the 72 hours test period.

Exposure Time	*30 mins*	*2 hours*	*4 hours*	*8 hours*	*16 hours*	*24 hours*	*32 hours*	*48 hours*	*72 hours*
ANODE	Outside	Outside	Outside	Outside	Outside	Outside	Outside	Outside	Outside
Potential Difference (mV)	4 ,6	8 , 9	7 , 8	5 , 5	4 , 4	3 , 4	4 ,4	4 ,4	4 ,4
Potential Difference – Average (mV)	5	8.5	7.5	5	4	3.5	4	4	4
Current passing From Anode to Cathode (μA)	0.2 , 0.3	0.7 , 0.8	0.8, 1	1.0 , 1.2	1.1 , 1.4	0.7 , 0.9	0.2 , 0.2	0.2 , 0.2	0.1 , 0.1
Current passing From Anode to Cathode (μA) – Average	0.25	0.75	0.9	1.1	1.25	0.8	0.2	0.2	0.1

Table 8.4. Electrochemical behaviour, potential difference, and galvanic current between the two areas on the concentric specimen of Cu-10%Ni.

8.1.2. Concentric specimens of Marinel.

8.1.2.1. Effect of time on erosion-corrosion processes for concentric specimens of Marinel.

The same techniques were employed as for the analogous study on Cu-10%Ni, i.e. experiments involved two separate specimens. One, 6mm diameter directly under the jet and the other, 8mm internal diameter, 25mm external diameter, separated by insulating resin. The respective areas were $0.28cm^2$ and $4.4cm^2$. These were subjected to a jet using a nozzle diameter of 1mm, at a velocity of 17m/s, at a temperature of 19±2°C.

8.1.2.1.1. <u>Linear polarisation type tests.</u>

One set of experiments involved a series of linear polarisation type monitoring exercises, undertaking at times of 30mins, 2, 4, 24, 48 and 72 hours under the impinging jet.

Figure 8.6a-b show the typical anodic polarisation curves for the central and the outer specimen respectively.

Table 8.5. and Table 8.6. show the values of $R_p^{'}$ and $1/R_p^{'}$ calculated from the gradient of the graphs on Figure 8.6a-b. The tables also include the analogous values for the composite specimen, (from Table 6.26.) for comparison purposes.

Figure 8.7a. and Figure 8.7b. present the $1/R_p^{'}$ versus time plots for the concentric samples and Figure 8.8. presents the $1/R_p^{'}$ average values versus time plots for the concentric samples. The time dependence of corrosion rate follows a huge increase for the first 2 hours, with a gratual decrease for the next 46 hours. Afterwards, a significant increase to the direct corrosion weight loss is detected.

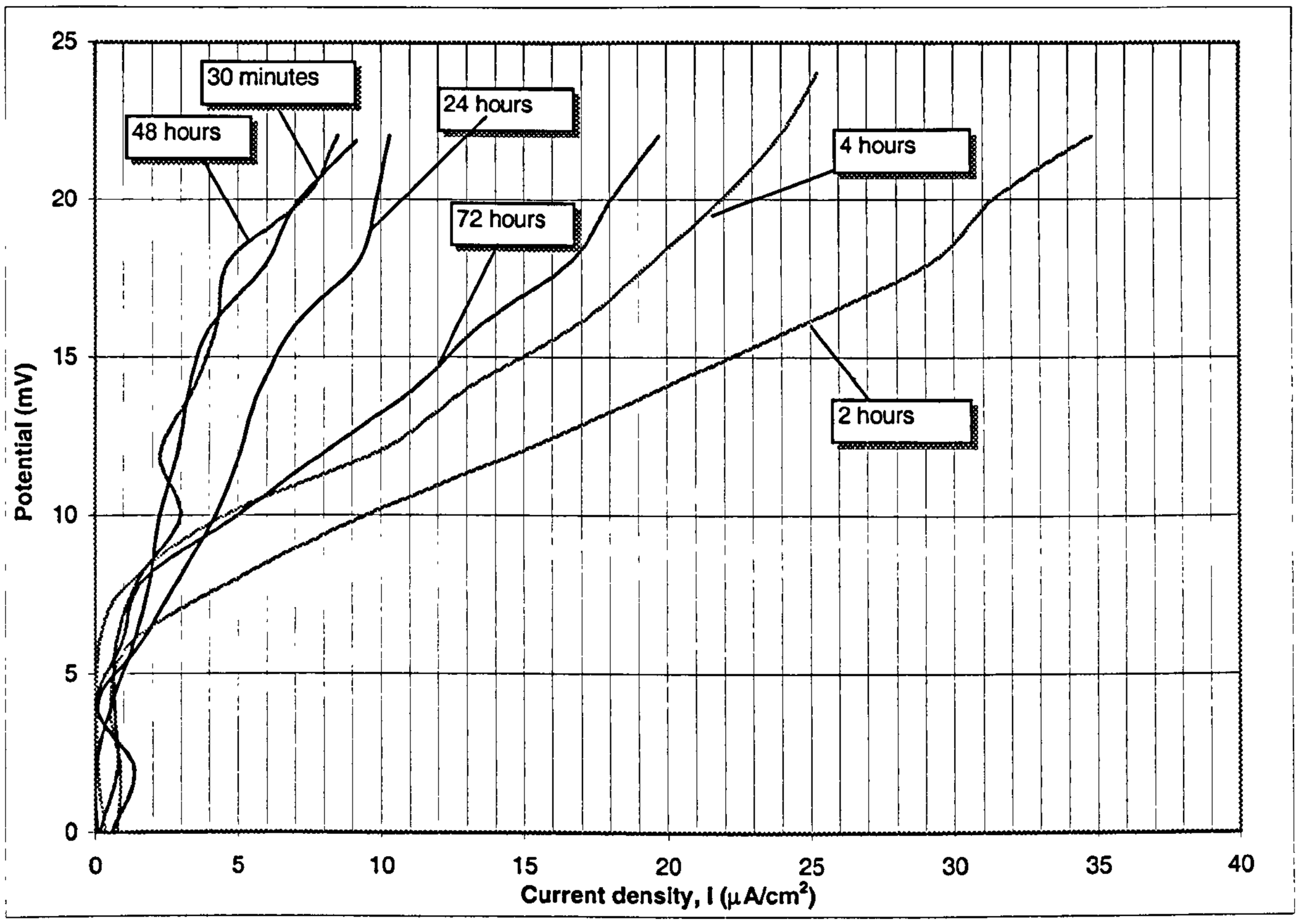

Figure 8.6a. Anodic polarisation curves of the *central* region of a concentric specimen of Marinel, for an increase by 22mV to the value of E_{corr}, upon exposures of 30 mins, 2, 4, 24, 48 and 72 hours under impingement velocity of 17 m/s.

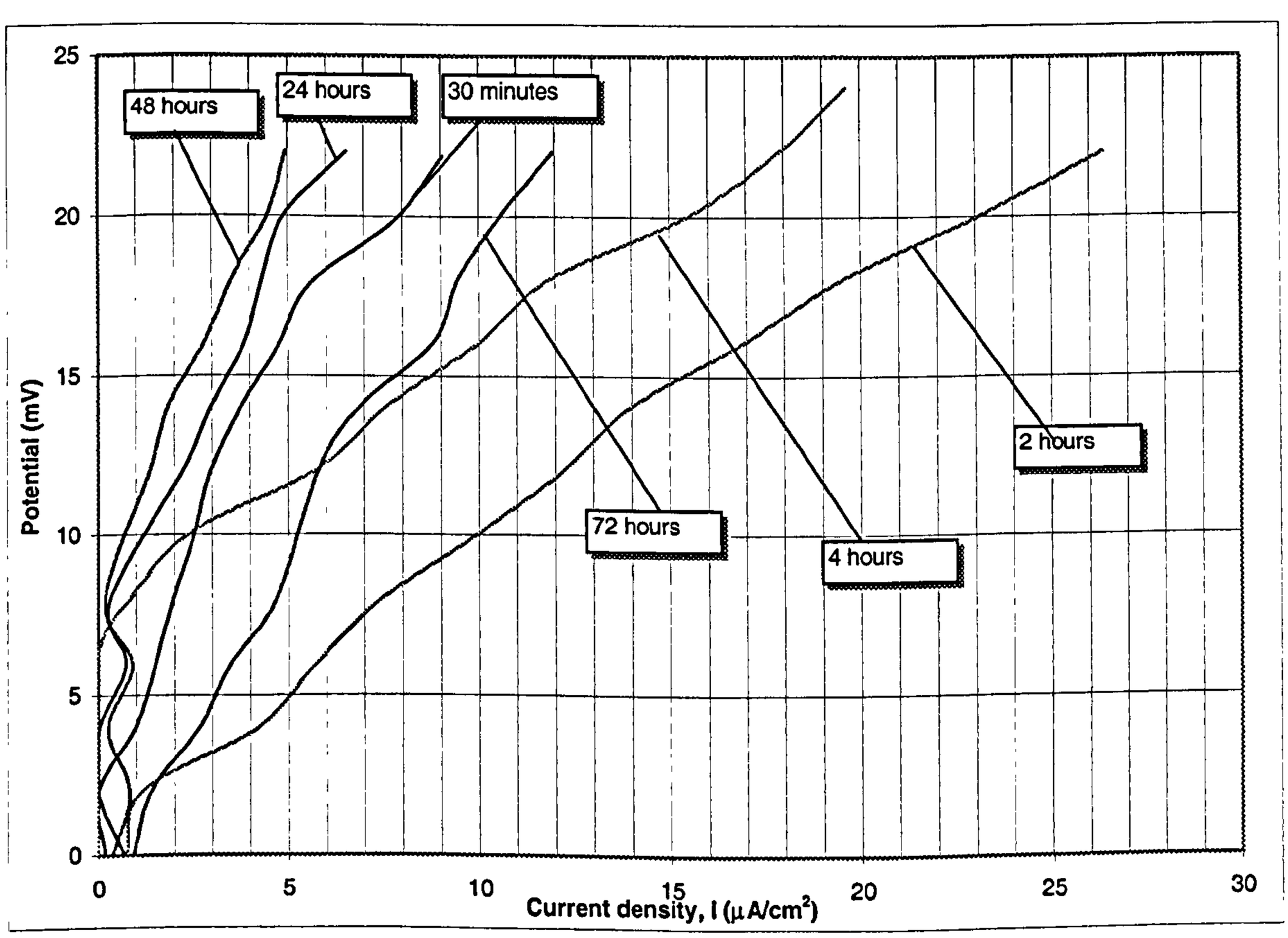

Figure 8.6b. Anodic polarisation curves of the *outside* region of a concentric specimen of Marinel, for an increase by 22mV to the value of E_{corr}, upon exposures of 2, 4, 24, 48 and 72 hours under impingement velocity of 17 m/s.

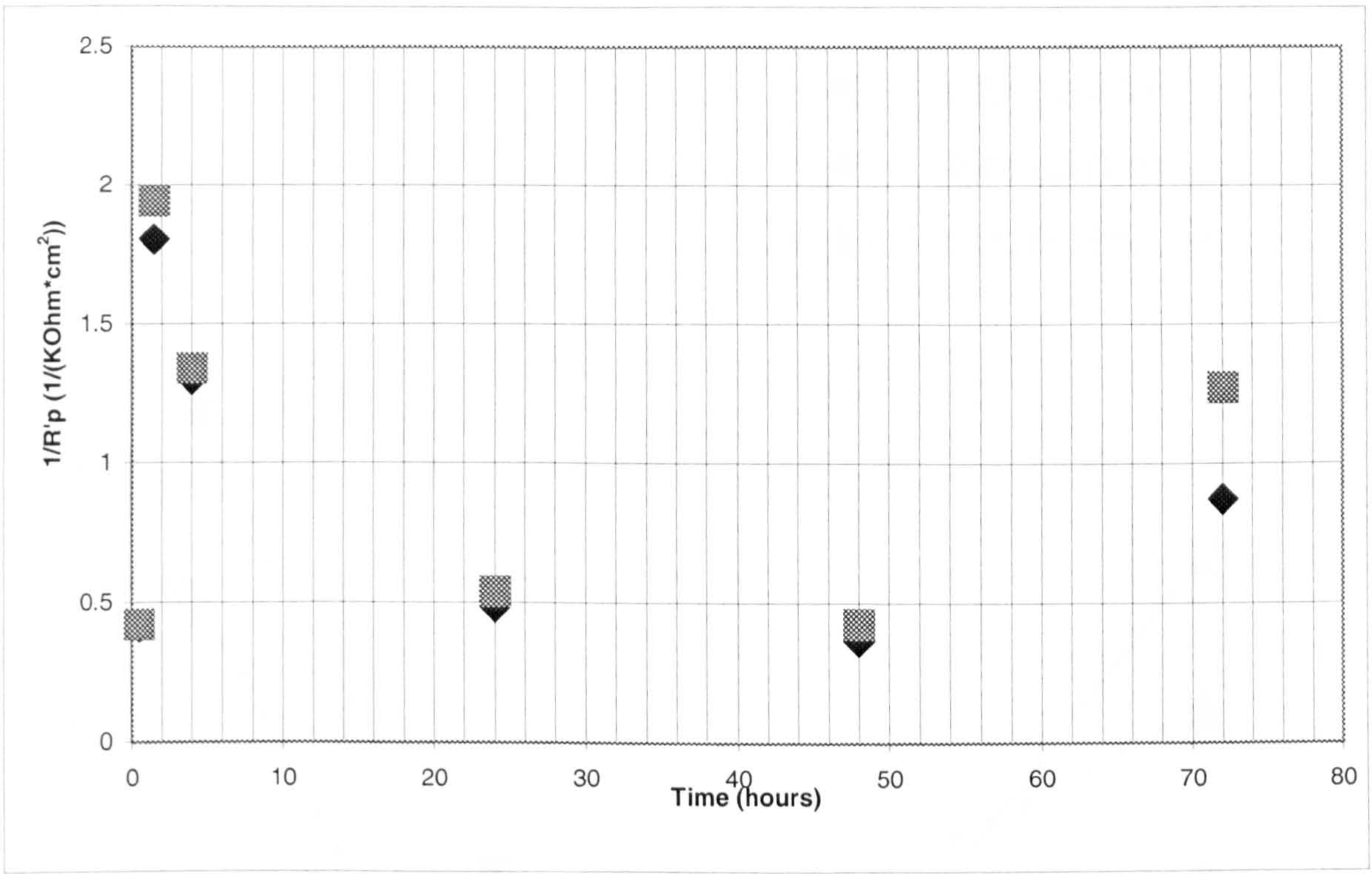

Figure 8.7a. $1/R_p$ values vs. Time curve for the *central* region of a concentric specimen of Marinel under impingement velocity of 17 m/s.

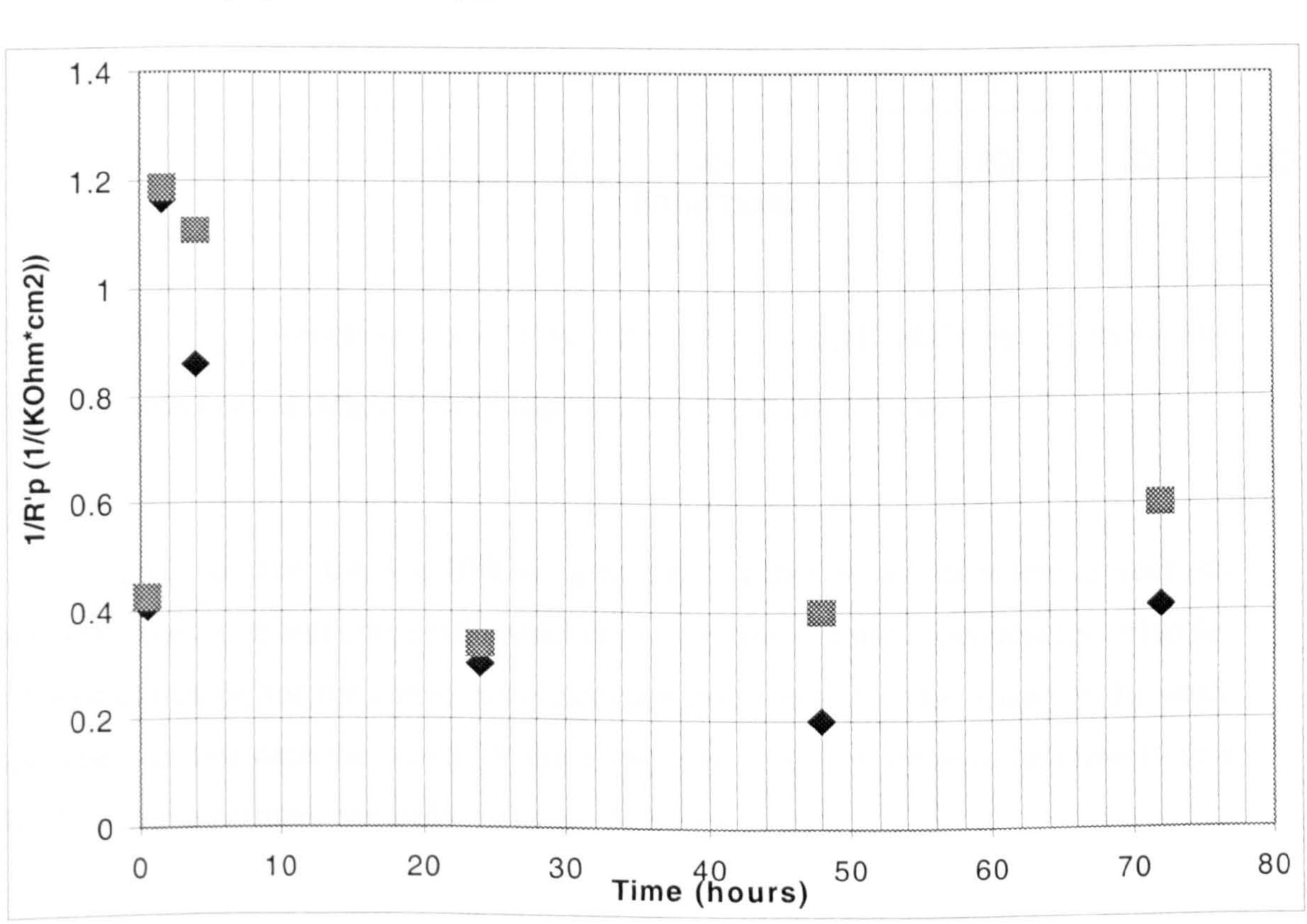

Figure 8.7b. $1/R_p$ values vs. Time curve for the *outside* region of a concentric specimen of Marinel under impingement velocity of 17 m/s.

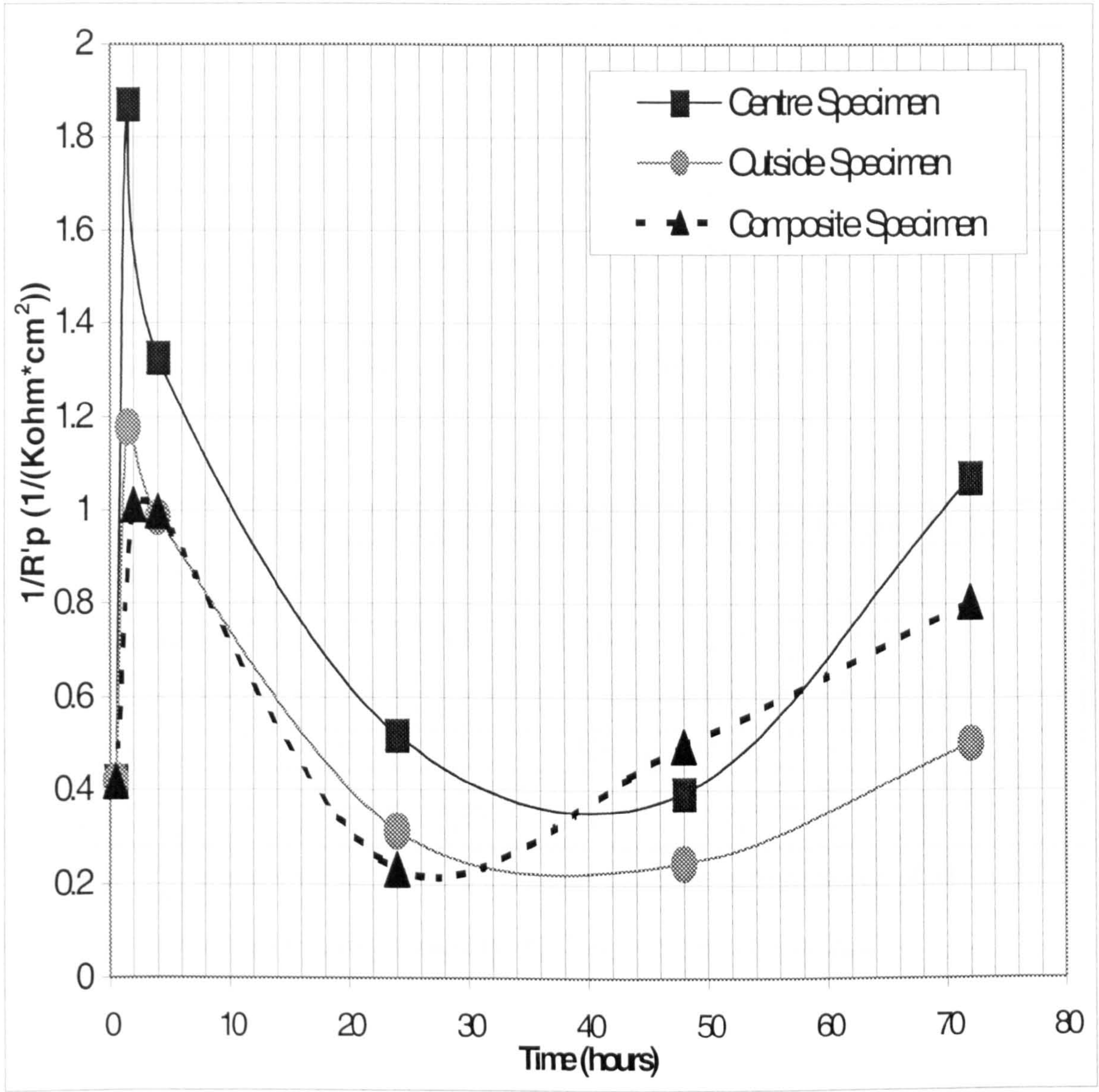

Figure 8.8. $1/R_p'$ average values vs. Time curve for the *central* and the *outside* region of a concentric specimen of Marinel under impingement velocity of 17 m/sec.

Again as for the Cu-10%Ni specimens, there is an excellent agreement between composite and concentric specimens, in terms of time dependencies. Also the rates of corrosion for the centre specimens are consistently higher than for the outer specimen. In this case the curve for the composite specimen tends to be close to that for the outer specimen, certainly up to the 24 hours.

Time	*30 mins*	*2 hours*	*4 hours*	*24 hours*	*48 hours*	*72 hours*
$R_p^{'}$ *(Kohm*cm²)*						
Composite specimen – Average	2.395	0.989	1.001	4.310	2.020	1.243
Centre – Average	2.382	0.534	0.754	1.929	2.538	0.932
Outside – Average	2.384	0.849	1.015	3.18	4.05	1.993

Table 8.5. $R_p^{'}$ average values for both the *central* and the *outside* region of Marinel, for different time exposures, for an increase by 22mV to the value of E_{corr}.

Time	*30 mins*	*2 hours*	*4 hours*	*24 hours*	*48 hours*	*72 hours*
$1/R_p^{'}$ *(1/(KOhm*cm²))*						
Composite specimen – Average	0.417	1.012	0.999	0.232	0.495	0.804
Centre – Average	0.419	1.872	1.326	0.518	0.394	1.072
Outside – Average	0.419	1.177	0.985	0.314	0.246	0.501

Table 8.6. $1/R_p^{'}$ average values for both the *central* and the *outside* region of Marinel, for different time exposures, for an increase by 22mV to the value of E_{corr}.

8.1.2.1.2. Full Anodic Polarisaton scans.

In addition to the "linear polarisation-type" tests, separate experiments were performed, again using the 1mm nozzle and 17m/s, in which full anodic polarisation scans were undertaking after 48 and 72 hours.

Figure 8.9a-b. show the resulting typical anodic polarisation curves for the central and the outer specimens, respectively. This is in agreement with the trend for 48 and 72 hours shown by the linear polarisation-type tests. Moreover, (and again in agreement with the linear polarisation type tests), the values of i_{corr}, (Table 8.7.), are greater for the central specimen.

Table 8.7. also shows that the instantaneous direct corrosion rates, calculated applying the Faraday's Law to the i_{corr} values, increase by exposure time, for the central, the outside region and the composite specimen, (from Table 6.24.).

Exposure time	*48 hours*			*72 hours*		
Specimen	*Centre*	*Outside*	*Composite*	Centre	Outside	*Composite*
Corrosion Current Density ($\mu A/cm^2$)	9 , 10	5 , 6	6.3 , 5.5	12 , 13	8 , 9	10 , 10
Corrosion Current Density – Average ($\mu A/cm^2$)	9.5	5.5	5.9	13.0	8.5	10.0
Instantaneous Direct Corrosion Weight Losses – Average (mg/h)	0.003	0.027	0.033	0.004	0.042	0.056

Table 8.7. Instantaneous weight loss values due to the direct corrosion component for the central, the outside and the composite specimen of Marinel.

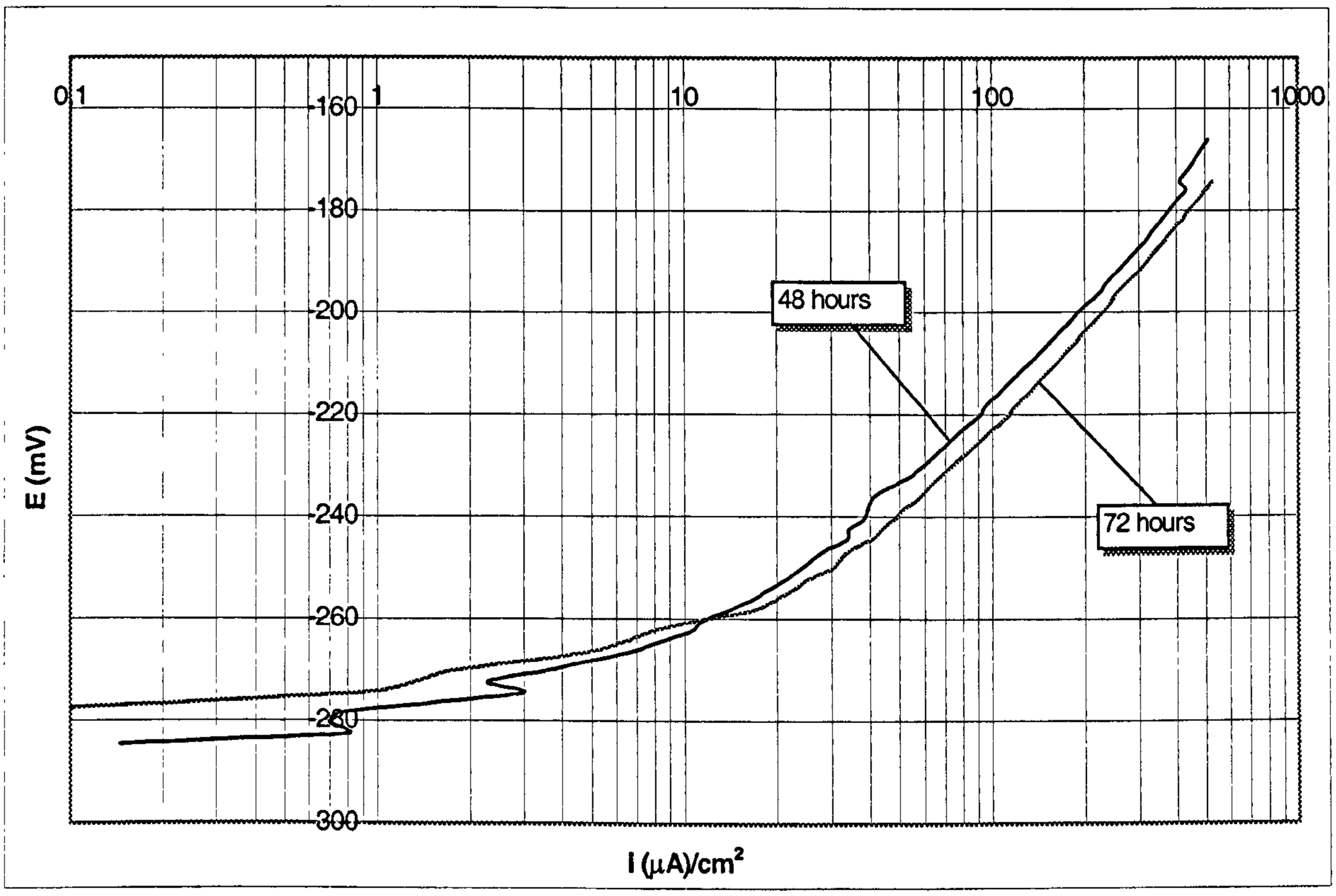

Figure 8.9a. Anodic polarisation curves of the *central* region of a concentric specimen Marinel upon exposures of 48 and 72 hours under impingement velocity of 17m/s.

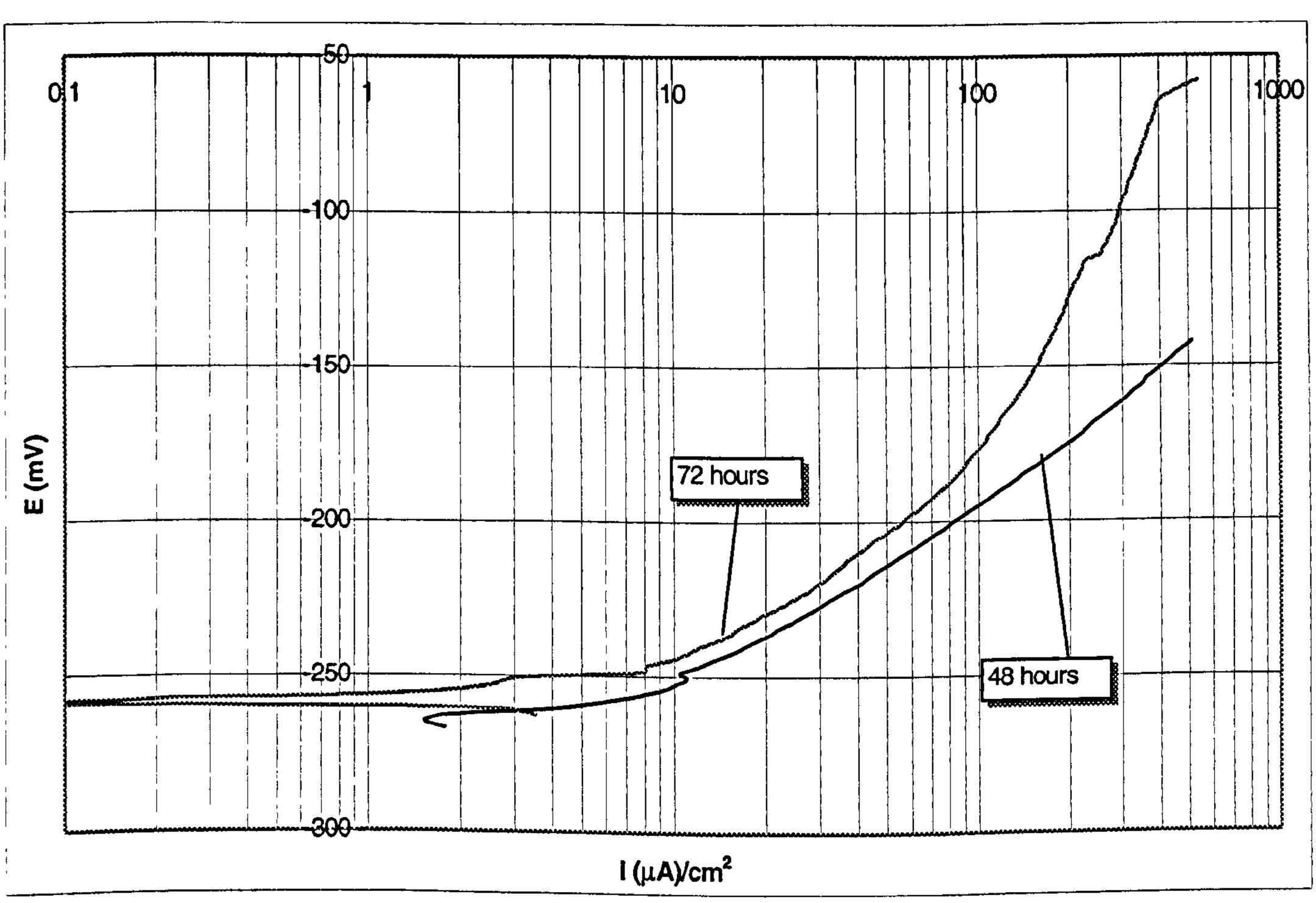

Figure 8.9b. Anodic polarisation curves of the *outside* region of a concentric specimen Marinel upon exposures of 48 and 72 hours under impingement velocity of 17m/s.

8.1.2.1.3. Galvanic Measurements.

A study of the galvanic interactions between the outer and the central specimens, following the same techniques like for Cu-10%Ni, was also undertaken.

Table 8.8. shows which area of the concentric specimen was more electronegative, (i.e. the anode), the potential difference between the two areas, and the measured galvanic current passing from the anode to the cathode.

According to the results the area which acts as an Anode, switches after the first 24 hours, from the outside to the centre specimen, and through the whole process very small galvanic currents are measured.

Exposure Time	*30 mins*	*2 hours*	*4 hours*	*24 hours*	*48 hours*	*72 hours*
ANODE	Outside	Outside	Outside	Equal	Centre	Centre
Potential Difference (mV)	2 , 4	5 , 9	6 , 8	0 , 1	1 , 1	7 , 11
Potential Difference – Average (mV)	3	7	7	0.5	1	9
Current passing From Anode to Cathode (μA)	1.0 , 1.2	1.3 , 1.5	1.3 , 1.4	0.1 , 0	0.1 , 0	1.4 , 1.4
Current passing From Anode to Cathode (μA) – Average	1.10	1.40	1.35	0.05	0.05	1.4

Table 8.8. Electrochemical behaviour, potential difference, and galvanic current between the two areas on the concentric specimen of Marinel.

In order to obtain more data to assist in the evaluation of trends in galvanic interactions between the outer and the central specimen, a series of linear polarisation type monitoring exercises was undertaken, with the jet impinging direct on the central specimen, but the outer specimen was placed well away from any direct influence from the impinging jet, (Figure 8.10.).

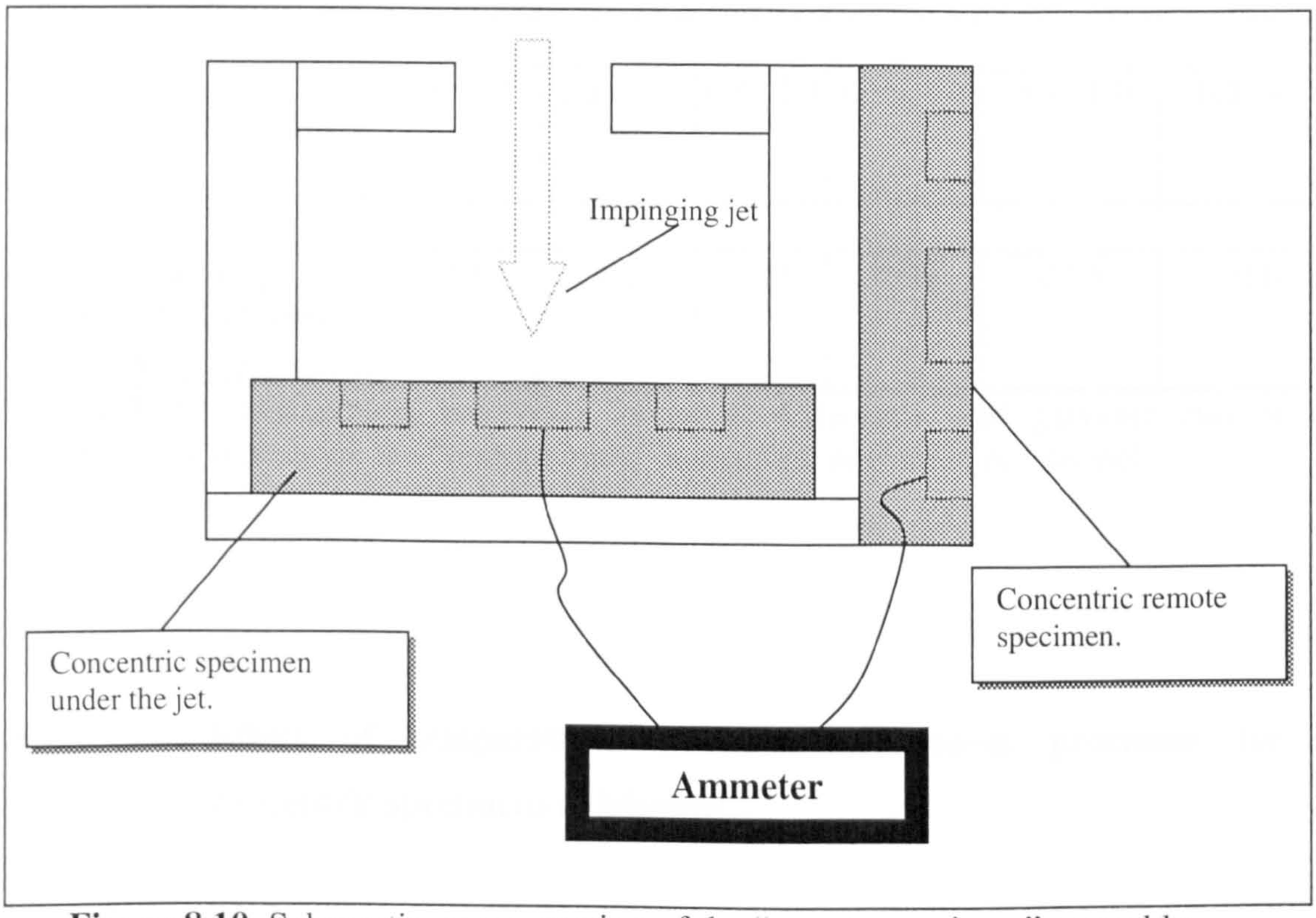

Figure 8.10. Schematic representation of the "remote specimen" assembly.

Table 8.9. shows which area of the "remote-outer" concentric specimen was more electronegative, (i.e. the anode), the potential difference between the two areas, and the measured galvanic current passing from the anode to the cathode.

The results in Table 8.9. are generally very similar to these in Table 8.8. with the exception that the switch of polarity between the remote outer specimen and the directly-impinged central specimen, appeared to be delayed to between 47→72 hours.

Exposure Time	*30 mins*	*2 hours*	*4 hours*	*24 hours*	*48 hours*	*72 hours*
ANODE	Remote Outer	Remote Outer	Remote Outer	Remote Outer	Remote Outer	Centre
Potential Difference (mV)	2 , 4	5 , 6	5 , 5	5 , 6	4 , 5	2 , 2
Potential Difference – Average (mV)	3	5.5	5	5.5	4.5	2
Current passing From Anode to Cathode (μA)	1.0 , 1.2	1.1 , 1.3	1.3 , 1.4	0.9 , 1.0	0.9 , 1.0	0.5 , 0.7
Current passing From Anode to Cathode (μA) – Average	1.10	1.2	1.35	0.95	0.95	0.6

Table 8.9. Electrochemical behaviour, potential difference, and galvanic current between the two areas on the "remote-outer" concentric specimen of Marinel.

8.1.2.2. Effect of temperature on erosion-corrosion processes for concentric specimens of Marinel.

These tests employed experiments involved a concentric specimen as described section 8.1.2.1. The specimen was subjected to a jet using a nozzle diameter of 1mm, at a velocity of 17m/s, at a temperature of 35±1°C.

8.1.2.2.1. Linear polarisation type tests.

Linear polarisation type monitoring exercises were undertaking at times of 30mins, 2, 4, 24 and 48 hours under the impinging jet.

Figure 8.11a-b shows the typical anodic polarisation curves for the central and the outer specimen respectively.

Table 8.10. and Table 8.11. show the values of $R_p^{'}$ and $1/R_p^{'}$ calculated from the gradient of the graphs on Figure 8.10a-b. The tables also include the analogous values for the composite specimen, (from Table 7.13a.) for comparison purposes.

Figure 8.12a. and Figure 8.12b. present the $1/R_p^{'}$ versus time plots for the concentric samples and Figure 8.13. presents the $1/R_p^{'}$ average values versus time plots for the concentric samples. The time dependence of corrosion rate decreases constantly for the exposure period of 48 hours, with the corrosion rates of all three specimens being generally very similar; the interesting exception to this occuring after 30 minutes of exposure, at which the corrosion rate on the central specimen is significanlty higher than on the outer specimen.

A study of the galvanic interactions between the outer and the central specimens was also undertaken.

Table 8.12. shows that the anode is always the central specimen. Although the potential differences were rather higher than in the analogous experiments at 19°C, the galvanic currents were tiny in the early hours of exposure and undetectable for exposure periods more that 24 hours.

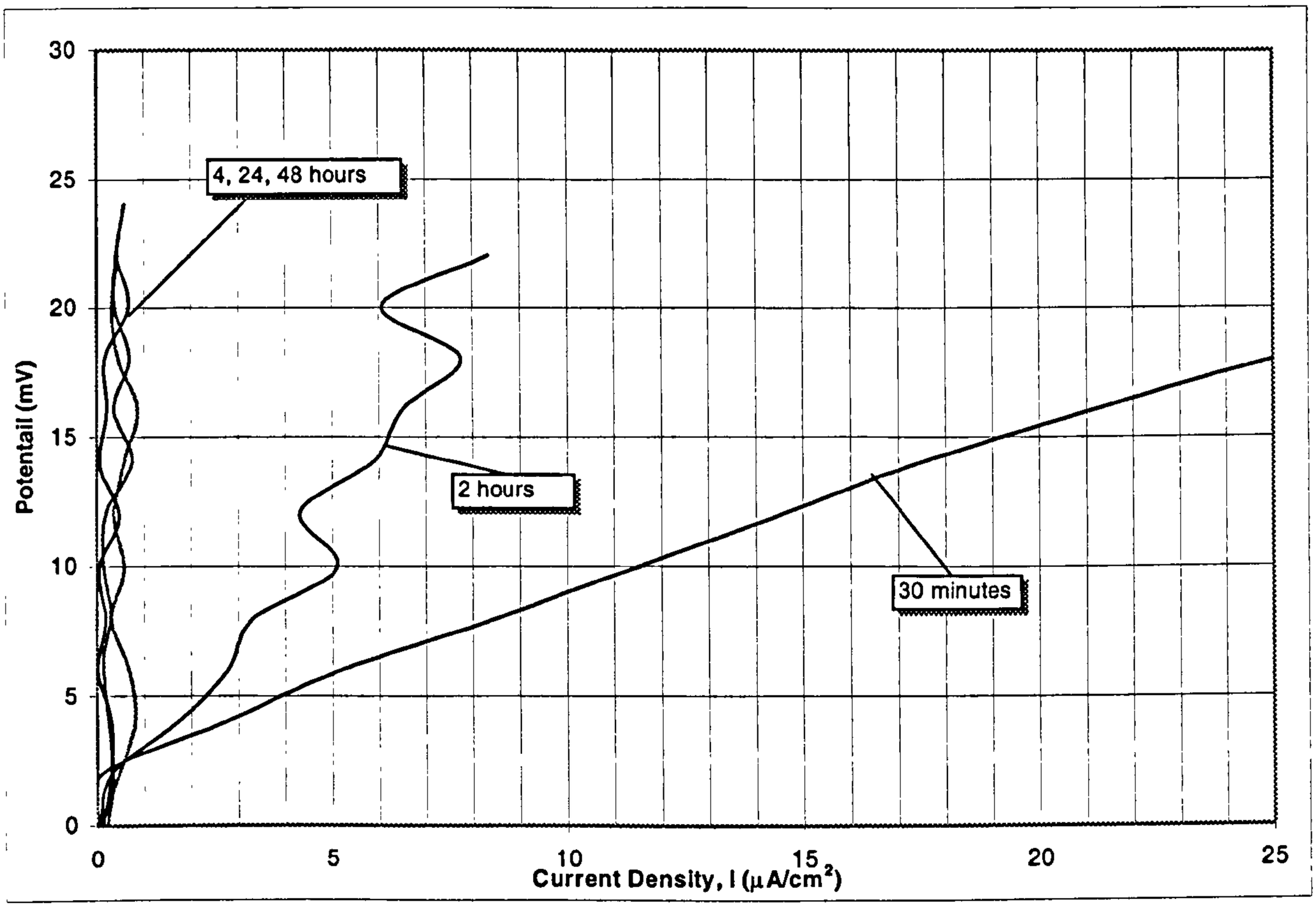

Figure 8.11a. Anodic polarisation curves of the *central* region of a concentric specimen of Marinel, for an increase by 22mV to the value of E_{corr}, upon exposures of 2, 4, 24 and 48 hours under impingement velocity of 17 m/s, at 35°C.

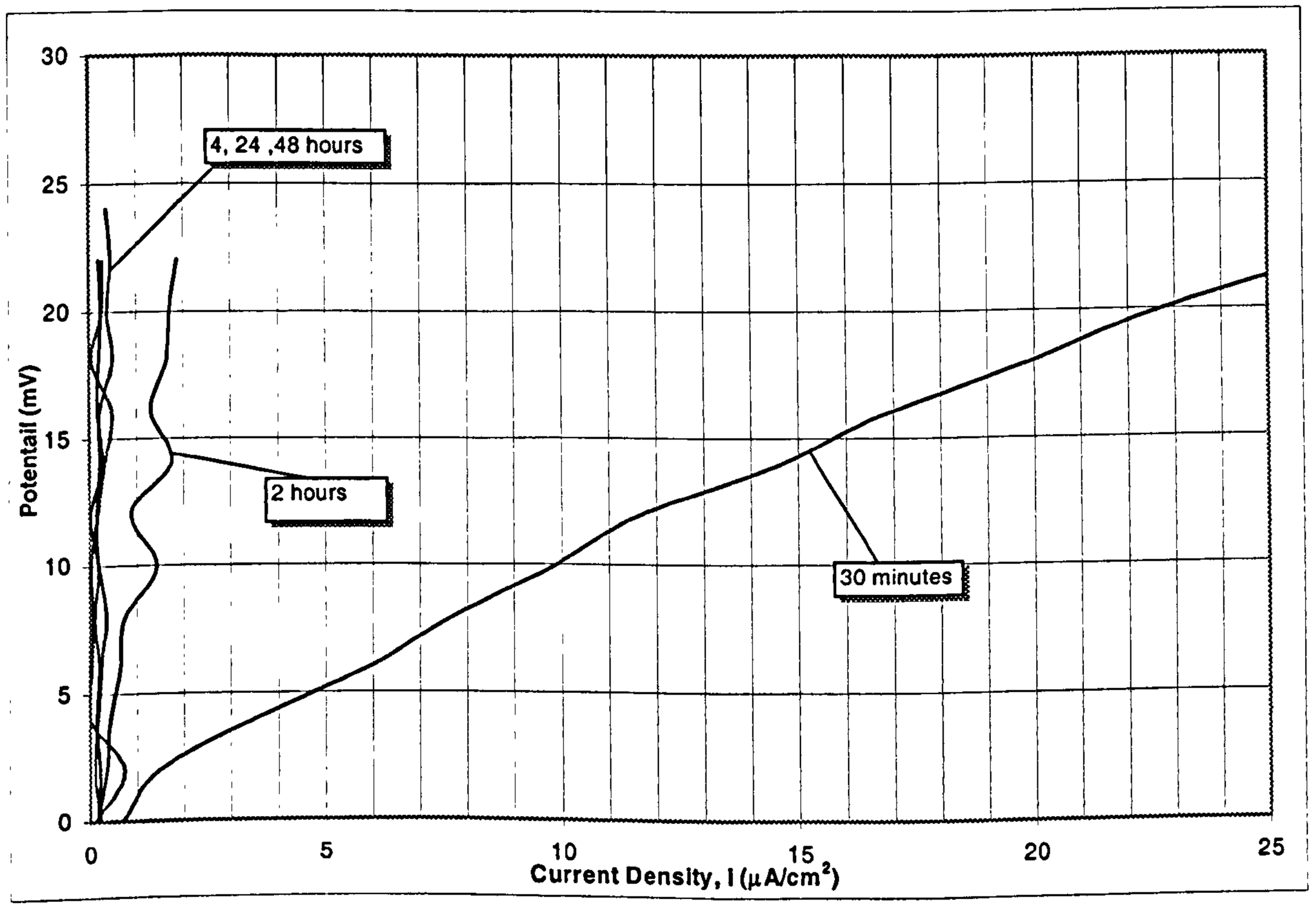

Figure 8.11b. Anodic polarisation curves of the *outside* region of a concentric specimen of Marinel, for an increase by 22mV to the value of E_{corr}, upon exposures of 2, 4, 24, 48 and 72 hours under impingement velocity of 17 m/s, at 35°C.

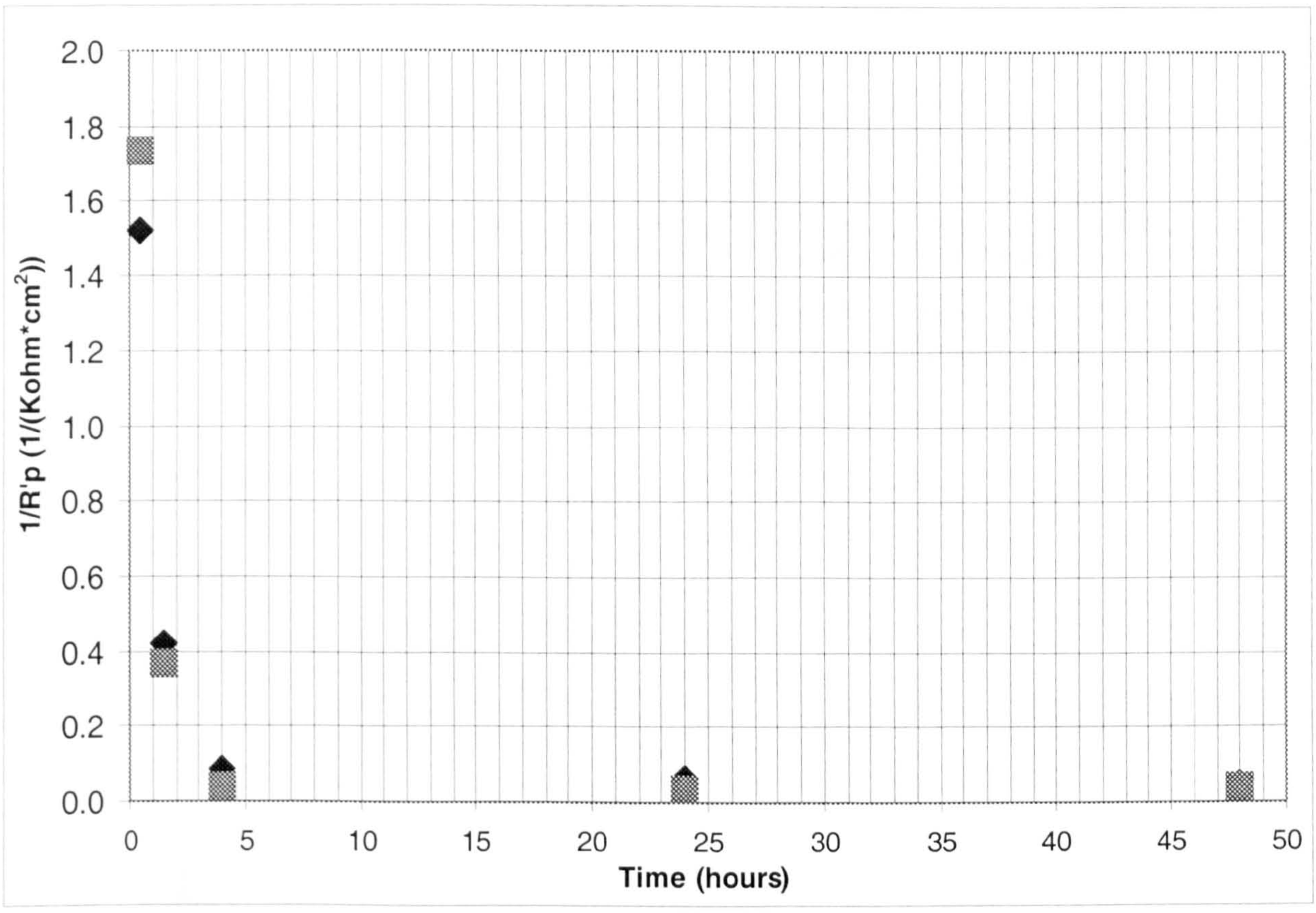

Figure 8.12a. $1/R_p'$ values vs. Time curve for the *central* region of a concentric specimen of Marinel under impingement velocity of 17 m/s, at 35°C.

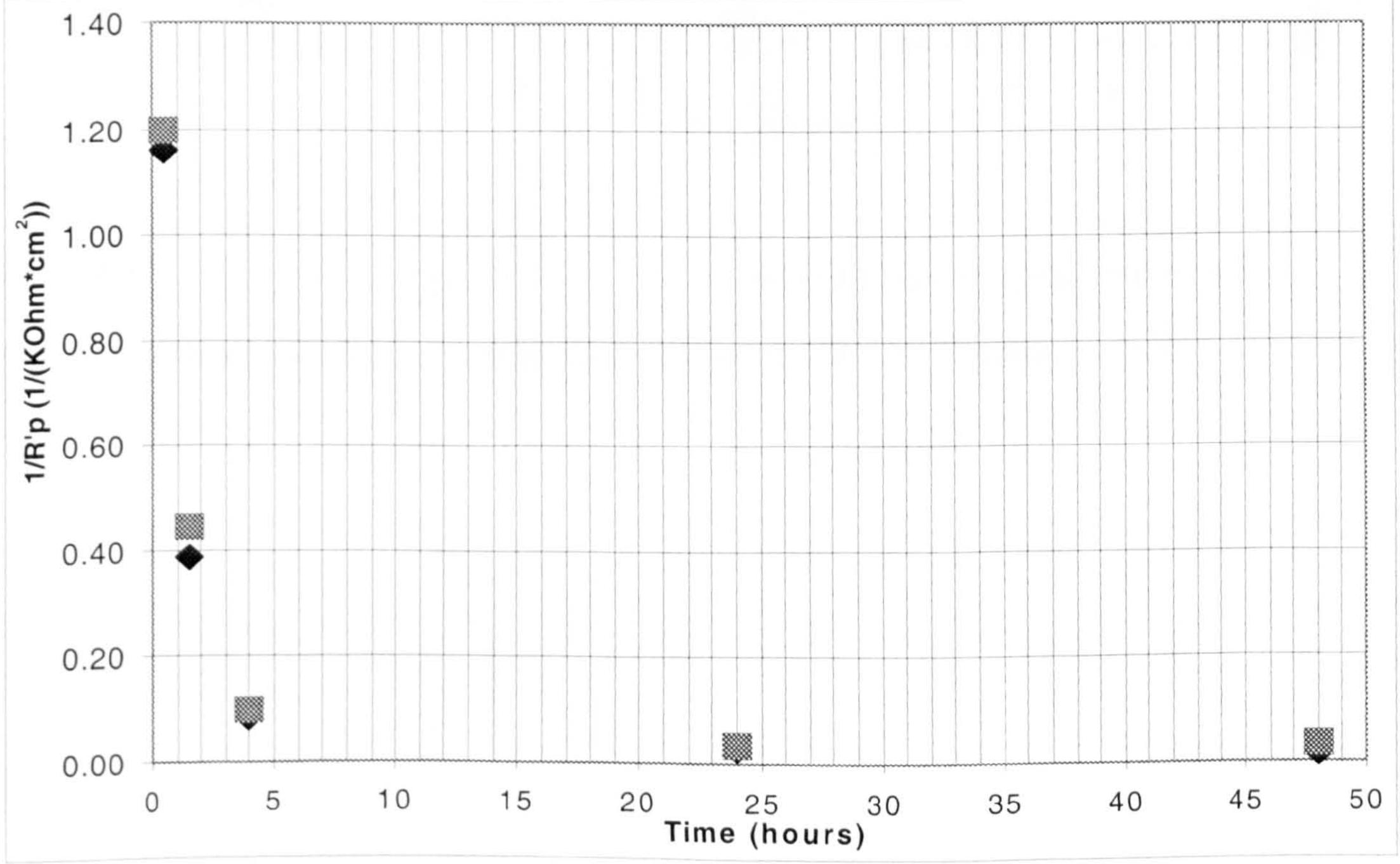

Figure 8.12b. $1/R_p'$ values vs. Time curve for the *outside* region of a concentric specimen of Marinel under impingement velocity of 17 m/s, at 35°C.

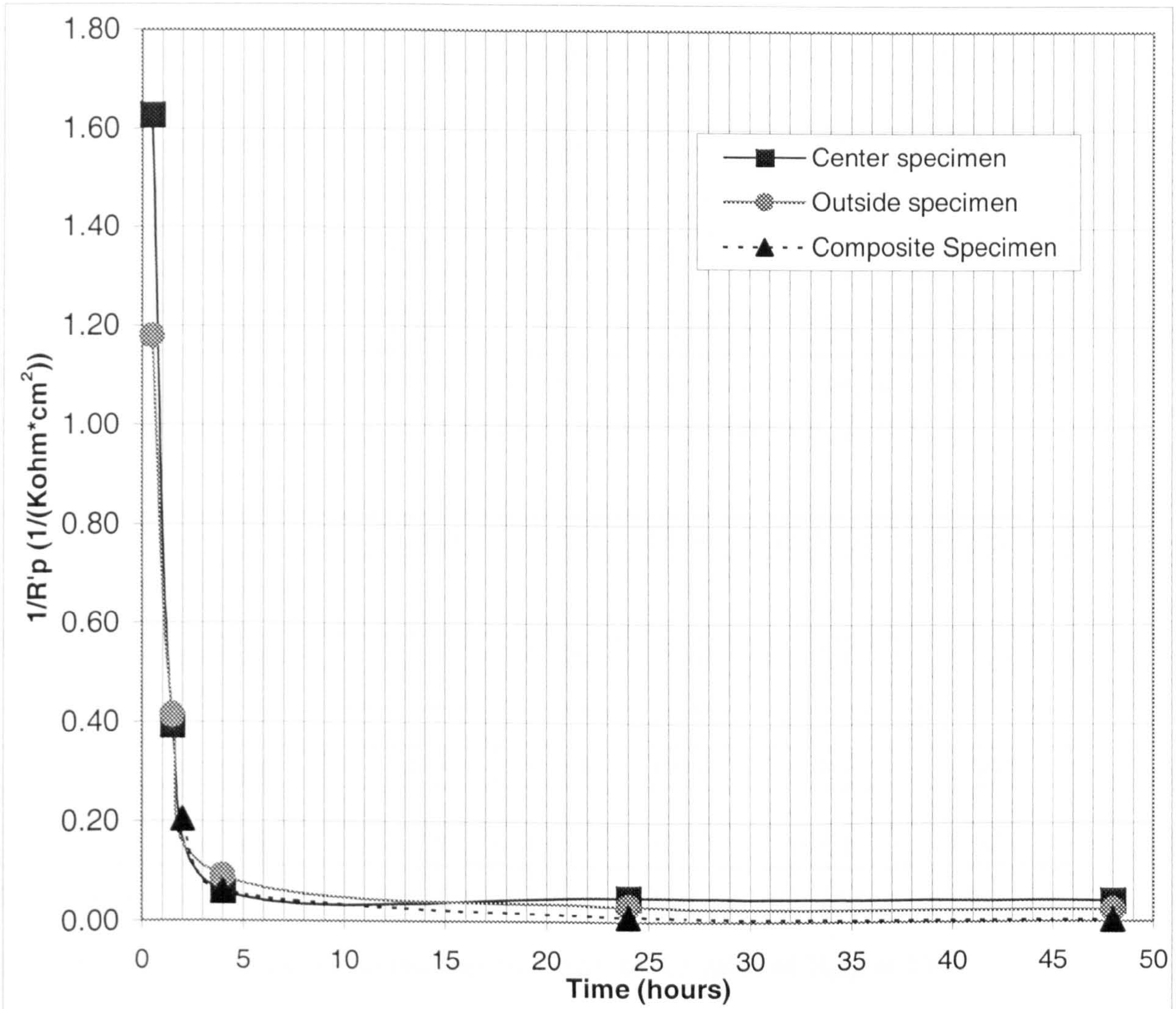

Figure 8.13. $1/R_p'$ average values vs. Time curve for the *central* and the *outside* region of a concentric specimen of Marinel under impingement velocity of 17 m/sec, at 35°C.

Time	*30 mins*	*2 hours*	*4 hours*	*24 hours*	*48 hours*
$R_p^{'}$ **(*Kohm*cm²*)**					
Composite specimen – Average		4.84	16.12	71.09	235.12
Centre – Average	0.61	2.54	16.43	20.45	23.26
Outside – Average	0.85	2.41	11.00	32.13	40.87

Table 8.10. $R_p^{'}$ average values for both the *central* and the *outside* region, for different time exposures, for an increase by 22mV to the value of E_{corr}, at 35°C.

Time	*30 mins*	*2 hours*	*4 hours*	*24 hours*	*48 hours*
$1/R_p^{'}$ **(*1/(KOhm*cm²)*)**					
Composite specimen – Average		0.206	0.062	0.011	0.004
Centre – Average	1.629	0.394	0.061	0.049	0.043
Outside – Average	1.179	0.415	0.091	0.031	0.024

Table 8.11. $1/R_p^{'}$ average values for both the *central* and the *outside* region, for different time exposures, for an increase by 22mV to the value of E_{corr}, at 35°C.

Exposure Time	*30 mins*	*2 hours*	*4 hours*	*24 hours*	*48 hours*	*72 hours*
ANODE	Centre	Centre	Centre	Centre	Centre	Centre
Potential Difference (mV)	4 , 5	5 , 6	6 , 7	11 , 11	11 , 11	11 , 11
Potential Difference – Average (mV)	4.5	5.5	6.5	11.0	11.0	11.0
Current passing From Anode to Cathode (μA)	0.2 , 0.3	0.2 , 0.2	0.1 , 0.1	0.0 , 0.0	0.0 , 0.0	0.0 , 0.0
Current passing From Anode to Cathode (μA) – Average	0.25	0.2	0.1	0.0	0.0	0.0

Table 8.12. Electrochemical behaviour, potential difference, and galvanic current between the two areas on the concentric specimen, at 35°C.

8.2. Microscopical examination.

The results of the microscopical examination on the concentric specimens after the tests, are presented in the following sections, 8.2.1. for Cu-10%Ni and 8.2.2. for Marinel.

8.2.1. Cu-10%Ni.

The appearance of the central and the outer specimen, of a concentric specimen, subjected to liquid impingement at 17m/s at ambient temperature 19°C, after an exposure of 48 hours and 72 hours, was very similar to the 48 hours composite specimen. Figure 8.14. shows that after 72 hours a black film covered the entire surface and the etched structure underneath the film was visible. This behaviour was typical for the centre and the outer specimen after 48 and 72 hours.

Figure 8.14. Cu-10%Ni, Concentric, V=17m/s, 72hours, T=35°C, T.W.L.
A black film covered the entire surface with the etched structure underneath the film still visible.

8.2.2. Marinel.

After exposures of 48 and 72 hours at ambient temperature 19°C, subjected to liquid impingement at 17m/s, the centre specimen was looking almost identical to the composite specimen after exposure of 48 hours, Figure 6.89 and Figure 6.90, with the entire surface covered with an almost continuous black film. A black film also covered the outer regions after 48 and 72 hours, but under the microscope it appears to be not quite as thick and continuous as the one at the centre of the specimen.

At 35°C, the appearance of the concentric specimen was the same as for the composite at the same high temperature.

Chapter 9

Discussion of Results of Cu-10%Ni and Marinel.

9.1. Comparison between Cu-10%Ni and Marinel for static exposures in 3.5% NaCl solution.

Table 6.1 shows the total material losses from static tests in 3.5% NaCl solution at 19±2°C on both alloys. It is quite clear that both alloys present the same weight loss values for the first 4 hours, but after 70 days and longer exposure periods Cu-10%Ni was more corrosion resistant than Marinel. Both alloys displayed behaviour typical of the gradual establishment of a protective film. A thin yellow film covers the surface of both alloys after a 4-hour exposure. The observed trends in this respect between 4 hours and 210 day exposures, guide us to make the postulation that the eventual establishment of the protective layer will probably reduce any differences in corrosion behaviour between the two materials.

Microscopic examination showed that the specimens that were exposed to 3.5% NaCl solution at 19°C exhibited uniform general corrosion with an almost amorphous appearance. The most prominent feature resulting from the tests for both alloys was the apparent gradual development of a thin, patchy, discontinuous surface film (see Figures 6.1, 6.2 for Cu-10%Ni and 6.3 for Marinel).

Some evidence of the metallurgical structure was also observed on the Marinel alloy after 70 days and longer exposure periods to 3.5% NaCl solution at 19°C. This provides more evidence that this higher-Ni alloy may be inherently somewhat less corrosion resistant than Cu-10%Ni.

These findings are consistent with the assumption that this uniform layer of corrosion products acts as a protective film and comes into agreement with information in the literature that copper-nickel alloys display significantly lower corrosion rates after initial protective film formation is complete [86,94].

The experimental results showed slight evidences that the Marinel alloy might not possess as good static corrosion resistance as the Cu-10%Ni.

9.2. Effect of impinging velocity on the short-term, erosion-corrosion, behaviour of Cu-10%Ni and Marinel in 3.5% NaCl solution.

This section discusses the erosion-corrosion behaviour for exposures up to 4 hours to 19±2°C.

9.2.1. Effect of impinging velocity on the total weight loss by erosion corrosion.

As Table 6.8 and Table 6.18 demonstrate, both alloys Cu-10%Ni and Marinel exhibited a general trend of increasing total weight loss with impinging velocities. Another general feature is the lower material loss experienced by Marinel, although this is somewhat less evident in some of the results at low velocities on account of the small weight losses relative to the accuracy of the balance, 0.1mg. As the impinging velocity increases, the superiority of Marinel, with lower total weight losses, becomes evident.

An interesting feature was the measurement, via cathodic protection tests, of a small amount of pure erosive losses on the Cu-10%Ni alloy, Table 6.9. In contrast pure erosion damage on Marinel was negligible except at the highest velocity of 86m/s.

The total weight loss data for Cu-10%Ni in Table 6.8 and for Marinel in Table 6.18, provide an indication of a step in the overall weight loss/velocity relation between 2.38-4.5m/s for Cu-10%Ni and between 4.5-17m/s for Marinel. However, these data are complicated somewhat by being comprised of tests with two different nozzle sizes. In an attempt to see if relating the weight loss to a more fundamental hydrodynamic parameter, the weight losses were plotted in terms of Reynolds number.

The Reynolds Number, R_e, is defined as:

$$R_e = \frac{Velocity * NozzleDiameter}{KinematicViscocity} = \frac{V * d}{\gamma}$$

where the kinematic viscocity of seawater at 20°C is $\gamma = 1.1*10^{-6}$ m^2/s, but for simplification reasons the used value in this work is, $\gamma = 10^{-6}$ m^2/s.

The impinging velocities expressed in Reynolds numbers are presented in Table 9.1.

Diameter. (mm)	0	1	4	4	4	4	1	1	1
Velocity. (m/s)	0	4.5	2.38	4.5	7.5	11.7	17	59	86
Reynolds No.	0	4500	9520	18000	30000	46000	17000	59000	86000

Table 9.1. Impinging velocity / Reynolds numbers data.

Although the weight losses/R_e graphs, (Figure 9.1, Figure 9.2), did provide more of an impression of a more smooth weight loss/hydrodynamic severity relation there was still some evidence, (especially for Marinel), for a step in the plot. This is of relevance to the analogous relationship, when the pure corrosion component of the total material loss is considered in the next section.

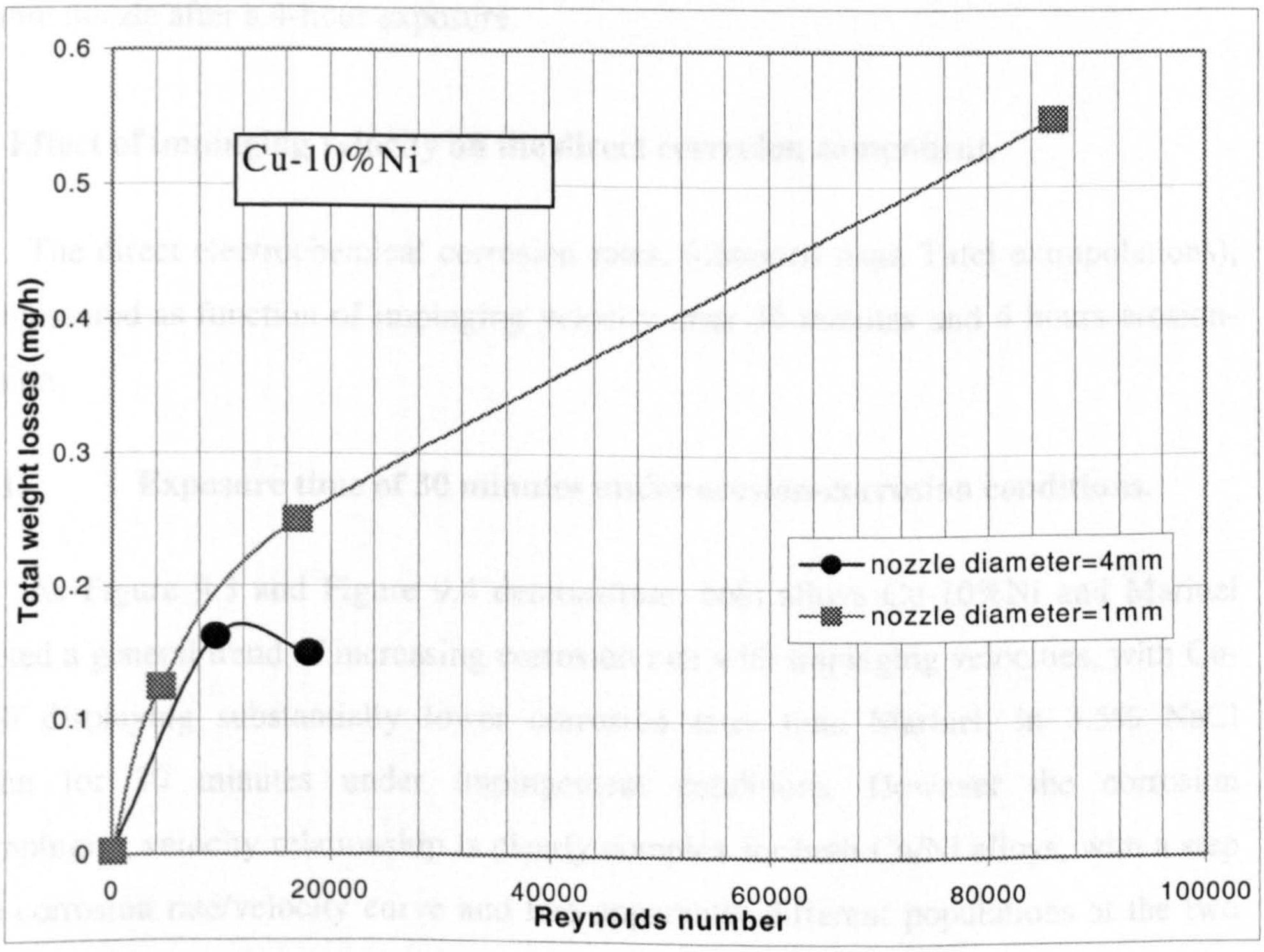

Figure 9.1. Total weight loss rate of Cu-10%Ni as a function of Reynolds number, at 1mm and 4mm nozzle after a 4-hour exposure.

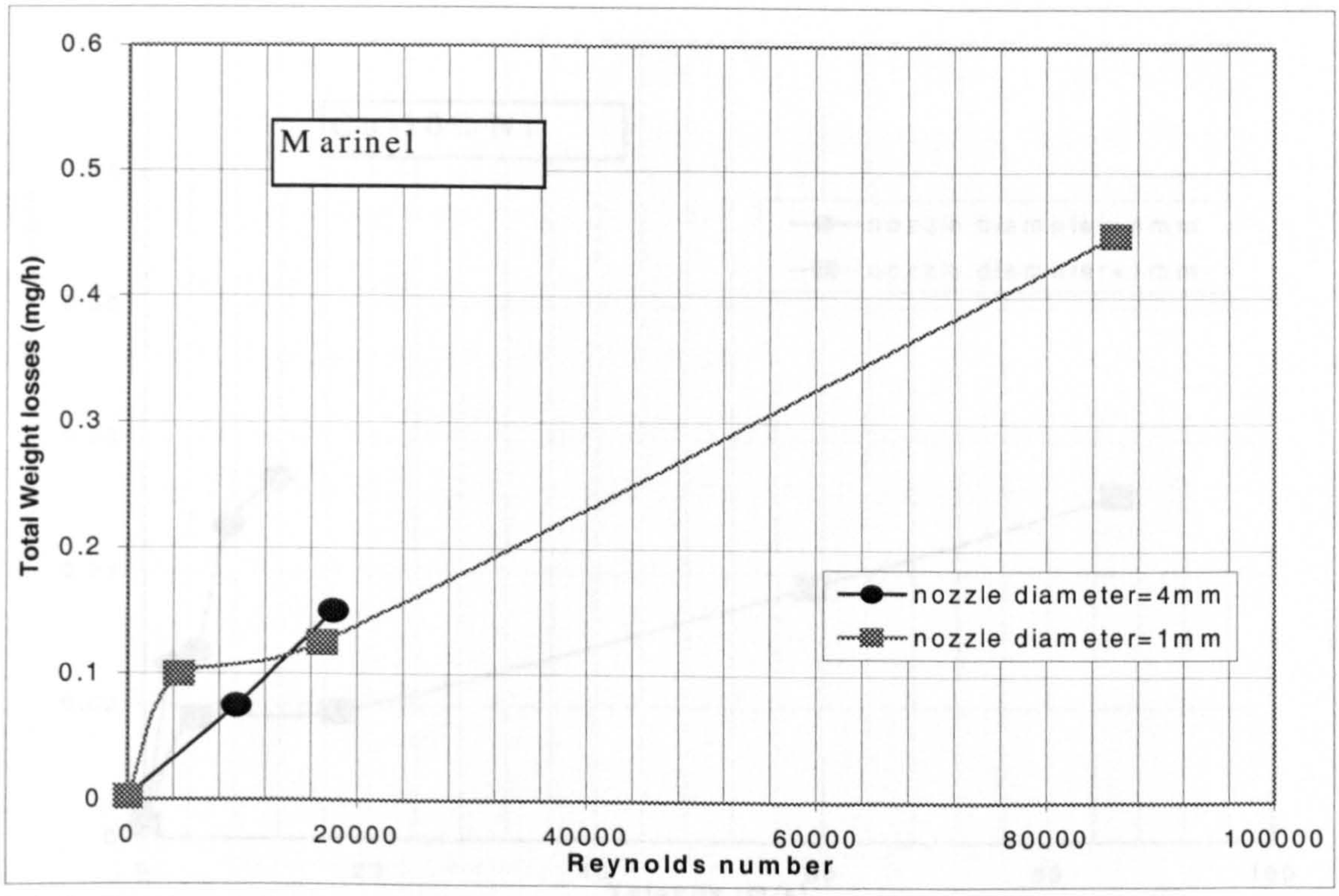

Figure 9.2. Total weight loss rate of Marinel as a function of Reynolds number, at 1mm and 4mm nozzle after a 4-hour exposure.

9.2.2. Effect of impinging velocity on the direct corrosion component.

The direct electrochemical corrosion rates, (obtained from Tafel extrapolations), were measured as function of impinging velocity after 30 minutes and 4 hours erosion-corrosion.

9.2.2.1. Exposure time of 30 minutes under erosion-corrosion conditions.

As Figure 9.3 and Figure 9.4 demonstrate, both alloys Cu-10%Ni and Marinel exhibited a general trend of increasing corrosion rate with impinging velocities, with Cu-10%Ni displaying substantially lower corrosion rates than Marinel, in 3.5% NaCl solution for 30 minutes under impingement conditions. However the corrosion rate/impinging velocity relationship is clearly complex for both Cu/Ni alloys, with a step in the corrosion rate/velocity curve and two apparently different populations at the two nozzle sizes. Moreover a plateau in the plot for Marinel was evident at the highest velocities. Another interesting feature was the different relative rates at the two nozzle sizes of the two alloys.

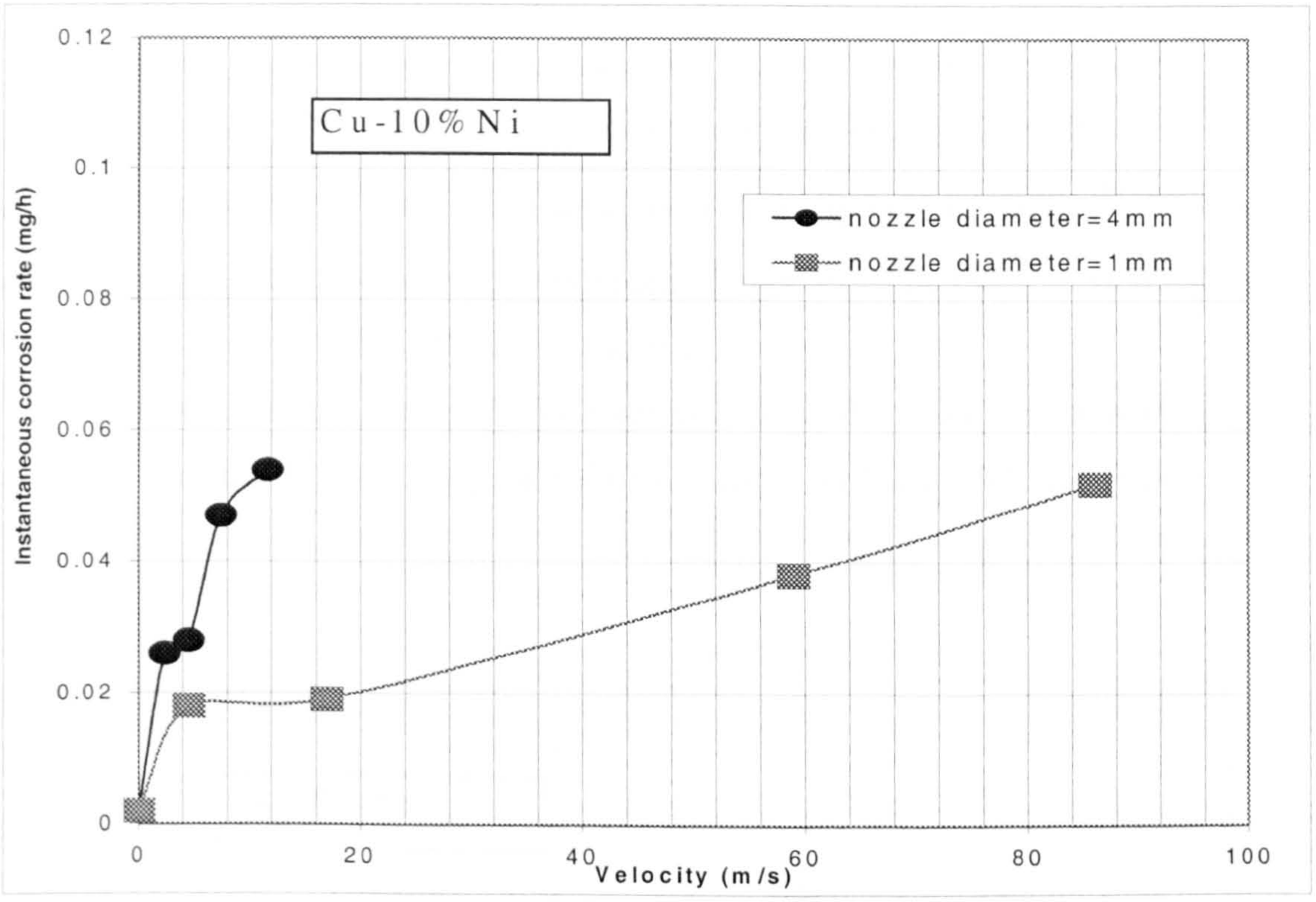

Figure 9.3. Instantaneous corrosion rate of Cu-10%Ni as a function of impinging velocity at 1mm and 4mm nozzle, after a 30-minute exposure.

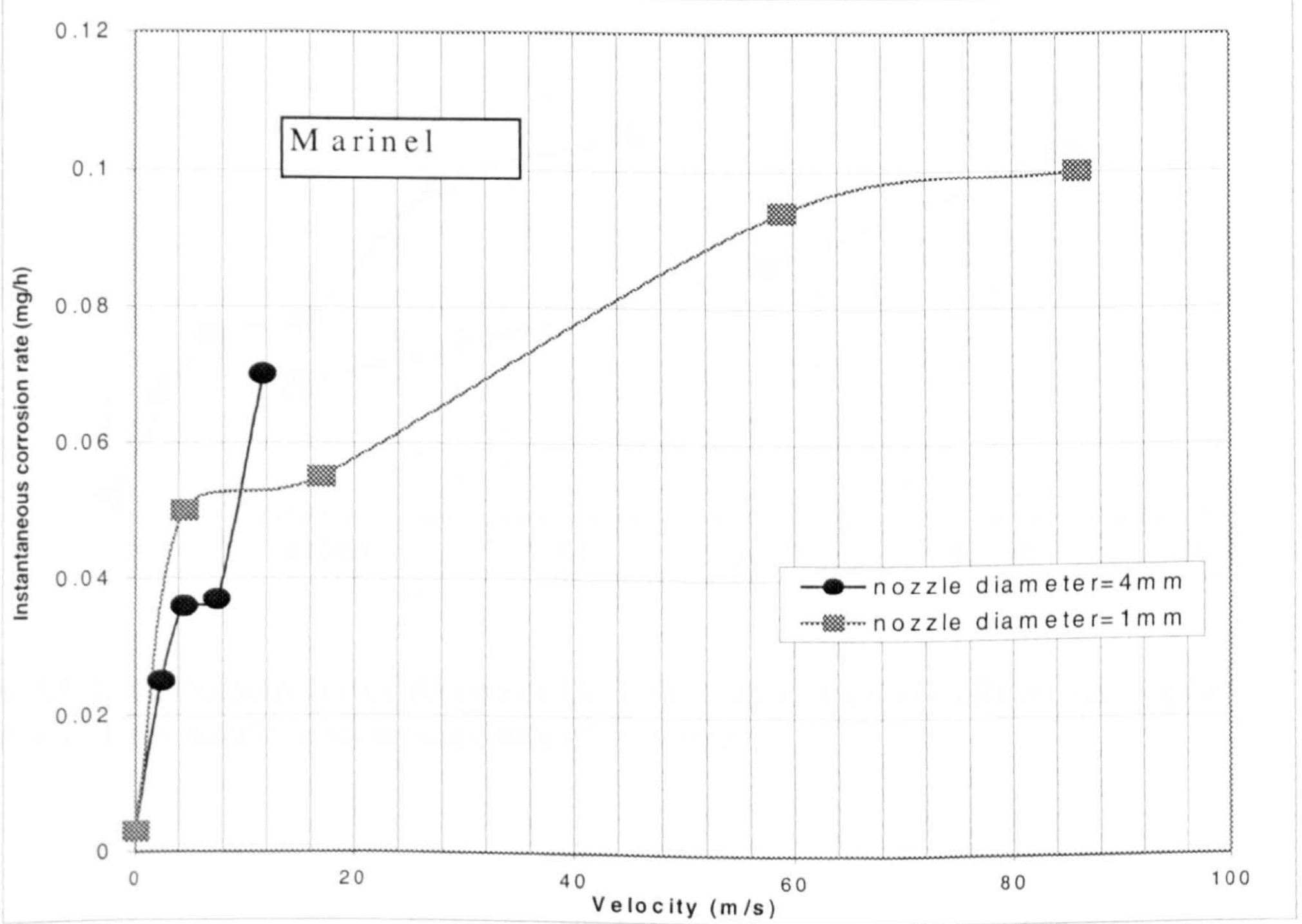

Figure 9.4. Instantaneous corrosion rate of Marinel as a function of impinging velocity at 1mm and 4mm nozzle, after a 30-minute exposure.

In order to assess a possible explanation for this complex relationship, an examination was made of the relationship between the corrosion rate and the Reynolds number, R_e. This approach comes into agreement with Syrett and Wing [106], who reported that in turbulent conditions it is more appropriate to relate the corrosion data to the Reynolds values rather than to the flow velocities.

The average corrosion rate/Reynolds numbers data at the two nozzle diameters for the Cu-10%Ni and the Marinel alloy, are shown directly in Figure 9.5 and Figure 9.6 respectively.

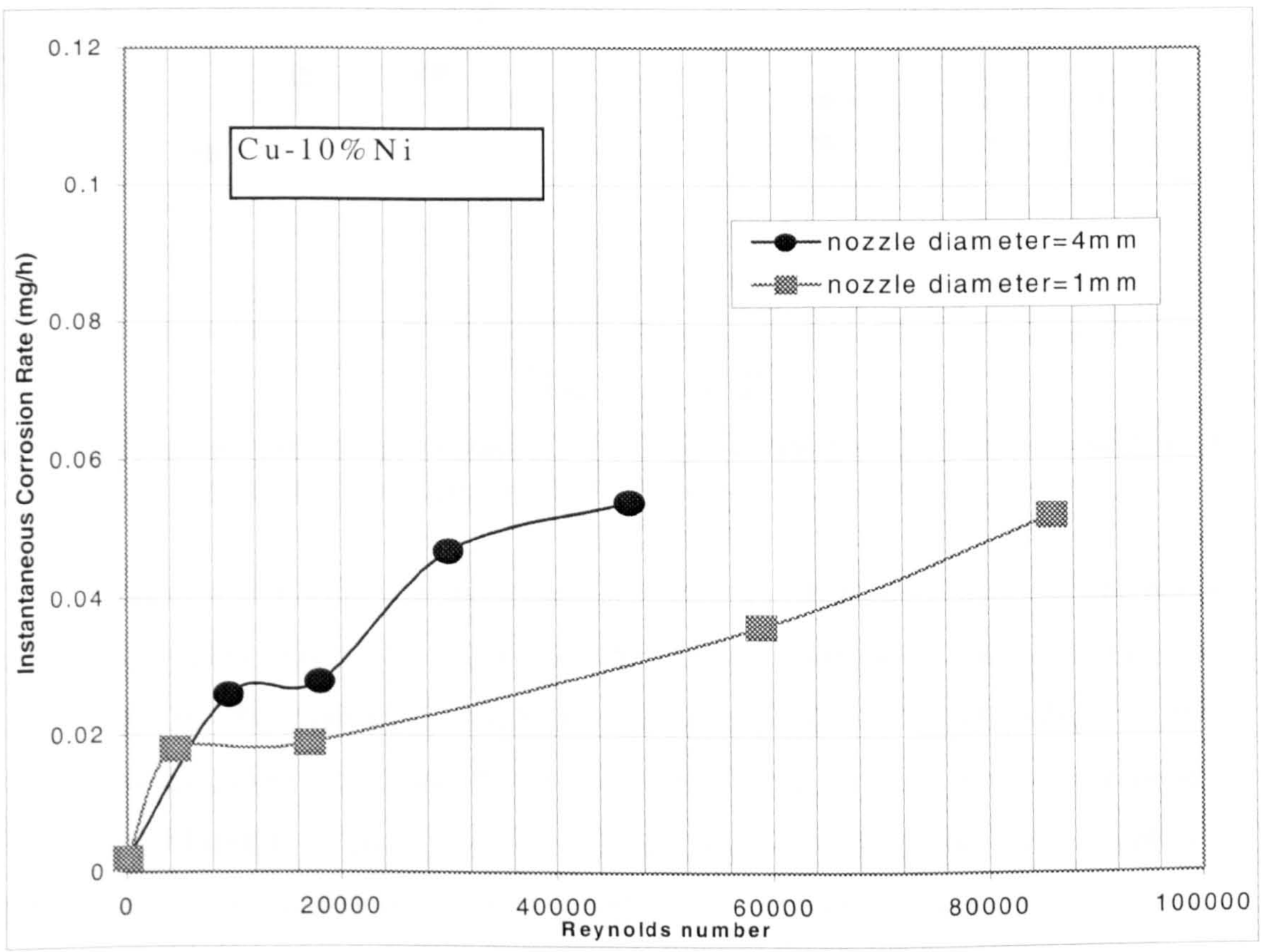

Figure 9.5. Instantaneous corrosion rate of Cu-10%Ni as a function of Reynolds number, at 1mm and 4mm nozzle, after an exposure of 30 minutes.

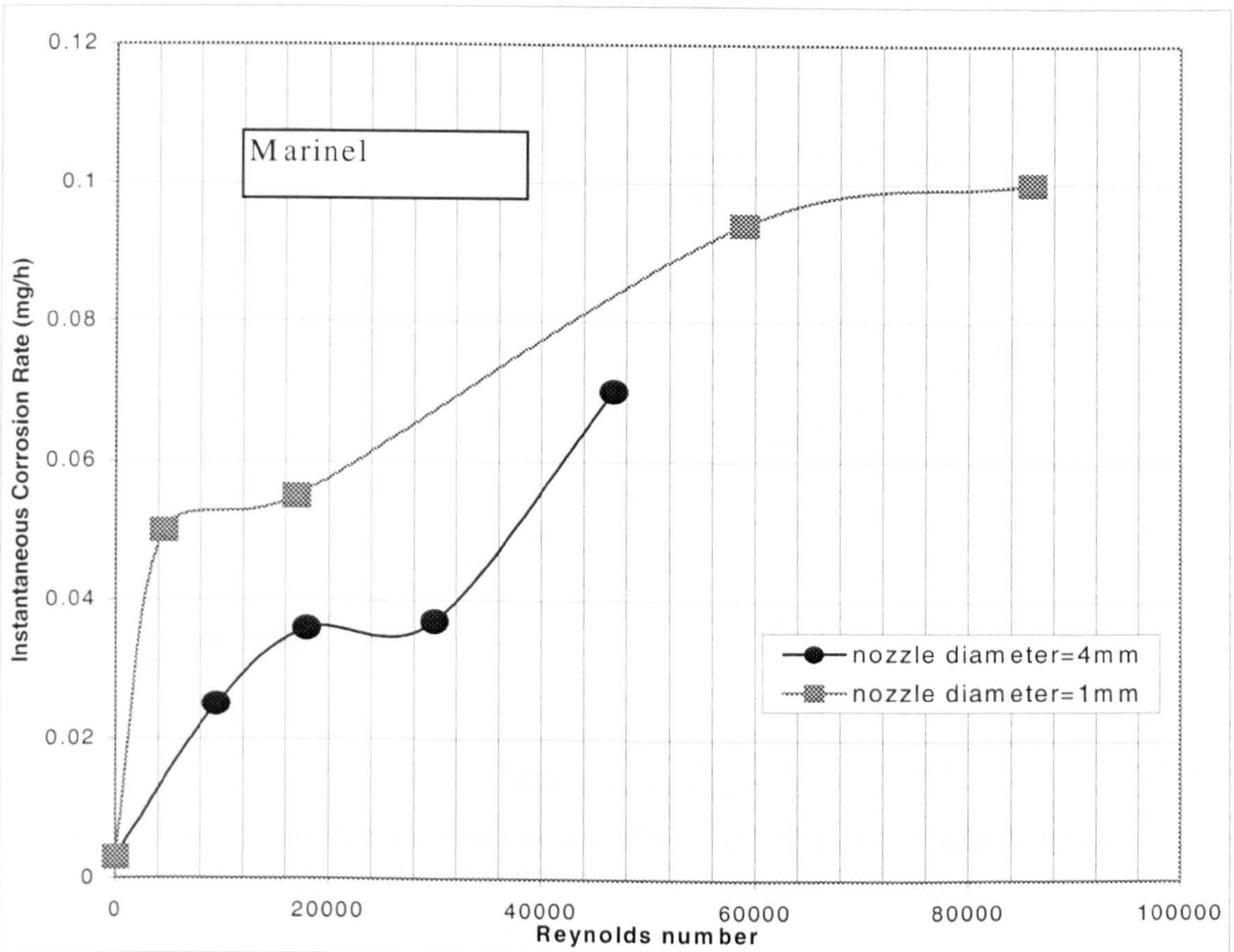

Figure 9.6. Instantaneous corrosion rate of Marinel as a function of Reynolds number, at 1mm and 4mm nozzle, after an exposure of 30 minutes.

Comparison of Figure 9.3 and Figure 9.5, (for Cu-10%Ni), shows that the results with the two nozzles move more closer together to the situation of one population, and also the step in the corrosion rate/hydrodynamic parameter relationship is more accentuated when plotted in terms of R_e than when plotted versus velocity. The same is also true for Marinel, (Figure 9.4 and Figure 9.6), although the two nozzle-size populations are still quite distinct in the R_e plots for this material, (Figure 9.6).

9.2.2.2. Exposure time of 4 hours under erosion-corrosion conditions.

The average direct corrosion rate/R_e data at the two nozzle diameters for the Cu-10%Ni and the Marinel alloy, are compared directly in Figure 9.7 and Figure 9.8 respectively.

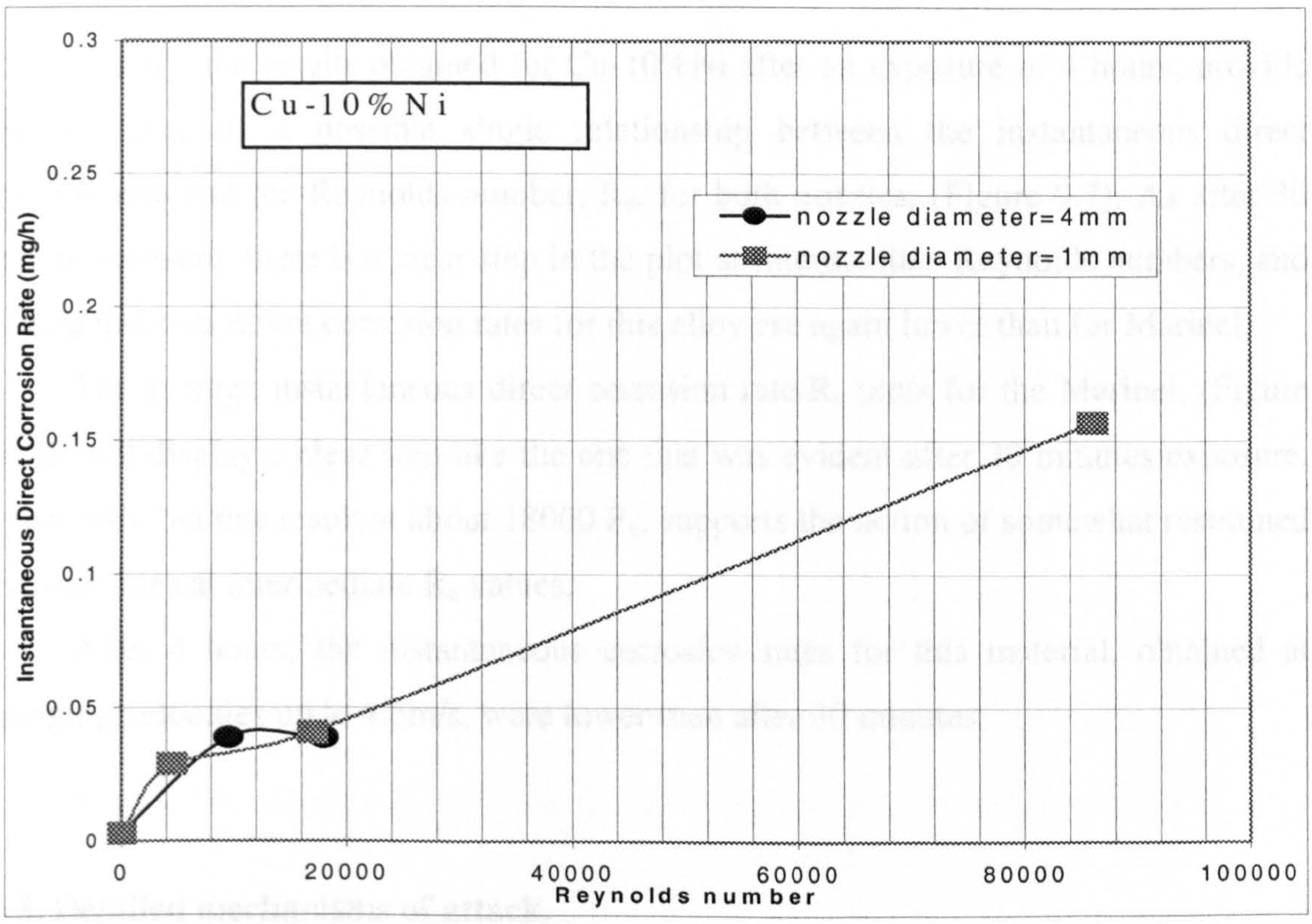

Figure 9.7. Instantaneous direct corrosion rate of Cu-10%Ni as a function of Reynolds number, at 1mm and 4mm nozzle, after a 4-hour exposure.

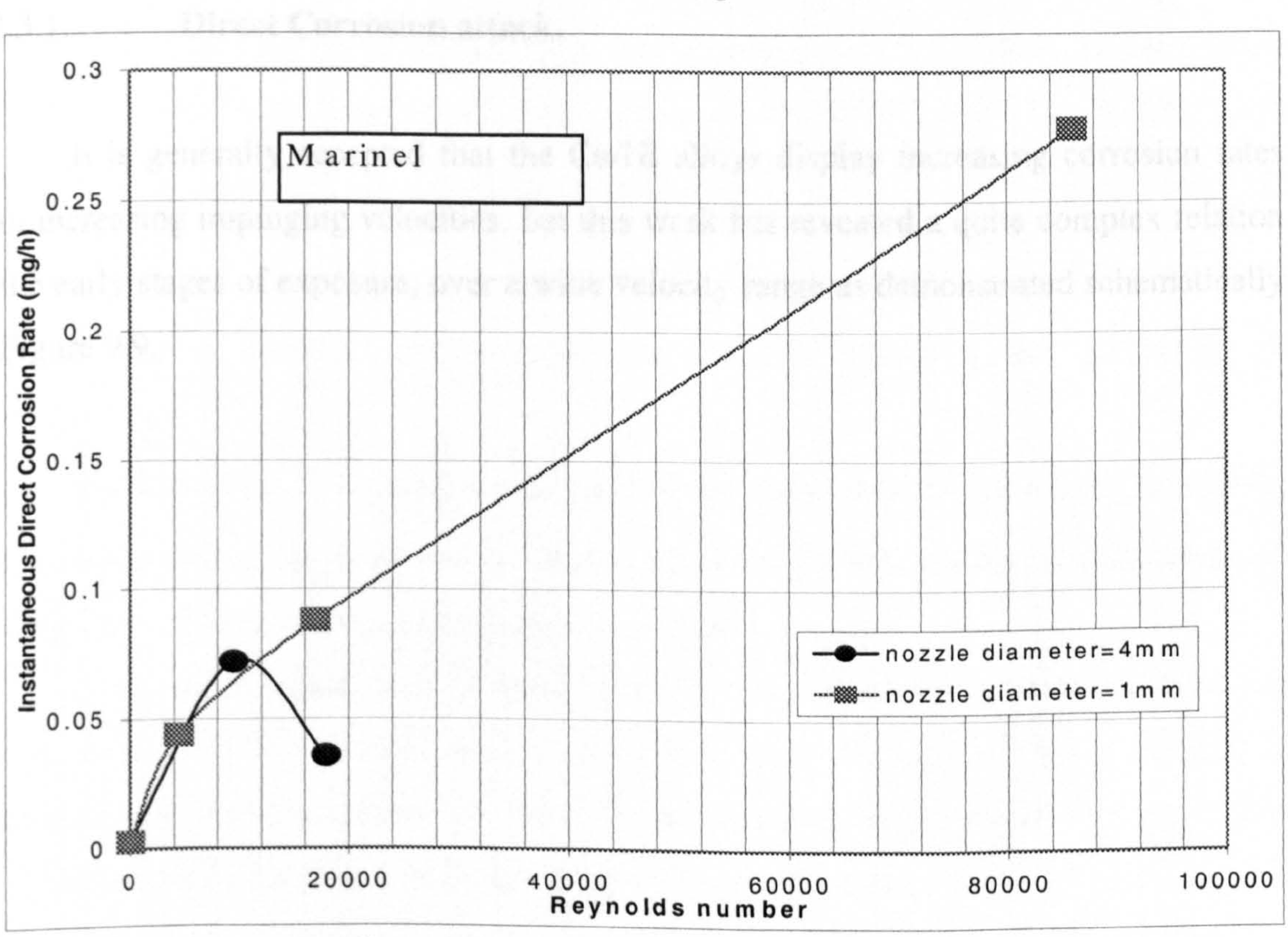

Figure 9.8. Instantaneous direct corrosion rate of Marinel as a function of Reynolds number, at 1mm and 4mm nozzle after a 4-hour exposure.

Clearly, the results obtained for Cu-10%Ni after an exposure of 4 hours, provide some evidence of a possible single relationship between the instantaneous direct corrosion rate and the Reynolds number, R_e, for both nozzles, (Figure 9.7). As after 30 minutes exposure, there is a clear step in the plot at intermediate Reynolds numbers, and the instantaneous direct corrosion rates for this alloy are again lower than for Marinel.

The average instantaneous direct corrosion rate/R_e plots for the Marinel, (Figure 9.8), do not display a clear step like the one that was evident after 30 minutes exposure, (Figure 9.6), but one result at about 18000 R_e, supports the notion of somewhat restrained corrosion rates at intermediate R_e values.

After 4 hours, the instantaneous corrosion rates for this material, obtained at impinging velocities up to 4.5m/s, were lower than after 30 minutes.

9.2.3. Detailed mechanisms of attack.

9.2.3.1. Direct Corrosion attack.

It is generally accepted that the Cu/Ni alloys display increasing corrosion rates with increasing impinging velocities, but this work has revealed a quite complex relation in the early stages of exposure, over a wide velocity range as demonstrated schematically in Figure 9.9.

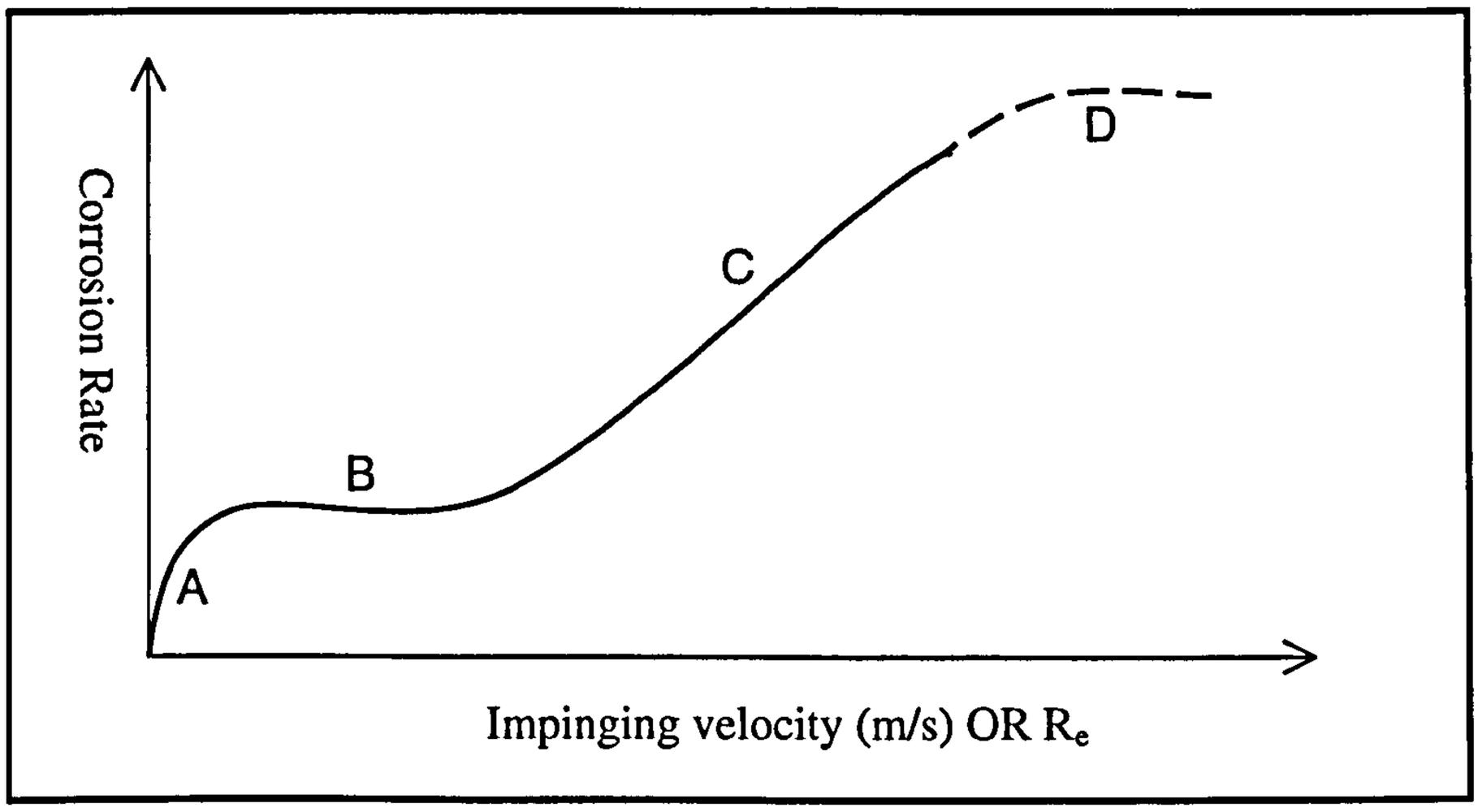

Figure 9.9. Schematic representation of the corrosion rate vs. impinging velocity.

The very interesting trends in instantaneous corrosion rate of Cu-10%Ni and Marinel with velocity, displayed in Figures 9.3 onwards and schematised in Figure 9.9, do not appear to have been reported previously except for a very short Russian paper published 30 years ago, which studied the corrosion rates of Cu-10%Ni at 1.5, 3, 5, 7 and 10m/s [115]. A schematic curve with some resemblance to Figure 9.9 has been suggested by Lotz [152] and was said to be representative of erosion-corrosion of (unspecified) copper alloys in seawater but no actual experimental examples were presented or referenced.

Some workers [158] using a rotating cylinder found that at high R_e, (up to 37000), the corrosion rate of Cu, brass and tin-bronze was virtually independent of velocity; these findings appear to be analogous to region B on Figure 9.9.

A plausible explanation of these trends is that the corrosion rates of the Cu/Ni alloys are subject to different modes of control, mass transfer or charge transfer at different flow rates, or even to mixed mass transfer/charge transfer control. The characteristics of each region in Figure 9.9 are discussed below:

Region A of Figure 9.9.

The relation in the first region A, can be correlated with other work on corrosion of copper in saline solutions. Workers over a period of decades [153-155,159], have either demonstrated or argued that the corrosion of this metal, under static and moderate-velocity conditions, is under mixed charge transfer/diffusion control via the following reactions:

$$Cu \rightarrow Cu^{+} + e^{-} \qquad \text{Anodic reaction.}$$

$$O_2 + 2H_2O + 4e^{-} \rightarrow 4(OH)^{-} \qquad \text{Cathodic reaction}$$

The products of the anodic reaction are said to undergo the following reaction:

$$Cu^{+} + 2Cl^{-} \rightarrow CuCl_2^{-}$$

and that the transport of the copper complex from metal surface into the bulk solution, represents the diffusion control reaction, which is accelerated as the velocity increases.

It has been postulated [155], that as the velocity increases, the balance between the diffusion and the activation control, shifts to the latter - this trend being reflected as a gradual levelling off of the corrosion rate/velocity plot, (analogous to the region B above, but this aspect is discussed later in more detail).

With regard to the diffusion control mechanism, it has been demonstrated and argued [153-155,158] that this does not involve the O_2-reduction reaction, because this reaction is under activation control at the rather positive free corrosion potential.

Turning to Cu/Ni alloys, a very recent paper [156], has reviewed previous works, largely on the basis of the temperature effect on seawater immersion corrosion of Cu-10%Ni alloy, but including a consideration of the corrosion behaviour in flowing seawater up to ~1m/s. The paper reports the findings of increased corrosion rate of Cu/Ni alloys at flowing velocities in comparison to static conditions, and suggests, (without

evidence), that the increase in rate is due to the corrosion rate being under diffusion control of the cathodic O_2-reduction reaction.

However the present work does not support this claim, but demonstrates that, (in common with the behaviour of Cu, as summarised above), the corrosion process of Cu/Ni and Marinel, under static and moderate velocities is under mixed diffusion/charge transfer control.

The evidences for this postulation are summarised as follows:

- The consistent findings of more negative E_{corr} values under impingement conditions than in static 3.5% NaCl solution for both alloys.

- The relation of the anodic polarisation curves, in the potential region immediately positive to E_{corr}, (this is most clearly demonstrated in Figure 9.10 for Cu-10%Ni after exposure of 4 hours, where the substantially-reduced slope of the anodic polarisation curve at 2.38 m/s compared to static conditions is clear). Also there is a further smaller reduction in slope for the 4.5m/s, obtained with the 4mm-nozzle, curve. These features, (as also indicated, but with less clarity in the 30-minute tests, Figure 6.4a and Figure 6.9a), would be expected if the anodic reaction was under partial diffusion control.

- The fact that the cathodic polarisation plots do not demonstrate concentration polarisation effects, even under static conditions near to E_{corr} as Figure 9.11 reveals. Figure 9.11 shows that, despite some fluctuation, the gradient of the static curve over a range of ~50mV negative to E_{corr} is very similar to that of all the curves at increasing velocities.

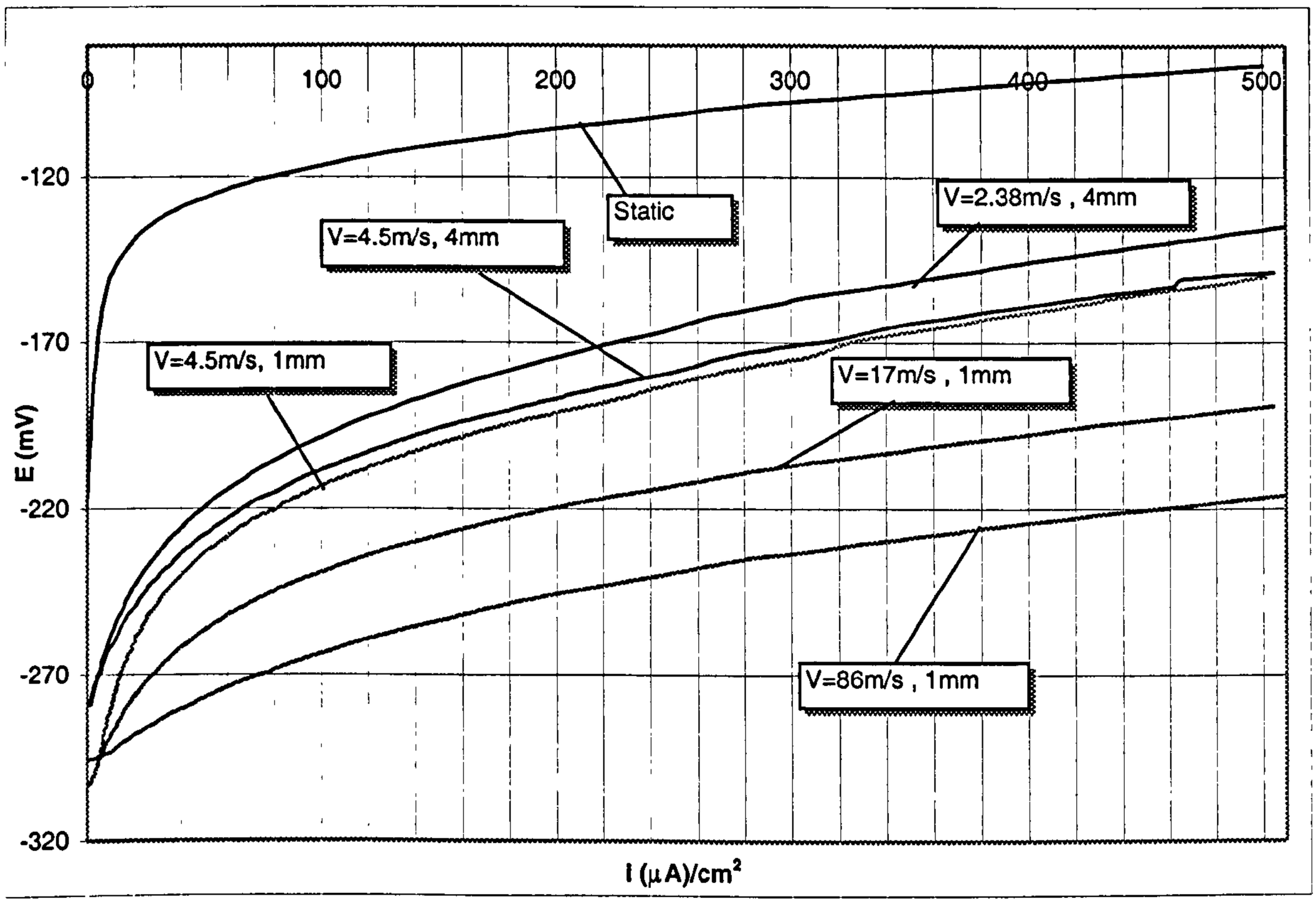

Figure 9.10. Anodic polarisation tests of Cu-10%Ni upon an initial exposure of 4 hours under the impinging jet.

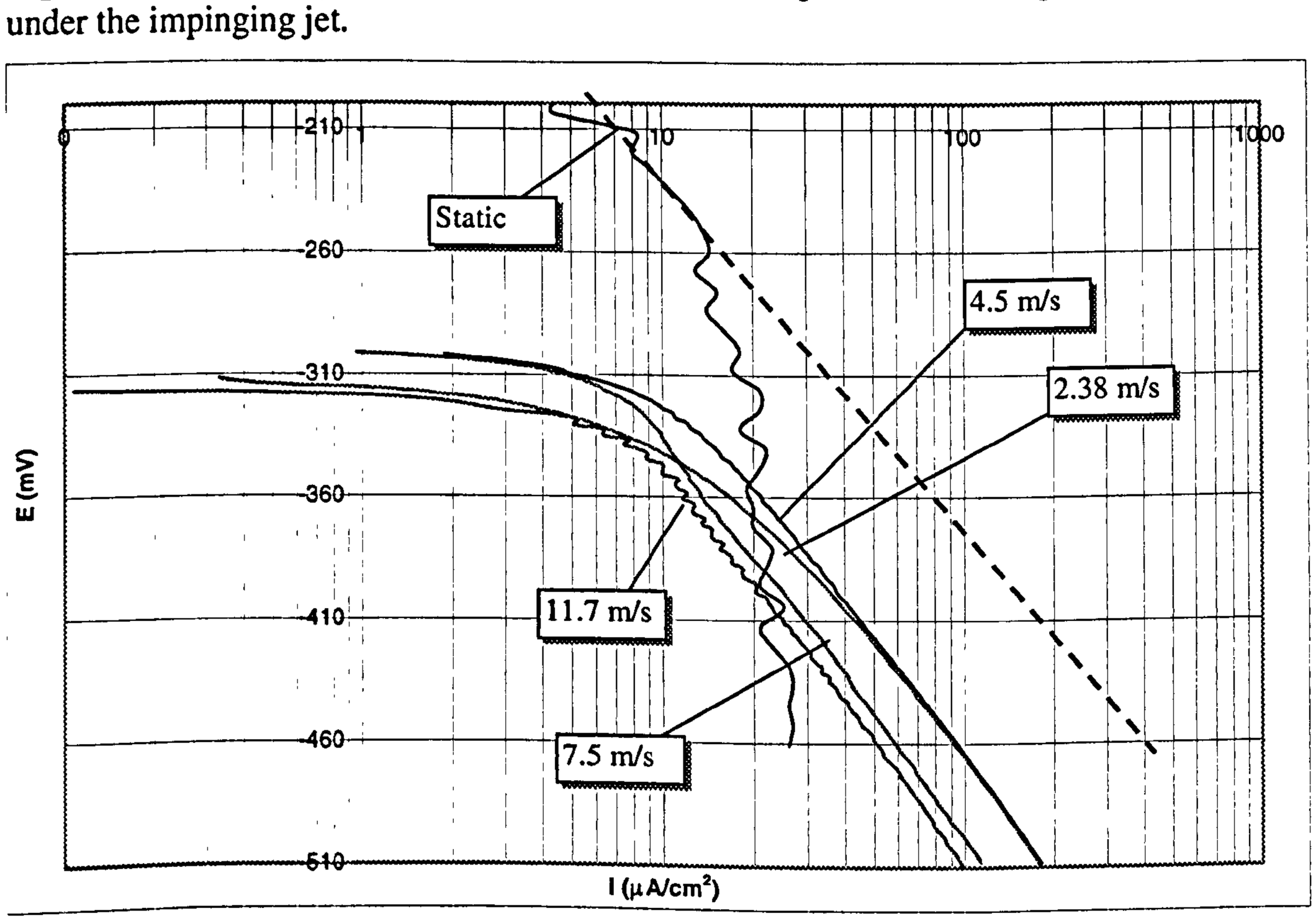

Figure 9.11. Cathodic polarisation tests of Cu-10%Ni upon an initial exposure of 30 minutes under the impinging jet, (dashed line shows the gradient of static curve in potential region of 50mV negative to E_{corr}).

The same effects of flow on anodic and cathodic reactions as described above for Cu-10%Ni were also evident for the Marinel. The cathodic polarisation plots for Marinel around E_{corr} were of similar gradient over the velocity range from static to 11.7m/s, (Figure 6.18b). On the other hand the anodic polarisation plots showed decreasing gradients in flowing conditions, (for instance compare 6.13b. and 6.17b. with the relevant corrosion weight loss/velocity plot, Figure 6.20).

It is suggested that the above evidence, points incontrovertibly to a scheme of the influence of impingement on the **active** corrosion behaviour of both Cu-10%Ni and Marinel alloys in the region A, essentially along the same lines as for Cu [152]. Thus the corrosion rate under static and these moderate hydrodynamic conditions is under mixed diffusion/charge transfer control of the anodic reactions, with the important step involving the outward diffusion of copper ions, or complexed copper ions, from anodic sites on the surface.

The increasing corrosion rate with velocity/R_e is due to accelerated outward diffusive flux of the anodic products through a diffusion boundary layer, δ_d, that decreases in thickness with increasing hydrodynamic severity. In other words, the instantaneous diffusive flux, $J_{(Cu)}$, is increased as δ_d reduces according to Fick's 1st Law of Diffusion:

$$J_{(C_u)} = -D\frac{(C_M - C_b)}{\delta_d}$$

where D is the Diffusion rate of outwordly-diffusing ions,

C_M is the concentration of the ions at the metal surface,

C_b is the bulk water concentration of the ions.

The situation is illustrated in Figure 9.12.

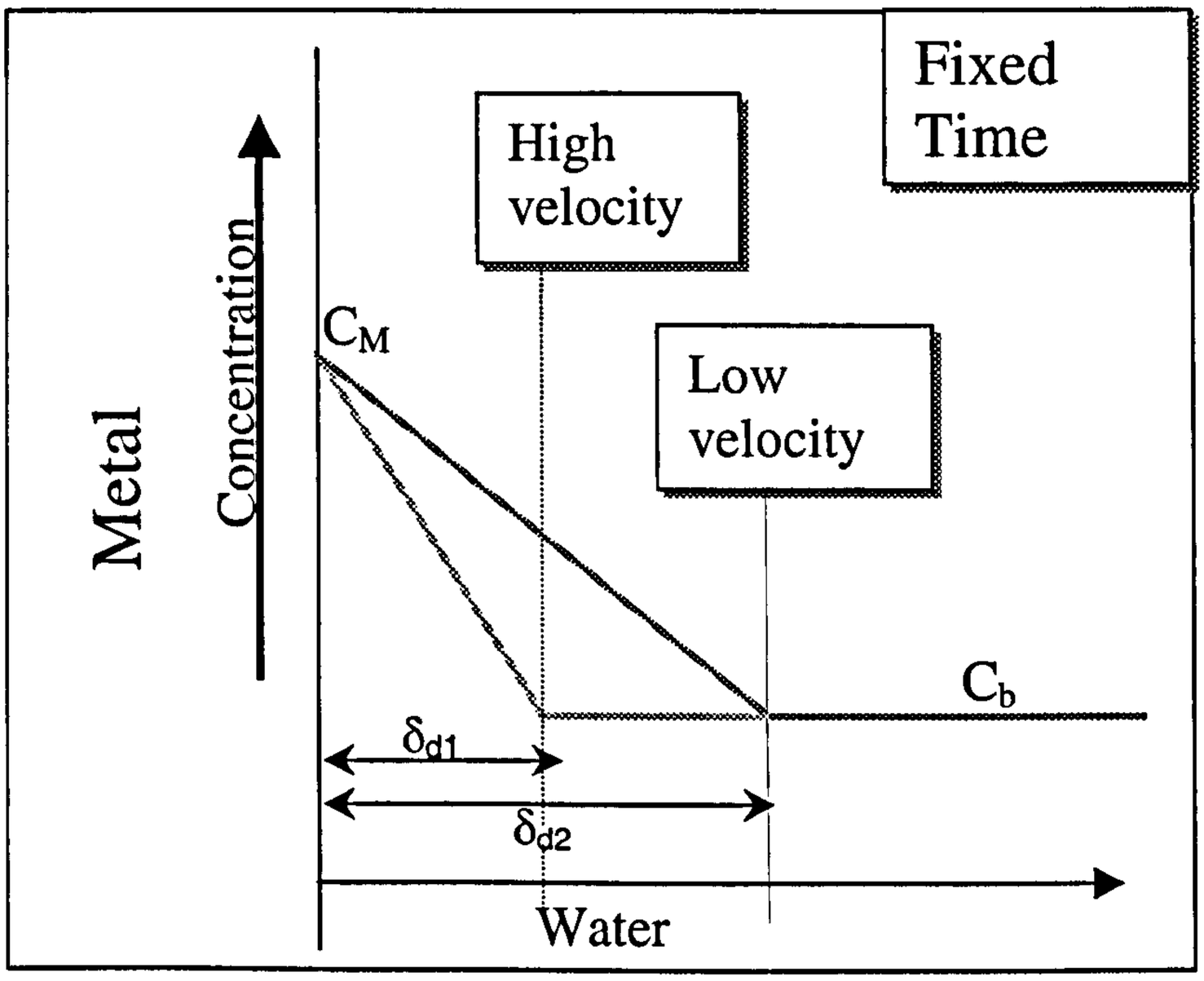

Figure 9.12. Schematic representation of concentration changes in diffusion boundary layer at different impinging velocities for a fixed time period.

This scenario implies that the alloying elements, (Ni, Fe, Mn in Cu-10%Ni, plus Al, Cr, Nb in the Marinel), do not play a crucial role in influencing the rate of active corrosion. This is further supported by the feature that the corrosion rate of Marinel in static conditions and region A, is greater, (despite its enhanced alloying components), than for Cu-10%Ni. The influence of alloying elements becomes paramount in the formation of a film. This factor will be discussed later.

Region B of Figure 9.9.

It is clear that must be a major change of corrosion mechanisms in this region compared to the region A. First it is worthwhile mentioning again the previous work on Cu, since some workers [155,158] have correlated their observations, of a gradual flattening off of the corrosion rate/impinging velocity relation, to a shift from predominant diffusion control to predominant charge transfer control in the mixed-control process. Such a mechanism might be thought to be also involved in the current

findings – especially with the recognition that pure activation control is consistent with the corrosion rate being independent of velocity, (as in region B). However, it is concluded that this scheme does not pertain to the present observations on Cu-Ni alloys for two reasons.

First, it would be difficult to reconcile such a mechanism with the region of increasing corrosion rate with impinging velocity, (Region C).

Secondly the observation in this work of the production of corrosion product films, on the surface of the specimens under the impingement conditions; there was some evidence of thin patchy films at 2.38m/s and 4.5 m/s, which is around about the velocity where the corrosion rate starts to become independent of velocity. The films were more prominent at 17m/s, as demonstrated by Figure 6.35 and Figure 6.36. Over the range to 17m/s, the evidence of the grain structure confirms that the Cu-10%Ni was undergoing general active corrosion. For Marinel the correlation between microscopic features of the corrosion and velocity were not as clearcut as for Cu-10%Ni. One clear distinction between the two materials was a greater tendency for Marinel, compared to Cu-10%Ni, to form films in all conditions studied.

Relatively thick but discontinuous films were evident on Marinel after exposures at 2.38m/s. At 17m/s the surface was extremely complex with patches of films of different colour and thickness, which might be interpreted as representing conditions where the hydrodynamic conditions are beginning to discourage a more uniform film formation. Again on Marinel at velocities up to 17m/s, the generally attacked metal structure could often be seen underneath the films formed.

In general the evidence of etched structures even beneath the films, demonstrates that these films under these conditions up to 4 hours exposure are not especially protective as indeed the corrosion measurements imply, (the corrosion rate of 0.05mg/h, see Figure 9.3 and Figure 9.4, extrapolates to about 0.01cm/year metal loss).

It is thus suggested, that the change in corrosion rate/hydrodynamic relation from region A to region B, is associated with the formation of a film on the surface of the specimens. This film is stable over the velocity/R_e range of region B, and its presence leads to a change of rate-control mechanism, to one of transport most probably of

products of anodic reaction through the film of constant thickness relating to a fixed time period.

Over the range of hydrodynamic conditions in which the film is stable, such a mechanism is consistent with anodic and cathodic reactions occurring at constant rates. In this respect, Figure 9.11 shows the cathodic polarisation curves of constant gradient over the range up to 11.7m/s, and the anodic curves in Figure 9.10 show an anodic polarisation curve at 17m/s of a very similar gradient to that of 4.5m/s.

Region C of Figure 9.9.

In this region both alloys exhibited rapidly increased corrosion rates with increasing hydrodynamic severity. The plausible explanation of this change is that, as the hydrodynamic severity increases, eventually the film present in region B becomes unstable. Lotz suggested [152] that a steeply rising component like the region C was associated with a transition from mass transfer hampered by the presence of a corrosion product scale, towards the erosion of the scale. The evidence from the polarisation curves is that the corrosion rate again becomes under mixed control of the anodic reactions. The evidence for this can be seen in Figure 6.5b, where the slope of the cathodic polarisation plots are similar over the range of 17→59-86m/s, providing evidence that the cathodic reaction is not controlling the overall corrosion rate. In contrast, as shown on Figure 9.10, there is a distinct flattening of the anodic polarisation curve at 86m/s compared to 17m/s.

Thus it appears that transport of products of anodic reaction from the metal surface to the solution again becomes rate determining. The higher corrosion rates at higher velocities are likely to be related to thinner boundary layers.

Strong evidence for this mechanism was provided by the absence of any film on the Cu-10%Ni after exposure at 86m/s for 4 hours.

The question arises as to what are the detailed mechanisms of breakdown of the films? These appear to be two possibilities:

- Film instability is due to increasing hydrodynamic severity promoting enhanced mass transfer [160], which is considered to enhance the film dissolution.

- Films are broken down or cannot form as a result of shear stresses [101]. It is of interest to make some estimates of shear stresses on impinged specimens and to compare these values with the critical values for Cu/Ni alloys in the literature [101].

By using $\tau_w = 0.0447\rho u^2 R_e^{-0.182}(\frac{r}{d})^{-2}$ from the literature [22,28], and assuming that the wall jet region commences at about r/d =2, the shear stresses within the wall jet region for different impinging velocities, (i.e. Reynolds numbers), were estimated and are presented in Table 9.2.

where ρ = 1020 Kg/m3 (density of seawater),

u = 4.5 m/s, 17 m/s and 86 m/s,

R_e = 4500, 17000 and 86000,

d = 10^{-3} m (diameter of the nozzle)

(r/d) = 2.

The maximum shear stresses were also estimated by using $\tau_m = \frac{0.16\rho u^2}{(H/d)^2}$, (although literature [27], recommends this equation only for H/d > 8), and are presented in Table 9.2.

Impinging Velocity (m/s)	Reynolds numbers	Max. Shear stress (Pa)	Wall-Jet region Shear stress (Pa)
4.5	4500	100	49
17	17000	2000	560
86	86000	50000	10000

Table 9.2. Wall-Jet region and maximum shear stresses for different impinging velocities.

Alloy	Temperature °C	Critical Shear Stress (Pa)
Aluminium brass	12	19
Cu-10%Ni	27	43
Cu-30%Ni	12	48
84-16 Cu-Ni + 0.5 Cr	27	297

Table 9.3. Critical shear stress of Cu-base alloys in seawater [101].

Clearly the calculated shear stresses are so small in magnitude that, as the literature suggests, (Table 9.3), it is hard to imagine it could cause erosion damage to a metallic surface, (320 MPa and 924-955 MPa are the tensile strengths for Cu-10%Ni and Marinel respectively).

However, the relationship between shear stress and flow rates is the matter of interest to the critical shear stress necessary for the breakdown of protective surface layers on metals [27], which can be the cause of accelerated erosion-corrosion rates.

At 4.5m/s, the calculated maximum shear stress clearly exceeds the critical value, 43 Pa, measured for Cu-10%Ni by Efird [101] and even in part of the wall jet regions, the shear stress is around the critical value. Efird's calculations for the critical shear stress, were obtained for more mature films formed after longer periods, (30 days), in contrast with these very short experiments in the current work. Consequently precise correlation between the calculated and the quoted critical shear stresses is unreasonable.

Nevertheless at 17m/s (R_e=17000), the calculated shear stresses are an order of magnitude or more in excess of the critical values for Cu-10%Ni, and it is of interest that

these are the R_e values at which the corrosion rate data showed a film breakdown, (Figure 9.5).

In contrast, the critical values obtained by Efird [101] for a 84Cu-16Ni+0.5Cr alloy were much higher than for Cu-10%Ni. It is reasonable to assume that this figure is more representative of the behaviour of films on Marinel and it is noticeable, (Figure 9.6), that some of the data obtained in the present work indicated that the transition to higher corrosion rates was at a higher R_e for Marinel than for Cu-10%Ni.

The above calculations and comparisons provide quite persuasive support for the idea that film breakdown occurs at critical values of shear stresses. Such a correlation does not necessarily prove that film breakdown involves a shear process; it could represent a correlation between shear stress and mass transfer, with the actual damage mechanisms involving instability of the film by increased mass transfer.

Region D of Figure 9.9.

This region was evident for Marinel only and involved a return towards much lower corrosion rate sensitivity to hydrodynamic conditions. The microscopic evidence revealed that most of the surface was covered by a much more continuous but thinner film at 86m/s, (Figure 6.96), compared to 17m/s, and this trend supports the idea of the development of a corrosion product film on the surface. This observation is in conflict with the suggestion by Lotz [152] that a plateau such as region D represents transport to the metal surface.

It might be considered to be somewhat inconsistent to suggest film stability in region B, followed by film breakdown in region C and film stability again in region D. However, the films formed on Marinel at 17m/s and 86m/s were clearly quite different, leading to the notion that different intensities of the hydrodynamic conditions might support in some way different types of film. Clearly though this tentative suggestion requires more investigation.

Nozzle size effect.

There was some evidence of different corrosion rates with the two different nozzle sizes – although these differences were much reduced when the corrosion rate was correlated with R_e rather than velocity, and also after a 4-hour exposure.

The directly impinged region of a composite specimen would be expected to heavily influence the measured overall corrosion rate of the sample. With a higher proportion of the specimen surface subjected to the high-velocity jet, higher currents would be flowing in the specimen involving the 4-mm nozzle and, in the conversion of current to current density by division by the total specimen area, a higher current density and hence a higher specimen corrosion rate would be monitored – as observed for the Cu-10%Ni material.

The different behaviour of Marinel, i.e. lower corrosion rates with the 4mm nozzle up to ~12m/s, may be associated with a more enhanced film formation on the surface, in the directly impinged zone, after the 30-minute exposure.

After 4 hours, the implied corrosion rates for this material were lower than after 30 minutes, implying a more established surface film, which might well diminish any nozzle-size effects.

9.2.3.2. Pure Erosion and Synergy.

The results indicated a contribution from pure erosion on erosion-corrosion of Cu-10%Ni even at the lower velocities, but the erosion material loss did not appear to be particularly sensitive to impinging velocities up to 17m/s. There was a significant increase in the erosion damage between 17 and 86m/s.

The erosion damage on Marinel was undetectable up to 4.5m/s, but modest levels of erosion were recorded at higher velocities. Substantial contributions from the synergetic factor were obtained for both materials but particularly high values, (>60%), for Cu-10%Ni were obtained at the highest velocities.

Discussions of the detailed mechanisms of pure erosion and synergy, are best accomplished after the general discussion of the findings over the entire range of conditions studied (including the effect of temperature); i.e. in section 9.5.

9.3. Effect of time on the erosion-corrosion behaviour of Cu-10%Ni and Marinel in 3.5% NaCl solution.

The effect of time, up to 48-72 hours, was studied in detail at the impinging velocity of 17m/s and to a lesser extent at 86m/s.

9.3.1. Total erosion corrosion.

As Table 6.12 and Table 6.22 demonstrate, both alloys Cu-10%Ni and Marinel showed an increased total weight loss with increased exposure time periods, with the only difference that, in the case of Cu-10%Ni, the rate of material loss appeared to be at a constant rate up to 8 hours with a fall somewhat thereafter, (from 0.25mg/h over an exposure period of 8 hours, to an averaged figure of 0.18 mg/h after 48 hours, impinged at 17 m/s). For the Marinel, the rate of material loss decreased constantly with the passage of time. The total weight losses for Marinel were lower than those for Cu-10%Ni, by a factor of 2-4 at 17m/s, but to a reduced extent at 86m/s. The films were more established on the surfaces of the alloys after these long time periods, but those on Marinel gave much better overall erosion-corrosion protection as discussed later.

As was observed in the 4-hour tests, the pure erosive component had a very small contribution to the total weight losses in Marinel's case, Table 6.23, especially at the lower impinging velocity of 17m/s, with the pure erosion weight losses found to be very low, as expected for a liquid impingement on a metal. The general trend for both alloys was the higher pure erosion weight losses at the higher velocities, and the noticeable decrease in the rate of erosion damage and its percentage contribution to the total material loss, with increasing time.

At the impinging velocity of 86m/s both alloys showed a greater rate of total weight loss damage.

9.3.2. Direct corrosion component.

9.3.2.1. General features.

Higher direct corrosion rates at 86m/s compared to 17m/s were clear for both alloys. The following discussion focuses mainly on the more-detailed study at 17m/s impinging velocity but with comments also on behaviour at 86m/s.

For Cu-10%Ni, there was good correlation between the Tafel extrapolation measurements and the linear polarisation monitoring exercise, which demonstrated (Figure 6.26b), a complex relationship between corrosion and time in jet impingement conditions. The overall impression was that the corrosion rate was 'cycling' between lower and higher values over the 72-hour test period.

The major feature of the direct corrosion behaviour of Marinel (again shown with good agreement from the two types of electrochemical measurement) was the substantial reduction in corrosion rate after a 4-hour exposure, which followed the initial period of increasing corrosion rate. This decline in corrosion rate was observed at both 17m/s and 86m/s, and was shown by the more detailed monitoring at 17m/s to be maintained until a higher corrosion rate was measured after the 48-hour exposure. Thus the time dependence of direct corrosion also seemed to be complex on Marinel. However, it might be appropriate to suggest that the corrosion rate of Marinel was also cycling but over longer periods of time than Cu-10%Ni. The corrosion rate of Marinel was greater than for Cu-10%Ni at short times (up to 8 hours), but was significantly lower at longer exposure periods.

For the impinging velocity of 17m/s, the detailed anodic and cathodic plots of Marinel, Figure 6.56a-b and Figure 6.57a-b, indicate that, as at the shorter times, (Figure 9.10), the corrosion rate was under anodic control. Thus, there is a substantially enhanced polarisation of the anodic reaction between 4 and 8 hours at 17m/s, followed by a slight depolarisation at longer time periods. This trend correlates extremely well with that in the $1/R_p$ results (Figure 6.59b). The depolarisation of the anodic reaction at 86m/s compared to 17m/s (Figure 6.56a-b) was confirmed. In contrast, all the cathodic polarisation curves were of similar gradient.

For the impinging velocity of 86m/s, both the anodic and the cathodic reactions after an exposure period of 8 hours impingement are slightly more polarised than at 4 hours.

Despite the very complex trends of corrosion rate with time, for Cu-10%Ni there was good correlation between the anodic polarisation curves and the linear polarisation data. Thus, from Figure 6.23a, the anodic polarisation curves after 4 and 8 hours were very similar implying similar corrosion rates – in agreement with the linear polarisation data in Figure 6.26b – and there was a clear additional degree of polarisation, evident on the anodic polarisation curve after 72 hours compared to 48 hours and again this is in agreement with the trend on Figure 6.26b. There was also an obvious feature of a clear depolarisation of the anodic polarisation curves after 4 hours and 8 hours at 86m/s compared to 17m/s. Most of the cathodic plots displayed similar gradients confirming the view that the corrosion process in not under cathodic control, during the periods of times and the range of velocities studied.

The most distinctive feature of the longer exposures at 17m/s of Marinel, was the more pronounced and more uniform surface film after 8 and 48 hours, as compared with the one established after the 4-hour exposure period. The presence of these films coincides with the much lower direct corrosion rates after 8-hour and 48-hour exposures, compared to the results after 4-hour exposure time, Table 6.24, and thereby demonstrates that these were conferring a substantial degree of corrosion protection even under the impinging conditions. Moreover the observed concurrent decreasing rate of total weight loss with the passage of time, (Table 6.22), indicates that these surface films on Marinel were providing a significant protection against *overall erosion-corrosion* damage.

Another interesting feature for Marinel is that the Ni/Nb particles were obvious even after an exposure period of 8 hours under 17m/s impingement Figure 6.82, showing that they are not directly involved either in the corrosion process or the film formation.

Microscopical examination of Cu-10%Ni specimens did not reveal any distinctive difference after erosion-corrosion at 17m/s for 4→8→48 hours exposure periods. Thus the constant feature was of fairly deeply etched structure over the entire surface. The etched surfaces displayed a variety of colours signifying the presence of very thin surface films. It should be emphasised that these films were very much less evident than the ones

on Marinel, described in the proceeding paragraph. It seems clear that there is a much less significant role of the surface corrosion products in conferring significant direct corrosion and erosion-corrosion protection on Cu-10%Ni under the impingement conditions of 17m/s and 86m/s over the exposure times studied in this research.

9.3.2.2. Corrosion mechanisms.

The most appropriate way of attempting to interpret the above-described complex features of the time trends in the corrosion processes is to commence with a consideration of the corrosion of Marinel at an impinging velocity of 17m/s. The following corrosion mechanism is proposed.

The corrosion rate in the early stages of exposures is under mixed diffusion/activation anodic control via diffusion, (as described in section 9.2.3), of products of the anodic reaction across a diffusion boundary layer. With the passage of time the concentration of the anodic products continually increases at the metal surface and this produces a steadily increasing concentration gradient across the boundary layer, as presented in Figure 9.13. This facilitates an increasing corrosion rate with time as observed for Marinel up to 2 hours. Eventually, the concentration of anodic products reaches a value that corresponds to the solubility limit of some copper-base compound, which thus forms a film on the metal surface. At this point in time, corrosion control switches from diffusion of soluble ions across a diffusion boundary layer, to diffusion across a solid film, i.e. corrosion is at a slower rate. Moreover, if it is postulated that the rate of film thickening is greater than that of dissolution at its outer surface, then the continual increase in film thickness accounts for the observed progressive fall in corrosion rate.

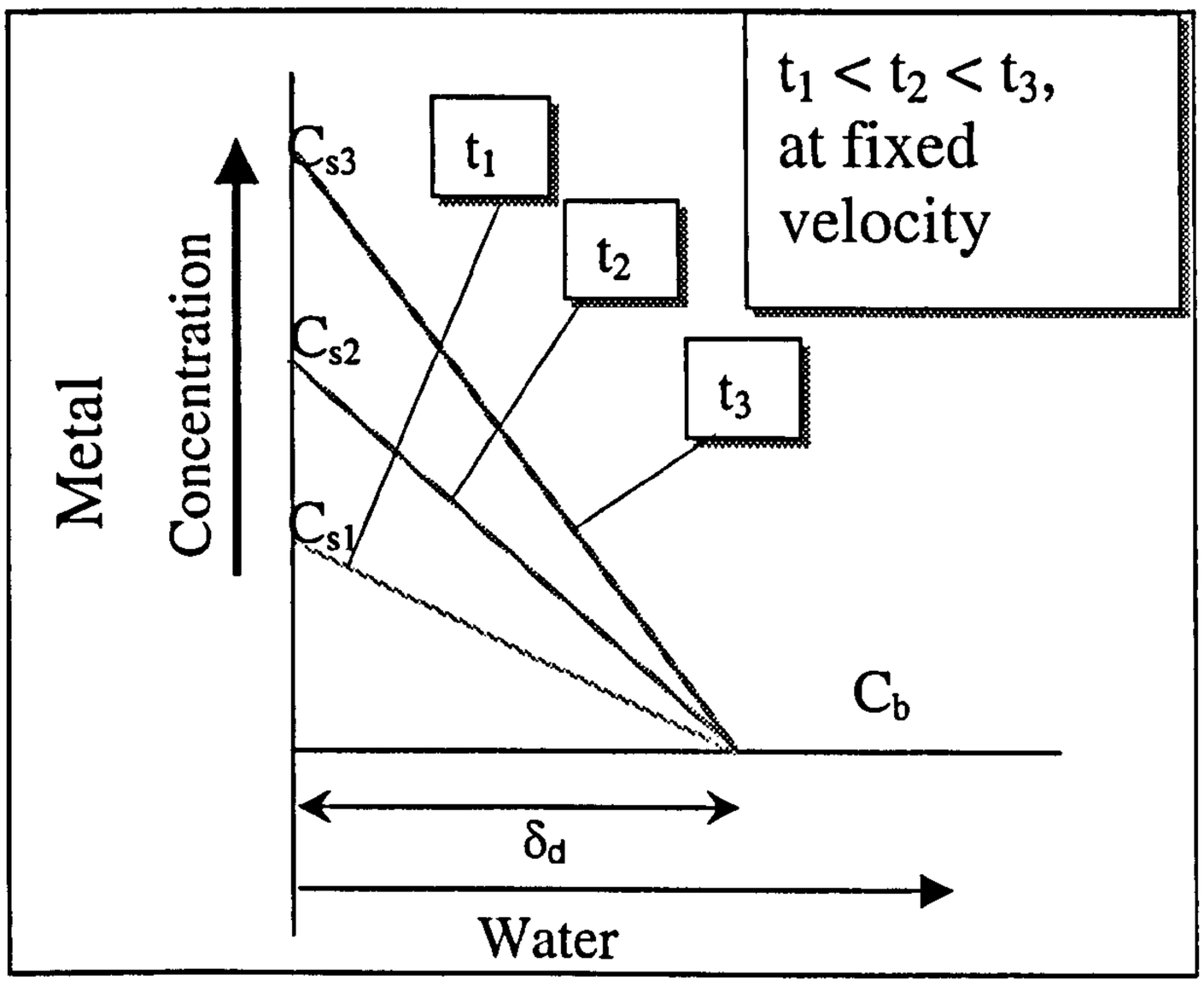

Figure 9.13. Schematic representation of concentration changes in diffusion boundary layer at different time periods for a fixed impinging velocity.

The films grown on Marinel were clearly observed (Figure 6.80) to be irregular, leading to an increasing degree of surface roughness on a micro scale. It is well known that rough surfaces promote local turbulence and hence accelerate mass transfer processes, and possibly elevate local shear stresses. It is thus considered that, after the period of steadily diminishing corrosion rates (Figure 6.59b), the surface roughness has become sufficient to lead to destabilisation of the film by one or both of the mass transfer/shear stress processes. It is quite likely that the above sequence would then be repeated on a cyclic basis, but only the first possible phase, of a second cycle of increasing corrosion rate with time, has been observed within the time-scales of these experiments in this research.

An additional question relates to what extent the proposed corrosion mechanism would pertain at different velocities than the 17m/s, the behaviour at which it has been applied. The fewer measurements and observations at 86m/s revealed the expected higher corrosion rates but with evidence that films can still form in such severe impinging conditions. At velocities lower than 17m/s it can be postulated that the films may take longer to establish, (on account of the lower corrosion rates that lead to the enhanced ion

concentrations at the metal surface), but might be stable for longer periods in the less-severe hydrodynamic conditions.

The clearer cycling of corrosion rate on Cu-10%Ni at 17m/s might be thought to support a similar mechanism as the one described above for Marinel. However, the films formed on Cu-10%Ni were never observed to be more than of interference-colour thickness, which implies a similar ratio of dissolution to growth of the film. Thus their formation would not be expected to confer the same degree of protection at 17m/s as these on Marinel, (this rationale would also support the findings of no observable films on Cu-10%Ni at 86m/s). Consequently although the presence of the film on Cu-10%Ni causes a reduction in corrosion rate, (as shown for instance between 16 hours and 24 hours in Figure 6.26b), the corrosion rate does not fall to as low values as the corrosion rate for Marinel. The periods of increasing corrosion rate, say after 40 hours, may also be caused by film destabilisation due to increased mass transfer caused by surface roughening. Supporting evidence comes from the observation of increased surface roughness of Cu-10%Ni with the passage of time as demonstrated in Table 9.4.

	Initial	4 hours	48 hours
R_a (μm)	0.02	0.06	0.35

Table 9.4. Roughness values for Cu-10%Ni at 17m/s for different exposure periods.

The above discussion has focused on the role of surface films in causing reductions in the corrosion rate. The question arises: what is the composition of the surface corrosion products? The investigations in this work focused on gathering information on the overall nature of the erosion-corrosion phenomenon on these Cu-Ni base alloys and no attempts have been made to identify the composition of the surface corrosion products. It is generally considered that, in the long term at low flow velocities, the protective corrosion product on Cu-10%Ni comprises a main inner layer of Cu_2O with an outer layer(s) containing CuO and various other compounds including possibly atacamite $Cu_2(OH)_3Cl$ and lepidokrokite (FeO(OH)) [86]. The lepidokrokite represents the beneficial effects of iron addition to Cu-10%Ni. Some authors [153,161] have

suggested that a top layer of atacamite provides the corrosion resistance on account of its low solubility, but others [106] have suggested atacamite to be present as porous patches on top of the oxide film, which are not likely to be protective.

The thicker and clearly more protective corrosion products forming on Marinel must be associated with the additional alloying components which can promote a quicker-forming and more hydronamically resistant film, than on Cu-10%Ni. The key alloying elements are almost certainly aluminium and chromium, with some limited previous studies to support this notion. The presence of Al in Cu/Ni alloys has been observed to yield improved durability in a recent investigation by Clark et al [149], who showed that Hiduron 191, (15%Ni, 5%Mn, 1%Fe, 1.4%Al, bal Cu), possesses superior jet impingement resistance at 9.2m/s after a 28-day exposure, and general corrosion resistance in sea water compared with both Cu-30%Ni and Cu-10%Ni., probably because of the beneficial effect of the aluminium additions in increasing hardness and promoting a more readily formation of a passive surface layer. Moreover Kear et al [154] reported in a very recent paper, that additions of aluminium form a protective corrosion product layer of aluminium oxide at nickel aluminium bronze, (which does, however contain much more Al, 9.58%, than on Marinel). It was therefore expected that because of its higher aluminium content Marinel should be at least as good as Hiduron 191.

Anderson and Efird [84] reported that the addition of chromium up to 3%, increase the hardness of Cu-10%Ni and allows its use in contact with flowing seawater at velocities higher, (6-8m/s), than those permitted, (2.5-4m/s) for the chromium free alloy. Also Efird [101] conducted experiments in flowing sea water at velocities up to 18m/s, and after 30 days exposure time, (direct corrosion or erosion-corrosion rates were not measured), he suggested that even a very small addition of chromium, up to 0.5% to a cupronickel with 16% Ni and balance copper, greatly increases the adherence or the protective film, thereby significantly extending the seawater velocity limits for the alloy. Alhajji [109] performed similar tests with a copper nickel alloy of similar type (16%Ni – balance Cu), with a chromium addition of 0.7%, and his results, obtained with the linear polarisation technique after 4-hours tests at 6.1m/s, confirmed Efird's postulation [101].

Laboratory seawater corrosion tests carried out by Anderson and Badia [127] confirmed that the addition of a nominal 0.5% Cr to copper-nickel alloys (15-38% Ni) can provide a marked improvement in sea water impingement corrosion resistance for a range of sea-water velocities up to 8m/s.

In summarising, these rather restricted previous studies provide evidence of beneficial association with separate additions of Cr and Al to Cu-Ni alloys. The present study has demonstrated in much more detail substantial improvements in erosion-corrosion resistance, brought about by the combined presence of both these elements in small quantities, (1.78-1.88%Al and 0.31-0.56%Cr).

Clearly it would be of interest to contact studies, (e.g. using X-ray photo-electron spectroscopy, "XPS"), to identify the films forming on the erosion-corrosion conditions studied in this work.

9.3.2.3. Further comments on the percentage contributions of the direct corrosion component to the total weight loss.

A surprising finding in this study was the low percentage contribution to total weight loss attributed to direct corrosion especially for Cu-10%Ni, under all conditions studied. This poses the question as to whether the evaluation of the instantaneous corrosion rates from the Tafel slopes, and/or the estimations of the 'integrated' weight loss due to the direct corrosion component, (i.e. 'area under the graph' method), have been seriously underestimated in this work.

To check this possibility, the results for Cu-10%Ni at 17m/s for an exposure period of 4 hours, are now re-evaluated. For this case the pure corrosion component was determined to be 11%, (Table 6.11). Let us, for the sake of argument, consider the possibility that the percentage of the true pure corrosion contribution is say 77%, and try to assess if it is possible, that the computations that resulted in the 11% value, could by re-assessment, reasonably move towards to the 77% value. There are two possible sources of error.

1) The 'integrated' technique represents a serious underestimate. With reference to Figure 6.22, the only reasonable re-assessment would be to assume that the instantaneous corrosion rate between 30 minutes and 4 hours is constant at the 4-hour value, as represented in Figure 9.14b.

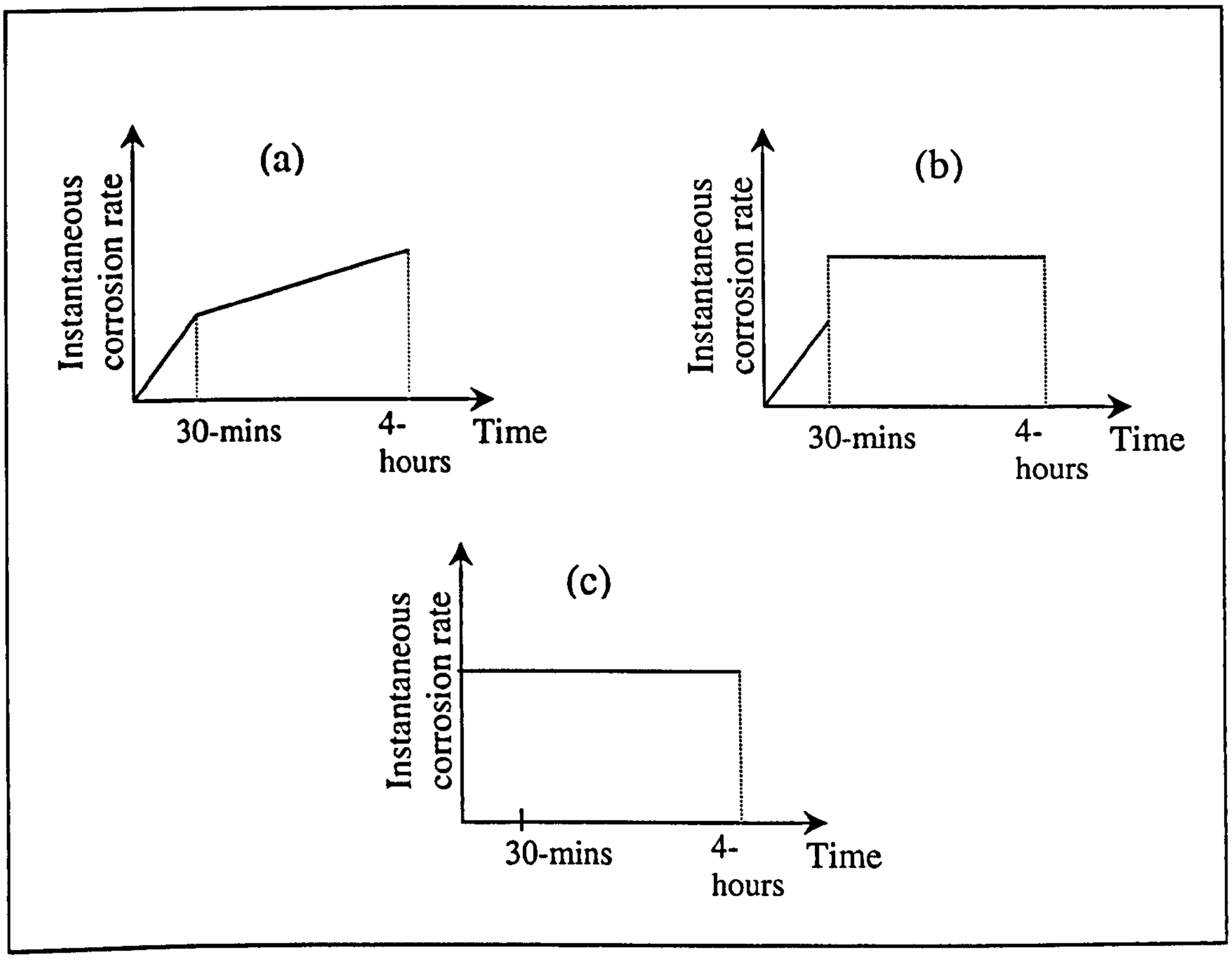

Figure 9.14. a) Figure similar to Figure 6.22, b) Constant instantaneous corrosion rate between 30mins and 4 hours, at the 4-hour value, c) Constant instantaneous corrosion rate for the whole 4-hour exposure, at the 4-hour value.

This would lead to an additional increment, (equal to A3 in Figure 6.22), to the 'area under the graph' calculations. Reference to the calculations in 6.3.1.1.3 reveals that this would yield a direct corrosion weight loss increased from 0.11mg to 0.15mg, which, (Table 6.11) would only increase the percentage corrosion contribution to about 15%.

Even assuming a constant rate of corrosion equal to that at the 4-hours value, as demonstrated at Figure 9.14c, (hence ignoring the 30-minutes result),

will lead, (Table 6.10) to a direct corrosion weight loss of 0.16 mg in 4 hours, which (Table 6.11), would still only represent a percentage of 16%.

2) The other possible source of error is the Tafel slope plot. In order for the direct corrosion component to be around say 80%, Table 6.10 and Table 6.11 would indicate that the i_{corr} value would need to be about 5-7 times that, obtained from the duplicate Tafel plots and presented in Table 6.10, i.e. 8.75 $\mu A/cm^2$. In other words i_{corr} would have to be around $45\mu A/cm^2$, which is clearly a completely unrealistic assessment of the Tafel slope. A similar checking exercise on the 86m/s for the Cu-10%Ni after a 4-hour exposure result, (Table 6.11), leads to the same conclusion, namely that the direct corrosion contributions have not been seriously underestimated, as presented in the Chapter 6.

As another example, in order to confirm the low direct corrosion percentage contributions, Figure 9.15 presents the obtained anodic and cathodic plots for the Cu-10%Ni after exposure of 4 hours under a 4mm impinging jet at 4.5m/s. From Table 6.11, for the direct corrosion to be equal to the total weight loss, the pure corrosion weight loss, (=0.13mg), would have to be elevated by a factor of 5, and even assuming a constant rate at the 4-hour instantaneous rate of $8.5\mu A/cm^2$, this would require an i_{corr} of over $40\,\mu A/cm^2$ which as shown by Figure 9.15 is clearly unrealistic.

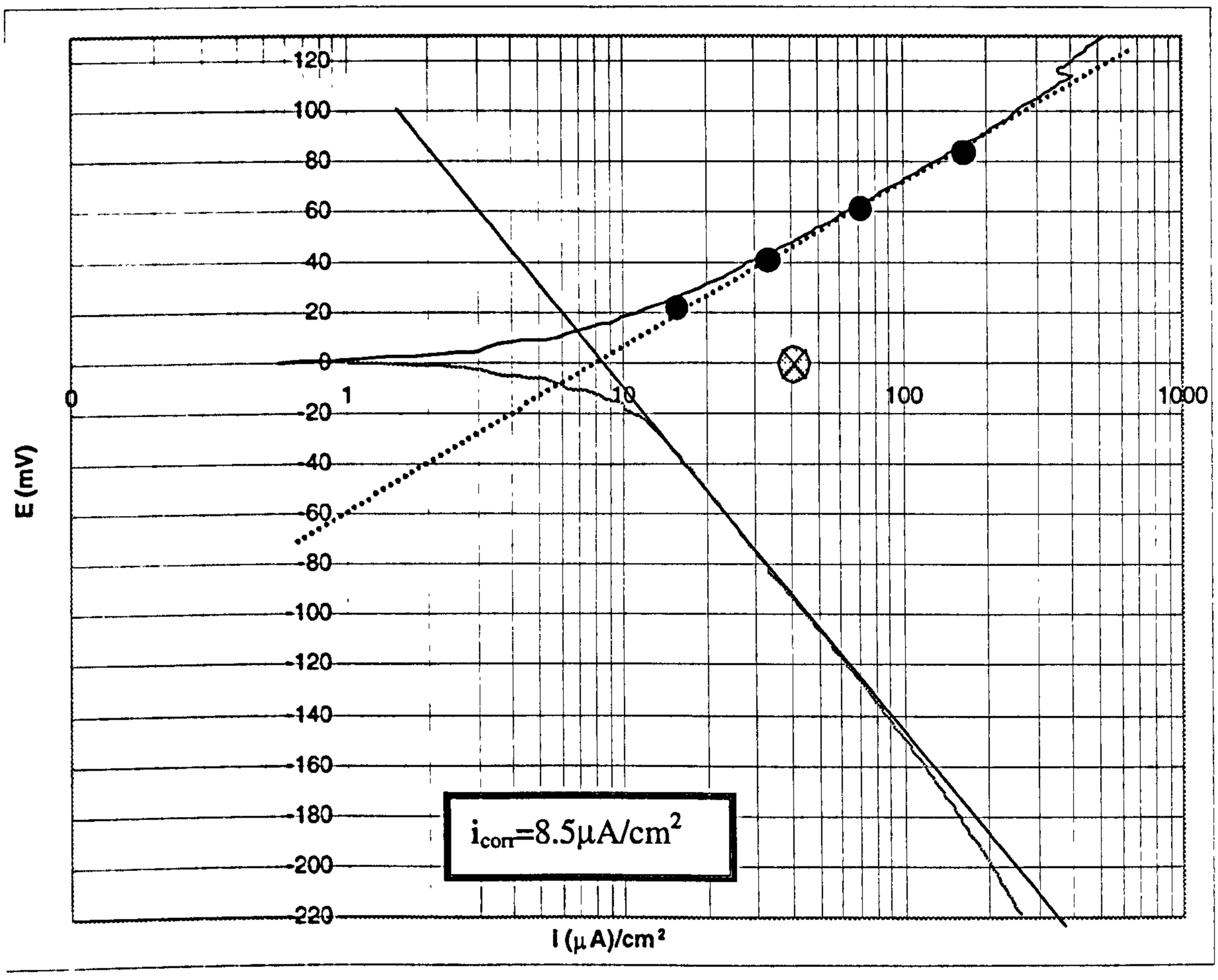

Figure 9.15. Anodic and Cathodic polarisation plots of Cu-10%Ni after exposure of 4 hours under a 4mm impinging jet at 4.5m/s. i_{corr}=8.5 μA/cm^2. The ⊗ indicates the necessary i_{corr} value for the total weight loss to be dominated by the direct corrosion.

It is of interest to refer to a paper [157], in which this issue was discussed against a background of a review of the literature. The author suggested plausible explanations, of overestimates of the total weight loss from electrochemical corrosion measurements, in terms of the electrochemical technique, but he considered that the many underestimates of the total damage from electrochemical measurements were more difficult to explain. He suggested that such underestimates arose because the discreet instantaneous corrosion rates obtained electrochemically can represent serious underestimates because they do not accurately account for the high rates of corrosion in the early stages of exposure. Others [156], have also made similar suggestions and there is little doubt that these represent at least partial reasons for underestimates. However, the present work demonstrates that, certainly under jet impingement conditions, an additional factor is the occurrence of pure erosion and synergetic modes of attack in erosion-corrosion circumstances.

9.4. Comparison between Cu-10%Ni and Marinel for the effect of other parameters on erosion-corrosion processes.

9.4.1. Effect of impingement angle on erosion corrosion processes.

Probably the most relevant point to make about the experiments at different impinging angles is that they did not reveal any clear-cut influences. Indeed it was impossible to infer any trends from the tests on Marinel (Table 7.6). A feature here was the rather low total weight losses exhibited by this material. Longer experiments might provide some clear relationships.

As indicated by Table 7.1. the Cu-10%Ni alloy, after an 8-hour test at 17m/s, exhibited two populations in terms of similar total weight loss rates, i.e. of about 0.20 mg/h for the ϕ=45° and the ϕ=60°, and of about 0.26 mg/h for the ϕ=30° and ϕ=90°. Clearly the rate of the total weight loss was higher for the ϕ=30° and ϕ=90°.

Further investigation of the total weight losses for the ϕ=30° and ϕ=90°, in terms of the detailed mechanisms of attack, revealed a complex situation in terms of the impinging angle influence. Even though the rate of the total weight loss was the same for Cu-10%Ni, for these two angles, the weight loss values of synergy and the pure erosion weight losses appeared to be higher at ϕ=90° than at ϕ=30°, with the converse situation to appearing for the instantaneous direct corrosion losses, (Table 7.4). This shows how complex the erosion corrosion behaviour is, emphasising the futility of simply transferring angular relationships obtained from dry erosion, through to aqueous erosion-corrosion.

The evidence of substantially higher direct corrosion rates at 30° compared to 90° impingement was obtained from the separate exercises of Tafel extrapolations (Table 7.3), linear polarisations (Figure 7.4) and examinations of the slope of anodic polarisation curves, (Figure 7.1a).

A possible explanation of the higher corrosion rates at 30° impingement is that a larger area, compared to the ϕ=90°, is influenced by the hydrodynamic effects, i.e. the turbulent conditions of the jet cover a larger area on the surface, resulting in faster anodic

and cathodic reactions. The similar trend was also noticed for Cu-10%Ni, when higher corrosion rates were presented with the 4mm nozzle after 30-minutes and 4-hour tests at ϕ=90°.

Microscopical examination of the Cu-10%Ni specimens after the tests at ϕ=30° and ϕ=45°, showed the same surface features as after the same exposure time at the same velocity, (8 hours, 17m/s), at ϕ=90°, i.e. the etched structure implying uniform attack on the metal with a tendency for a thicker surface film away from the impinged zone. For Marinel a discontinuous acicular surface film was apparent under the jet at all impinging angles, supporting the evidence that the more enhanced film formation on the surface of Marinel occurs in the directly impinged area. A clear difference between the behaviour at ϕ=90° and the other angles was the appearance of the film at the outer regions of the specimen. At ϕ=90° a more discontinuous dark film was present, but at the other angles an etched structure together with the Ni/Nb particles was apparent, with a slight evidence of a thin film formation.

9.4.2. Effect of salinity on erosion corrosion processes.

As indicated by Figures 7.5a-b. the direct corrosion rate remained the same with salinity variations, (1.75% NaCl and 3.5% NaCl solutions), for the Cu-10%Ni alloy. This is in agreement with previous work [119], suggesting that the results obtained by the linear polarisation method showed no significant difference for Cu-10%Ni, in film-forming tendencies between the normal sea water and the double-concentration type.

9.4.3. Effect of temperature on erosion corrosion processes.

When the temperature was increased from 19°C to 35°C, the Cu-10%Ni as indicated by Table 7.7. demonstrated a clear trend of increasing weight loss with increasing temperature, from about 8.8mg at 19°C, to 10.9 at 35°C. A recent review [156]

of the literature on effect of temperature on corrosion resistance of Cu-10%Ni concluded that exposure to sea water with low flow rates, (e.g. 0.6 - 1.5m/s), leads to much lower short-term (4-days) and long term (6 years), corrosion rates at 40°C than around 15-25°C. The short-term trends at 40°C were attributed to a rapid formation of a protective surface layer.

The present work did not reveal a clearly visible enhanced tendency for the production of thicker surface corrosion products at 35°C, (Figure 7.15), than at 19°C, and these corrosion products did not appear to be especially uniform or very protective. It thus appears that the impinging velocity of 17m/s override the tendency for a faster protection film to form on Cu-10%Ni at 35°C, but the situation might well be more conductive to protective corrosion products at these elevated temperatures, when the velocities are lower. Moreover, as Ijsseling et al pointed out [93], there may be benefits associated with a pre-conditioning of Cu-10%Ni at temperatures perhaps around 35-50°C, in inducing longer term improved corrosion resistance. It certainly would be interesting to test this idea to erosion corrosion behaviour with such a pre-treatment at low velocity followed by assessment of its effectiveness at high velocity.

For Marinel, the obtained total weight losses at 35°C showed lower values than the ones at 19 °C. After the end of the experiment the film formed on this material at 35°C was more difficult to remove that the one formed at 19°C. The film was more abundant at the centre than at the outer areas of the specimen. It appeared that between the patches of the film, only a faint evidence of he etched structure was apparent, supporting the better erosion-corrosion resistance of Marinel at high temperatures. This provides an indication that the development of the films on Marinel, is not only time - and velocity dependent, but also temperature dependent. It is apparent that the film formed on Marinel at 35°C contributes to the measured increase in erosion-corrosion resistance compared to 19°C.

When the specimens were cathodically protected the same pure erosion weight losses were obtained for the 35°C as for 19°C, Table 7.9, supporting the trend that the increase in temperature did not affect the erosion component.

In accordance with the microscopical observation, the anodic polarisation curves, Figure 7.6a-b, indicated the gradual establishment of a passive film on Marinel at 35°C,

and this was accentuated with the passage of time. Clearly, as Figure 7.7 suggests, Marinel exhibited better corrosion resistance at 35°C than at 19°C. This trend is supported by the linear polarisation tests, Figure 7.9c, which confirm that the corrosion rate decreases dramatically, supporting the notion of a rapid development of a protective film on the surface even in the severe 17m/s impingement velocity. The results also show, that the temperature increase did not significantly affect the E_{corr} values.

Another interesting feature is the large proportion due to the synergy to the total weight losses at the high temperatures, i.e. from 0.06mg and 3% of the total weight loss at 19 °C, to 0.87mg and 70% at 35 °C, after a 48-hour exposure.

As already mentioned at the end of section 7.3.2.4, it was decided to run another experiment at 35°C at 4 hours at 17m/s. The average total weight loss of this test was 0.4mg, demonstrating the fact that the total erosion-corrosion rate was falling with time, (as were the direct corrosion rates), at 35°C. Further estimates of the approximate values of pure erosion and direct corrosion in the initial 4 hours of exposures at 35°C were made as follows.

Table 7.10 shows that the instantaneous direct corrosion weight loss after a 4-hour exposure at 17m/s at 35 °C is 0.018 mg/h. Assuming a constant direct corrosion rate for the whole 4-hour exposure period, the weight loss due to the direct corrosion component is 0.018*4 = 0.072mg.

Table 7.9 shows that the pure erosion loss at 17m/s at 19°C after a 48-hour exposure was 0.2mg, and this weight loss value remained unaffected with the temperature increase. As a consequence it is expected that the pure erosion weight loss at 19°C at 17m/s after a 4-hour exposure, (=0.1mg), will remain the same even at the elevated temperature of 35°C

Summarising the above trends, the percentage contribution of the synergy on the total weight loss after a 4-hour exposure at 35°C at 17m/s, is calculated and presented in Table 9.5, together with the 48-hour results from Table 7.12. The data in Table 9.5 demonstrate the large contribution of synergy throughout the entire 48-hour duration of the experiment.

Exposure time (hours)	Average total weight loss (mg)	Average pure erosion weight loss (mg)	Average direct corrosion weight loss (mg)	Synergy – average (mg)
4	0.4	0.1	0.07	0.23
	%	25	17.5	57.5
48	1.25	0.2	0.18	0.87
	%	16	14	70

Table 9.5. Weight losses due to pure erosion, direct corrosion and indirect corrosion (synergy) effect, at 35°C after a 4-hour and a 48-hour exposure at 17m/s.

An important feature of the data in Table 9.5 is that it demonstrates a clear trend of reducing rates of total material loss with time. Thus the average total weight loss in the period 0→4 hours is 0.1 mg/h, where the average total weigh loss in the period 4→48 hours is 0.85/44 = 0.02 mg/h, i.e. an approximate five-fold reduction in erosion-corrosion rate. This implies extremely good long-term performance of Marinel at 35°C but clearly this indication needs to be verified by longer-term experiments.

9.5. Erosion and Synergy mechanisms.

An interesting finding in this work was the involvement of pure erosion in the erosion-corrosion phenomena, on the Cu-10%Ni alloy, even at the lower velocity impingement. It may seem surprising that pure mechanical damage should occur in liquid impingement conditions, but this has been detected [64,162] during the erosion-corrosion of cast iron and Ni-Cr-Si-B-C cermet, in the same general test conditions as these employed in the current research.

The calculations in section 9.2 and by others [101], demonstrate clearly that direct damage to the metal by the shear stresses occurring from the hydrodynamic conditions are not implicated.

It is considered that a factor in the production of the pure erosion damage was the presence of air bubbles entrained in the impinging jet. A number of workers have previously demonstrated or postulated [67,161], that impinging air bubbles can cause enhanced damage during erosion-corrosion of Cu-Ni alloys. In the present work the re-circulation system was open to the atmosphere and conditions in the reservoir tank were very agitated. Support for this notion was provided by:

i) the observation of pits on the surface of specimens in the direct impingement zone even after the cathodic protection tests,
ii) the severely pitting damage directly under the jet, on Cu-10Ni at 86m/s during erosion-corrosion tests, (Figure 6.49),
iii) and the existence of the pits on Marinel although to a much lesser extent, (Figure 6.102).

Surface damage caused by collapsing air bubbles, might be thought of as somewhat akin to cavitation and it may be that this phenomenon is involved in the erosion process. Indeed sharp distinction between erosion and cavitation is probably difficult in conditions of high-velocity impinging jets.

At low velocities the superiority of Marinel, as a designed high strength material, over the Cu-10%Ni was unquestionable, with the total absence, (in the range of the balance), of the pure erosion contributor on the total material loss, as indicated by Table 6.11 and Table 6.21. Even at the impinging velocity of 17m/s, the pure erosion weight losses for Marinel are low, and only at the highest velocity of 86m/s was the erosion component significant on this alloy. Moreover previous and concurrent studies in this laboratory on titanium alloys [96], have not revealed any obvious signs of pure erosion damage.

The short study at elevated temperatures on Marinel revealed that erosion rates ere not greater than at 19°C which seems to be a reasonable expectation.

The contribution of synergy was significant, (and in some cases substantial), on both alloys. The experiments on Marinel under potentiostatic anodic-polarisation conditions demonstrated, section 6.3.2.3, the important role of synergy in the overall erosion-corrosion process. The actual mechanisms involved are not easily apparent. In the work of high velocity impingement on cast iron [64], the synergetic factor was related to corrosion attack at graphite/matrix interfaces, but no similar large-scale microstructural features are present in the two alloys studied in this work.

For Cu-10%Ni for both velocities and at all times, the dominant contributor to overall erosion-corrosion material loss is the synergy, with values remarkably similar in the range 60-69%, (Table 6.15). One realistic synergy mechanism was indicated by the observation that after cathodic protection at 86m/s, (and to a slight extent after 48 hours at 17m/s), two pitted regions were apparent on the Cu-10%Ni, (Figure 6.50), but surface profiles demonstrated that the penetration of this pits was very small. The relative intensity of attack at these pitted zones under free erosion-corrosion conditions and conditions of cathodic protection, is indicative of a synergy mechanism on Cu-10%Ni – namely accentuating of the pitting erosion damage by simultaneous corrosion processes. Another minor contribution to synergy on Cu-10%Ni might have been the erosive dislodgement of non-metallic inclusions promoted by corrosion at the interfaces.

The proportions of total material loss attributed to synergy for Marinel ranged substantially from a few % over long exposures at 19°C to 70% over the same exposure and the same impinging velocity (17m/s) at 35°C, Table 7.12.

It is suggested that this may be associated with the film properties. At 19°C, the instantaneous corrosion rate at 48 hours is much higher (0.033mg/h) than at 35°C (0.0006mg/h), Table 7.10. Since this level of corrosion protection at 35°C was achieved gradually over the first few hours (Figure 7.9c), the implication is that, during this period the film was growing at a faster rate than it was dissolving. If the growing film is considered to have become increasingly rough on a microscale, this would result in high local turbulence which would accelerate the film "dissolution". This could be either by mass-transfer-accelerated chemical dissolution or by mechanical processes associated possibly with shear or turbulence-promoted forces (i.e. turbulent bursting stresses), as suggested by Poulson [38]. It is suggested that this "film-loss" process represents the synergy mechanism which accounts for a high proportion of material loss in these low-corrosion, stable-film, conditions at 35°C.

This suggested synergy mechanism implies that, eventually the film would thin down and corrosion protection would be lost. Indeed this mechanism is essentially the same as that proposed in section 9.3.2.2, to account for the eventual upturn in corrosion rate after ~40hours at 17m/s at 19°C. Longer experiments at 35°C would "test" this notion.

In contrast, at 19°C and 48 hours, the corrosion rates were higher implying the absence of a highly-protective film. In other words at 19°C the material loss is dominated by the direct corrosion process with only minor synergy contributions. If this concept is correct, total material loss measurements and synergy calculations in the time period 16-40 hours at 17m/s, at 19°C (Figure 6.59b), would yield to high values for the synergy.

9.6. Local Hydrodynamic Aspects.

As summarised in Chapters 2, an important feature of the jet impinging test is that there exist a variety of local hydrodynamic regions over the specimen surface with, for example, variations in mass transfer and degree of turbulence. Thus the expectation is, for the different hydrodynamic zones of the specimen, to exhibit significant variations in degree and type of corrosion and erosion-corrosion attack. The longer exposures led to the clear **visual evidence** of hydrodynamic zones on the surfaces of the specimens for both alloys. Moreover in the most-severe conditions in this programme, 86m/s impingement velocity, localisation of the damage, in the form of pitting in central regions and also in a zone of pitting about 4.5mm out from the directly impinged zone, was evident, Figure 6.49. This implies a hydrodynamic effect associated with a turbulent zone outside the stagnation zone as is generally supported – as discussed in Chapter 2.

Notwithstanding the above points, the overall evidence from most of the observations in this study was of **no major** difference between the erosion-corrosion behaviour in the different hydrodynamic zones of the specimens. The justification for this statement is as follows:

- With the exception of Cu-10%Ni at 86m/s, the microscopical examination did not reveal any substantial differences in the various hydrodynamic zones – even on specimens where hydrodynamic zones had been apparent visually.
- Evidence, especially on Cu-10%Ni, of a generally etched surface – signifying general active corrosion.
- Similar surface profiles across the entire specimen; e.g. Figure 6.41, which demonstrates the Cu-10%Ni specimen after an exposure period of 48 hours at 17m/s.
- Almost identical electrode potentials for central and outer specimens.
- Extremely low galvanic-currents flowing between the central and outer specimens.

Of course, there were some variations in behaviour of the different hydrodynamic zones in the impinged specimens. Thus higher corrosion rates (inferred from the linear

polarisation tests) were measured in the central specimens compared to the outer one in the concentric sample experiments. It should be noted that the diameter of the central specimen, (4mm for Cu-10%Ni and 6mm for Marinel), was greater than the jet diameter (1mm); thus this specimen would have included the highly-turbulent zone which jet-impingement-theory predicts. Consequently thinner different boundary layers would be present on the central specimen and this would explain the higher corrosion rates. Nevertheless, the degree of corrosion rate enhancement was not very large; the ratios of corrosion rates, central specimens:outer specimens were only about 2.3-3 for Cu-10%Ni and about 1.5 for most of the test on Marinel. The experiments on Marinel at 35°C, indicated similar, very low corrosion rates on both the central and outer specimens after the initial 4 hours (Figure 8.13).

The (admittedly tiny) electrode potential differences between the outer and central specimens, i.e. the outer sample being slightly anodic for the entire exposure period on Cu-10%Ni and the initial exposure period with Marinel, are difficult to rationalise. The polarity reversal on Marinel (in which central specimen eventually became the anode) was probably associated with the breakdown of the corrosion product film, because of its roughness – as argued earlier in section 9.3.2.2. It is of interest in this respect that this switch in polarity coincides with a rise in $1/R_p'$ (Figure 8.8), which was of greater magnitute for the central specimen.

The microscopic examinations revealed the presence of surface film in many of the contitions studied, but it is difficult to determine clear differences in the films formed on different parts of the impinged surfaces. In any case the films on Cu-10%Ni were generally extremely thin – interferance with colours.

The corrosion products on Marinel were often non-uniform on a microscopic scale but with a general impression of thinner, more-continuous films in the outer zones of the specimens.

In summary, the jet impinging conditions employed in this research have induced active corrosion on the specimens and hence have provided information of relevance to:-

- The behaviour of Cu-Ni-base alloys under erosion-corrosion conditions and the tendency towards the formation of protective or partially protective corrosion product films on the surface.
- The anodic, active regions of active/passive cells in practical circumstances of localised corrosion of Cu-Ni-base alloys.

In relation to the second point above, substantial galvanic interactions have been measured or postulated [107,153,161], (with much lower galvanic currents than these measured in this work), to pertain between highly-turbulence active and lower-turbulence passive areas in copper and its alloys. This feature highlights the fact, mentioned above, that the hydrodynamic conditions, performing in the experiments conducted in the present work, did not simulate active/passive cells. The latter situation would require specimens of larger size than the ones employed in this study.

9.7. General comments on relevance of findings to overall behaviour of copper-nickel-base alloys.

The extensive previous investigations of corrosion behaviour have been largely concentrated (for obvious reasons) on long-term studies. The major outcomes of the previous work have been:-

- demonstration of a gradual decrease in corrosion rates over long periods (e.g. years) of time [86],

- realisation of velocity limits for satisfactory performance of copper-nickel alloys. Although it has been recognised that such velocity limits must be "conditions dependent", figures of around 3-4 m/s are widely quoted for Cu-10%Ni pipes.

This research has focused on the detailed short-term, erosion-corrosion behaviour of these materials and has validity on its own, contributing to the understanding of behaviour in these circumstances. The previous sections of this chapter have discussed the results in that context. Nevertheless, it is of interest to discuss how the present findings might relate to erosion-corrosion over longer timescales.

The first point to consider relates to the fact that the most of the experiments were conducted at velocities substantially in excess of those for which these alloys are recommended. The rationale for this strategy was to produce accelerated effects that would yield information (whilst hopefully of relevance to less-severe hydrodynamic conditions) amenable to interpretation with more confidence than from smaller effects (e.g. low weight losses) obtained at lower velocities. In any case, the choice of 17 m/s for most attention represented a velocity at the upper end of a velocity range at which corrosion rates (and to an extent total material losses) were found to be constant.

The findings of substantial contributions to the overall material loss from pure erosion and corrosion-induced erosion ("synergy") are entirely novel. (Incidentally, this represents a justification of experiments at relatively-high velocities since such contributions were indicated on Cu-10%Ni at the low velocities of 2.38m/s, but were

confirmed at the higher velocities.). Although the mechanisms of pure erosion and synergy were not particularly-well elucidated, the erosion process was demonstrably associated with "impact events" which are considered to involve entrained air bubbles which are likely to be present in many practical circumstances.

As attested by the many previous investigations, the jet impingement set-up employed in this research is recognised to reasonably simulate practical situations where "local geometry" (e.g. obstacles) can cause fluid jets. The finding, that the material losses are not especially severe simply at perpendicular impingement, implies a wider spectrum of vulnerability.

In this study, no significant galvanic interactions were detected between the directly-impinged and wall-jet regions. Galvanic effects have been postulated in the past as an important feature in the hydrodynamically-induced, localised corrosion of copper-base alloys. As discussed in section 9.6 the obvious interpretation of this feature (supported by other observations) is that, in the experimental set-up utilised in this study, the entire specimen was acting as an actively- corroding element.

The benefits of alloying with aluminium or chromium separately on the durability of copper-nickel alloys have been indicated by limited previous studies, as discussed earlier in section 9.3.2.2. This research work has considered this aspect over a range of conditions and has shown that an alloy containing both aluminium and chromium, (Marinel), possesses rather lower corrosion resistance than Cu-10%Ni in quiescent saline solution, but it has demonstrated unequivocally the superior performance of Marinel in a range of erosion-corrosion conditions.

The behaviour of Marinel at 35°C, points to important aspects of improved erosion-corrosion resistance of this material at temperature elevated above 20°C. Although the same benefits were not found for the Cu-10%Ni alloy in the limited investigation of this aspect, there is reason to believe from some previous studies that similar effects may prevail for this alloy in some circumstances (e.g. less-severe hydrodynamic conditions?).

The observations of the complex time effects on erosion-corrosion behaviour perhaps represent the most intriguing aspect of this investigation. Thus the measurements of erosion-corrosion rates of Cu-l0%Ni and Marinel indicated a decreasing rate with

time, but the more-frequent monitoring of the pure corrosion rate demonstrated (certainly for Cu-10%Ni) that this was exhibiting cyclic behaviour. It seems reasonable to postulate that more-frequent measurements of total material loss would have revealed the same time effects as the pure corrosion ones. In any event, the early decline in the rates of both total weight loss and direct corrosion were observed for Marinel to coincide with the formation of surface films which are thereby postulated to provide a degree of protection.

However, calculations of the metal loss by corrosion at the minima of Figure 6.26b and Figure 6.59b, show that the instantaneous corrosion rates, (equivalent to 0.08 mm/year for Marinel and 0.1mm/year for Cu-l0%Ni) at 17 m/s, are an order of magnitude greater, than the long-term rates in "flowing" seawater [86]. The question arises as to whether, as in the case of the evolution of corrosion rates over long periods in less hydrostatically demanding conditions, these early-forming corrosion products in impingement corrosion conditions could be a precursor to more-protective surface films becoming established - perhaps after numerous rate cycles of diminishing amplitude?

9.8. Comments on relevance of findings to general erosion-corrosion of engineering materials.

One of the objectives of the research was to study the erosion corrosion of copper-nickel alloys because of their "intermediate property location" between materials (e.g. carbon steel, cast iron) with extremely poor corrosion and erosion-corrosion resistance, and materials (such as stainless steel and titanium) with good durability at least to aqueous streams without solids.

In this respect the major finding of the work was that of substantial pure erosion and synergy contributions in liquid impingement. Actually this is not the first such observation. As mentioned in section 9.5, a similar situation has been observed [64] during the liquid impingement of grey cast iron BS 1452 in 3.5% NaCl, where contributions of 16% erosion and 60% synergy were determined at 17 m/s and 18°C. Also pure erosive contributions of 20-30% have been measured during erosion-corrosion of Ni-Cr-Si-B-C cermet at 17m/s in 3.5% NaCl.

Of course, during solid/liquid erosion-corrosion it is well accepted that pure erosive damage and interactive mechanisms such as synergy (or related phenomena) are involved.

In contrast stainless steels and titanium possess excellent resistance to liquid impingement. Recent studies have demonstrated good resistance of even standard austenitic stainless steel (316L) up to 70- 100 m/s at ambient temperature, and titanium appears to resist attack at 72m/s even at the elevated temperature of 50°C. Such contrasting behaviour points to the crucial role of a rapidly forming, hydrodynamically resistant and re-forming passive film in resisting attack (by corrosion or erosion) during liquid impingement.

This research revealed a complex time effect on the direct corrosion process during liquid impingement, but it is not known if this is a general feature in liquid impingement of vulnerable materials or just specific to Cu-10%Ni.

Whilst discussing aspects of the erosion corrosion of Cu/Ni and stainless steels, it is worthwhile noting that there is a fundamental mechanistic difference in that localised corrosion of stainless steels, initiates at low-flow areas (e.g. under crevices) whereas localised corrosion of Cu/Ni alloys can be initiated at high-flow zones.

Further to these comparisons of the two groups of materials, it could be suggested that the behaviour of Marinel in this study, in some ways implies intermediate behaviour between the conventional Cu/Ni alloys and the stainless steels – in the sense of forming protection films more easily in high-flow conditions and more hydrodynamically resistant than conventional Cu/Ni alloys.

Chapter 10

Conclusions and Further Work.

10.1. Conclusions.

A detailed study of the behaviour of the two Cu-Ni-base alloys under jet impingement conditions has demonstrated the extreme complexity of the erosion-corrosion process. The experimental arrangements resulted in behaviour which, apart from the most-severe conditions of 86m/s impingement on Cu-10%Ni, did not exhibit major differences between the various hydrodynamic zones, laminar, high turbulent and wall jet, of the specimen. The velocity-dependencies and the time-dependencies of erosion-corrosion damage were extremely complex and there were substantial differences in the behaviour of the two alloys studied. The main separate conclusions are listed below.

- Over long periods, (7 months), the static corrosion resistance of Marinel appeared to be inferior to that of Cu-10%Ni at 19°C.

- Over the entire range of conditions studied, the erosion-corrosion resistance of Marinel was substantially superior to that of Cu-10%Ni.

- At 86m/s on Cu-10%Ni, the erosion-corrosion damage showed intense pitting attack on the central directly impinged zone and in a narrow region at a radial distance of about 4.5 mm, which undoubtedly corresponds to the maximum turbulence region associated with an impinging jet.

- Apart from the above case, the erosion-corrosion damage was found to be generally similar in type over the entire surface and comprised general attack, manifested by etching of the surface, plus film formation.

- In the first few hours of exposure to impingement over the velocity range of 2.38m/s-86m/s, (R_e=4500-86000), the direct corrosion resistance of Marinel was inferior to that of Cu-10%Ni.

- ❖ Over longer exposure periods at 17m/s, the direct corrosion rates of Marinel were lower than for Cu-10%Ni.

- ❖ In most of the conditions studied it was found that the direct corrosion accounts for only a proportion of the total material loss with significant amounts of pure erosion and often substantial proportions of corrosion-assisted erosive damage ("synergy").

- ❖ The hydrodynamic conditions stimulated film formation on the surface of Marinel and to a lesser extent on Cu-10%Ni, but the films became unstable in some circumstances. The complex patterns of film formation and destabilisation appear to account for the complex effects of impinging-velocity and time on the erosion-corrosion damage rates.

- ❖ The effect of increasing the impinging velocity on erosion-corrosion after 30 minutes and 4 hours exposure was observed to lead to a general increase in total material loss but with some indications of a step in the weight loss/velocity relationship at intermediate velocities/R_e. The direct corrosion rate was clearly seen to increase with velocity up to a range of velocities, at which the corrosion rates stabilised, followed by a subsequent increase in corrosion rate at higher velocities.

- ❖ The direct corrosion mechanism corresponding to the above trends, was rationalised in terms of mixed charge transfer/diffusion control of the anodic reaction at low velocities, corrosion rate stabilisation due to film formation at intermediate velocities and film breakdown, (leading to anodic rate control), at high velocities.

- ❖ At the impinging velocity of 17m/s the rate of the pure erosion declined with increasing time, but the corrosion rate/time relationships appeared to be cycling between high and low values. It is postulated that the initial phase of increasing corrosion rate with time is associated with increasing diffusion rates of anodic products across a diffusion boundary layer. Later, film formation introduces a period of decreasing corrosion rate. The subsequent period of increasing corrosion rate is thought to be associated with film breakdown possibly due to surface

roughness and mass transfer effects. It is thought that the above mentioned phases may be repeated to produce continued cycling behaviour.

- The erosion contributions were found to be significant on Cu-10%Ni, but only on Marinel at very high velocities. Microscopical observations indicated that the erosion damage was due to impact events, for instance from air bubbles.

- Synergy mechanisms have been proposed but it is recognised that in some respects (particularly for Marinel), these need to be clarified by further experiments.

- Experiments with concentric specimens revealed a higher corrosion rate on the specimen, which encompassed the directly impinged and highly turbulence zones, than on the specimen comprising the wall jet regions. However, extremely low galvanic currents flowing between the two components of a concentric specimen, further demonstrated the absence of substantial differences in erosion-corrosion behaviour between the various zones of the specimens employed in this study. Thus the hydrodynamic conditions, performing in the experiments conducted in the present work, did not simulate active/passive cells.

- The damage mechanisms for both alloys at different impingement angles were very complex, emphasising the futility to simply transfer angular relationships obtained from dry erosion, through to aqueous erosion-corrosion.

- For Cu-10%Ni salinity variations did not appear to affect the direct corrosion rate.

- Although the erosion-corrosion rates for Cu-10%Ni were higher at 35°C than at 19°C, the opposite was the case for Marinel. This interesting and potentially important finding for Marinel was correlated with a great attendance for the formation of more protective surface films at the higher temperature.

10.2. Recommendations for further work.

- ❖ To conduct studies, (e.g. using X-ray photo-electron spectroscopy, "XPS"), to identify the films forming during the erosion-corrosion of the Cu-Ni alloys.

- ❖ To conduct experiments at longer exposures to obtain trends for the complex time effects on erosion-corrosion behaviour of Cu-Ni alloys.

- ❖ To test the idea of a pre-treatment at elevated temperatures in static conditions and also at low velocities, followed by assessment of its effectiveness at higher velocity and ambient temperature.

- ❖ To expand on the findings of galvanic interactions between the inner and outer regions of specimens by a more detailed study of the behaviour of the concentric type specimens. It would be of great interest to try to simulate active/passive cells using specimens of larger size than ones employed in this study.

- ❖ The mechanisms of synergy should be the subject of further investigation.

- ❖ To conduct studies with impinging saline water containing moderate burdens of suspended solids, to ascertain if the deterioration mechanisms change from these in the absence of solids.

- ❖ To conduct tests, in order to investigate the possible influence of specimen size on the erosion-corrosion process.

LIST OF REFERENCES

[1] Herbert H. Uhlig , 'Corrosion and corrosion control', John Wiley & Sons Inc., 1971, 2-43.

[2] L.Giuliani and R.Cigna, 'Corrosion problems of copper alloys in desalination plants', Desalination, 22, 1977, 379-384.

[3] Part II Report Naval postgraduate school Monterey California, 'Effect of hydrodynamic variables on corrosion study of 90/10 Cu-Ni', 1978, 35.

[4] T.Hodgkiess, 'Basic mechanisms of aqueous corrosion', course notes, 1998.

[5] Joan Perry, Ph.D. Thesis, University of Glasgow, 2001.

[6] T.Hodgkiess and A. Neville, 'An assessment of the corrosion behaviour of high-grade alloys in seawater at elevated temperature and under a high velocity impinging flow', Corrosion Science, Vol.38, No.6, 1996, 927-956.

[7] E. Heitz, 'Flow-dependent corrosion – II. Ferous materials in pure and particulate chloride solutions', Werkstoffe und Korrosion, 36, 1985, 163-173.

[8] Gabriel Silva, "Wear generation in hydraulic pumps", SAE Technical paper series, International Off-Highway and Powerplant Congress and Exposition, Milwaukee, Wisconsin, September 10-13, 1990.

[9] B. Todd, "Corrosion and materials selection in seawater systems", I Mech E, 1979.

[10] T. J. Glover, 'Recent developments in corrosion-resistant metallic alloys for construction of seawater pumps', Materials Performance, 1988, 27, 51-56.

[11] J.Madadnia, I. Owen, 'Accelerated surface erosion by cavitating particle-laden flows', Wear, 1993, 165, 113-116.

[12] Chandler K. A., 'Marine and offshore corrosion', Butterworths Ltd, 1985.

[13] Engel. L. and Klinegele H., 'An atlas of metal damage', translated by Murray S. Wolfe Publishing Ltd. London and Carl Hanser Veriag, 1981.

[14] J. R. Zhou, S. Bahadur, 'Effect of blending of silicon carbide particles in varying sizes on the erosion of Ti-6Al-4V', Wear, 1989, 132, 235-246.

[15] S. Yerramareddy, S. Bahadur, 'Effect of operational variables, microstructure and mechanical properties on the erosion of Ti-6Al-4V', Wear, 1991, 142, 253-263.

[16] M. Emiliani, R. Brown, 'The effect of microstructure on the erosion of Ti-6Al-4V by spherical particles at 90° impact angles', Wear, 1984, 94, 323-338.

[17] Taishi Omote et al, 'Interaction between impingement angles and materials on sand erosion', 27th international SAMPE Technical Conference October 9-12, 1995.

[18] A. Venugopal Reddy, G. Sundararajan, 'The influence of grain size on the erosion rate of metals', Metallurgical Transactions A, 1987, 18A, 1043-1052.

[19] R. L. Howard, A. Ball, 'The effect of test temperature on the particle erosion performance of titanium aluminide alloys', Wear, 1997, 205, 11-14.

[20] J. A. C. Humphrey, 'Fundamentals of fluid motion in erosion by solid particle impact', Int. J. Heat and Fluid Flow, 1990, 11, 170-195.

[21] M. Bjordal et al, 'Erosion and corrosion properties of WC coatings and duplex stainless steel in sand-containing synthetic seawater", Wear, 1995, 186-187.

[22] Francesc Giralt, Olev Trass, 'Mass transfer from crystalline surfaces in a turbulent impinging jet part 2: Erosion and diffusional transfer', Canadian Journal of Chemical Engineering, 1976, 54, p.148.

[23] D.C.Silverman, 'Rotating cylinder electrode – geometry relationships for prediction of velocity – sensitive corrosion', Corrosion – NACE, 1987, 44, p.42.

[24] Frederick G. Hammit, Frank J. Heymann, 'Liquid erosion failures', in ASM Metals Handbook, Vol. 10, 8th ed., p.160-167.

[25] J. T. Davies, 'Turbulence phenomena', Academic press, New York and London, 1972.

[26] D. T. Chin, C. H. Tsang, 'Mass transfer to an impinging jet electrode', J. Electrochem. Soc., 1978, 125, 1461-1470.

[27] N.Rajaratham, 'Turbulent jet – developments in water science', Elsevier, 1976.

[28] Francese Giralt, Olev Trass, 'Mass transfer from crystalline surfaces in a turbulent impinging jet. Part 1: Transfer by erosion', Canadian Journal of Chemical Engineering, 1975, 53, p.505-511.

[29] Carolyn M. Preece, 'A comparison of liquid impact erosion and cavitation erosion', Wear, 1980, 60, 269-284.

[30] Chu-Jen Chia et al, 'Mass transfer in axisymmetric turbulent impinging jets', Ind. Eng. Chem. Fundam., 1977, 16, 28-35.

[31] U. Meyer et al, 'A new impinging jet test rig used to identify the important parameters in service erosion-corrosion in Bayer liquor and to study the damage morphology', Wear, 1994, 176, 163-171.

[32] J. M. Esteban et al, 'The impinging jet electrode: Measurement of the hydrodynamic constant and its use for evaluating film persistency", Corrosion, 1990, 46, 896-901.

[33] J. L. Dauson et al. Corrosion-NACE 87, pp. 453.

[34] K. D. Efird et al, 'Correlation of steel corrosion in pipe flow with jet impingement and rotating cylinder tests', Corrosion Engineering-NACE, 1993, 49, 992-1003.

[35] Bryan Poulson, 'Electrochemical measurements in flowing solutions', Corrosion Science, 1983, 23, 391-430.

[36] H. Q. Becerra et al, 'The corrosion of carbon steel in oil-in-water emulsions under controlled hydrodynamic conditions', Corrosion Science, 2000, 42, 561-575.

[37] R. G. Woolam et al, 'Electrochemical methods of corrosion research', Ed. By M. Duprat, Materials Science Forum (1986), 8, 53-68.

[38] Bryan Poulson, 'Complexities in predicting erosion-corrosion', Wear, 1999, 233-235, 497-504.

[39] Bryan Poulson, 'Advances in understanding hydrodynamic effects on corrosion', Corrosion Science, 1993, 35, 655-665.

[40] B. T. Ellison, C. J. Wen, 'Hydrodynamic effects on corrosion', The American Institute of American Engineers, 1981, 77, 161-169.

[41] G. Hoff et al, 'Rain and sand erosion, phenomena of material destruction caused by repeated loads', Characterisation and determination of erosion resistance, ASTM STP 474, American Society for Testing and Materials, 1970, 353-382.

[42] Kozyrev, S. P., 'The genesis of cavitation wear', Trenie Iznos, 1980, 1, 793- 808.

[43] Iain Finnie, 'Erosion of surfaces by solid particles', Wear, 1960, 3, 87-103.

[44] Hector Mac. Clark, 'The influence of the flow field in slurry erosion', Wear, 1992, 152, 223-240.

[45] A. A. Grant, 'Wear in slurry pumps', Technical Bulletin, Warman Group Development No 9, May 1991.

[46] A. Neville, T.Hodgkiess, J.T. Dallas, 'A study of the erosion-corrosion behaviour of engineering steels for marine pumping applications', Wear, Vol. 186, 1995, pp 497-507.

[47] T. Hodgkiess, A.Neville and S.Shrestha, 'Electrochemical and mechanical interactions during erosion-corrosion of a high velocity oxy-fuel coating and a stainless steel', Wear, 233-235, 1999, pp 623-634.

[48] M.Bjordal, E.Bardal, T.Rongne and T.G. Eggen, 'Erosion and corrosion properties of WC-coatings and duplex stainless steel in sand containing seawater', Wear, Vol. 186-187, 1995, pp 508-514.

[49] S. Zhou et al, 'Electrochemical studies of anodic dissolution of mild steel in a carbonate-bicarbonate buffer under erosion-corrosion conditions', Corrosion Science, 1996, 38,1-14.

[50] M. M. Stack et al, 'Some thoughts on the construction of erosion-corrosion maps for PVD coated steels in aqueous environments', Surface and Coatings Technology 1999,113, 52-62.

[51] G. Rocchini, 'The determination of Tafel slopes by the successive approximation method', Corrosion, June 1995, Vol. 37, Issue 6, 865-1029.

[52] A. Neville and T. Hodgkiess, 'Towards novel ceramic-base coatings for corrosion-wear applications', British Corrosion Journal, 2000.

[53] T. Hodgkiess, 'The role of advanced materials to combat erosion-corrosion in aqueous environments', Stainless Steel World, July/August 1999, 39-42.

[54] R. J. Wood, S. P. Hutton, 'The synergistic effect of erosion and corrosion: trends in published results', Wear, 1990, 140, 387-394.

[55] X. X. Jiang et al, 'Accelerative effect of wear on corrosion of high-alloy stainless steel, Corrosion-NACE, 1993, 49, 836-841.

[56] J. P. Tu, 'The effect of TiN coating on erosion-corrosion resistance of a-Ti alloy in saline slurry', Corrosion Science, 2000, 42, 147-163.

[57] ASTM Standard Guide for determining synergism between wear and corrosion, G199-93.

[58] B.W.Madsen, 'Measurement of erosion-corrosion synergism with a slurry wear test apparatus', Wear, Vol.123, 1988, pp 127-142.

[59] S.Zhou, M.M. Stack, R.C.Newman, 'Characterisation of Synergistic Effects between erosion and corrosion in an aqueous environment using electrochemical techniques', Corrosion Science, Vol.52, No.12, 1996, pp 935-946.

[60] H. Abd-El-Kader and S.M. El Raghy, 'Wear-corrosion mechanism of stainless steel in chloride media', Corrosion Science, Vol.26, No.8, 1986, pp 647-653.

[61] M. Lesser, 'Thirty years of liquid impact research: A tutorial review', Wear, Volume 186, Part 1, July 1995, 28-34.

[62] H.W.Wang and M.M.Stack, 'The erosive wear of PVD and CrN coatings', Tribology Letters, Vol.6, 1999, pp 23-36.

[63] M.C.Wang, S.Z.Ren, X.B.Wang and S.Z.Li, 'A study of sand erosion of W-alloy cast iron', Wear, Vol.160, 1993, pp 259-264.

[64] A.Neville, T.Hodgkiess and H.Xu, 'An electrochemical and microstructural assessment of erosion-corrosion of cast iron', Wear, 233-235, 1999, pp 523-534.

[65] D.Eleftherakos, 'History of metals in the Mediterranean region', Syros press, 1993, 124-132.

[66] D.Papaharisis, N.Rigos, P.P.Cazzola, D.Inda, 'Metal processing', APT press, 1996, 3rd edition, 246-265.

[67] F.L.LaQue, 'Theoretical studies and laboratory techniques in sea water corrosion testing evaluation', Corrosion-NACE, May 1957, Vol.13, 33-44.

[68] A.M. Shams El Din, 'Copper Alloys for Desalination Plants', Desalination, 93 (1993) 499-516.

[69] M.S.Parvizi, 'Corrosion behaviour of Cu-10%Ni in aqueous environments', Materials performance, 1987, 59-79.

[70] T. Hodgkiess & J.Akhtar, 'Observations on the Corrosion Behaviour of Copper in Glasgow Tap Water', Proceedings of a conference held at the Society of Chemical Industry, London, U.K., December 1992.

[71] H.Siedlarek, D.Wagner, M.Kropp, B.Fussinger, I.Hanssel & W.R.Fischer, 'Effects of Water Composition and Operating Conditions on the Corrosion Behaviour of Copper in Potable Water', Proceedings of a conference held at the Society of Chemical Industry, London, U.K., December 1992.

[72] T.Kaunisto, 'Corrosion in Potable Water Systems – The Situation in Finland', Proceedings of a conference held at the Society of Chemical Industry, London, U.K., December 1992.

[73] H.S.Campbell, A.H.L. Chamberlain & P.J.Angell, 'An Unusual Form of Microbially Induced Corrosion in Copper Water Pipes', Proceedings of a conference held at the Society of Chemical Industry, London, U.K., December 1992.

[74] T.H.Rogers, 'Marine Corrosion', George Newsness, London, 1960.

[75] E.A.Culpan & G.Rose, 'Corrosion Behaviour of Cast Nickel Aluminium Bronze in Seawater', Br.Corros.J., 1979, Vol.14, No.3.

[76] Robert J. Ferrara & Thomas E.Caton, 'Review of Dealloying of Cast Aluminium Bronze and Nickel-Aluminium Bronze Alloys in Seawater', Materials Performance, National Association of Corrosion Engineers', 1982, 30-34.

[77] Dipendra Nath Roy & Ashwini K. Sinha, 'Aspects of Localised Corrosion of Condenser Tube Materials in Chloride Media', 203-218.

[78] G.A.Bokov, I.K.Marshakov, I.A.Malakhov, A.Tarkhini, & A.K.Khachaturov, 'Corrosion Resistance of Copper-Nickel Alloys and Stainless Steel in Cooling Industrial-Domestic Waste Waters', Khimiya I Teknologiya Vody, Vol.16, No.3, pp. 295-300, 1994.

[79] G.L.Bailey et al, 'Copper-nickel-iron alloys resistant to sea-water corrosion', J. Inst. Met., 1951, 79, 243

[80] Peter T.Gilbert, 'A Review of Recent Work on Corrosion Behaviour of Copper Alloys in Seawater, National Association of corrosion engineers', 47-53, 1982.

[81] Peter T.Gilbert, 'Corrosion Resisting Properties of 90/10 Copper-Nickel-Iron Alloy With Particular Reference to Offshore Oil And Gas Applications', Br.Corros.J., 1979, Vol.14, No.1.

[82] Keith C Bendall, 'A Longer Life in the Ocean Waves', December 1997, 711-713.

[83] K.D.Efird, 'The Synergistic Effect of Ni and Fe on the Seawater Corrosion of Copper Alloys', Corrosion-NACE, Vol.33, No.10, October, 1977.

[84] D.B.Anderson and K.D.Efird, 'Proc. 3rd int. cong. on marine corrosion and fouling', Wrightsville Beach, NC, 1974, International Nickel Co. Inc., 264-276.

[85] M.S.Parvizi, A.Aladjem & J.E.Castle, 'Behaviour of 90-10 Cupronickel in Seawater', International materials preview, 1988, Vol.33, No.4, 169-199.

[86] Arthur H.Tuthill, Brian Todd & Dr. John Oldfield, 'Experience With Copper Alloy Tubing Waterboxes and Piping in MSF Desalination Plants', Proceedings of world congress on desalination and water re-use, Madrid, October 1997, 251-270.

[87] C.Kato, B.G.Ateya, J.E.Castle & H.W.Pickering, J.Electrochem.Soc., 'On the mechanism of corrosion of Cu-9.4Ni-1.7Fe alloy in air saturated aqueous NaCl solution', 127, 1980, 1890.

[88] C.Kato, 'Discussion', J.Electrochem.Soc., 127,1980, 1904.

[89] Harvey Hack & Howard Pickering, 'The Influence of Corrosion Product Film Formation on the Corrosion of Copper-Nickel Alloys in Aqueous NaCl', Electrochemical impedance, 220-236.

[90] M.Popplewell, R.J.Hart & J.A.Ford, Corrosion Science, 1973, 13, 295.

[91] B,Todd, 'Factors in the choice of materials for marine engineering', Corrosion-NACE, 1970, 161-179.

[92] F.P.Ijsseling, 'The Application of the Polarisation Resistance Method to the Study of the Corrosion Behaviour of Copper-based Alloys in Seawater', Cebelcor Tech, 122, 209.2/1-209.2/9, 1973.

[93] F.P.Ijsseling, L.J.P.Drolenga & B.H.Kolster, 'Influence of Temperature on Corrosion Product Film Formation on CuNi10Fe in the Low Temperature Range. I. Corrosion rate as a function of temperature in well aerated sea water', Br.Corros.J., 1982, Vol.17, No.4, 162-167.

[94] Arthur H. Tuthill, 'Guidelines for the Use of Copper Alloys in Seawater', National Association of corrosion engineers, Materials performance, 1987, 12-22.

[95] F.P.Ijsseling, 'The Corrosion Behaviour of the System CuNi10Fe/seawater – The Protective Layer of Corrosion Products – A Literature Review', 269-324.

[96] Dimitris Mantzavinos, Ph.D. Thesis, University of Glasgow, October 2001.

[97] Ralph W.Ross.Jr. & David B.Anderson, 'Hot Seawater Corrosion of Copper-Base Alloys', Material performance, Vol.14, September 1975, 27-32.

[98] F.P.Ijsseling and J.M.Krougman, Proc. 4th Int. Conf. Marine Corros. Fouling, Juan-les-Pins, 1976, 297.

[99] F.W.Fink, 'Alloys for sea water conversion – Copper-base alloys for heat exchange equipment', Mater. Prot., 1967, 6, (5), 40.

[100] B.C.Syrett, 'Liquid erosion-corrosion of copper nickel alloys', 1975, 30, 462-486.

[101] K.D.Efird, 'Effect of Fluid Dynamics on the Corrosion of Copper-Base Alloys in Seawater', Corrosion NACE, Vol.33, No.1, January 1977, 3-8.

[102] S.Sato & K.Nagata, 'Factors Affecting Corrosion and Fouling of Metal Condenser Tubes of Copper Alloys and Titanium', Sumitomo light metal technical reports, Vol. 19, Nos. 3 and 4, p.83, 1978.

[103] Ralph W.Ross.Jr. & David B.Anderson, 'Hot Seawater of Copper-Base Alloys – Part II', Materials performance, July 1976, 45-64.

[104] B.Todd, 'The Corrosion of Materials in Desalination Plant', Desalination, 3 (1967), 106-117.

[105] D.H.Foxall & G.Wildsmith, 'Some Aspects of the Use of Copper Alloys for Seawater Cooling Systems', I Mech E, 1979, 46-48.

[106] Barry C.Syrett & Sharon S.Wing, 'Effect of Flow on Corrosion of Copper-Nickel Alloys in Aerated Seawater and in Sulphide-Polluted Seawater', National Association of corrosion engineers, Corrosion NACE, Vol. 36, No.2, February 1980, 73-85.

[107] F.P.Ijsseling, 'The Application of the Polarisation Resistance Method to the Study of the Corrosion Behaviour of CuNi10Fe in Seawater', Corrosion Science, 1974, Vol. 14, 97-110.

[108] D.C.Vreeland, 'Review of Corrosion Experience With Copper-Nickel Alloys in Seawater Piping Systems', 15, 1976, 38-41.

[109] J.N.Alhajji & M.R.Reda, 'The Conflicting Roles of Complexing Agents on the Corrosion of Copper-Nickel Alloys in Sulphide Polluted Seawater', J.Electrochem.Soc., Vol. 141, No. 6, June 1994, 1432-1438.

[110] A.Cohen & L.Rice, 'Recent Experience With Copper Alloy in Desalting Environments', Materials Protection, December 1969, 67-69.

[111] A.Cohen & L.Rice, 'Experience With Copper Alloys in the Desalting Environment', Materials Protection, November 1970, 29-35.

[112] A.Cohen & L.Rice, 'Recent Experience With Copper Alloys in Desalting Plant Environments', Proc. 25th Conf. National Association of Corrosion Engineers, Denver, CO, 1969, 342-345.

[113] J.F.Nahman & E.R.Duffy, 'Effect of alloying additions on sea water corrosion resistance of iron-aluminium base alloys', Corrosion ,1974, 30, 357.

[114] R.C.Miffin & D.B.Bird, 'Performance of Tube Alloys Cooled by Brackish Delaware River Water', Materials protection, September 1969, 72-77.

[115] K.Yandushkin & V.Kuris, Zashch. Met., 1971, 7 ,(3), 317.

[116] C.A.Clark & P.Guda, 'High Strength Cupro-nickel for Marine Service', Br. Corros. J., 1982, Vol. 17, No.4, 159-161.

[117] L.E.Eiselstein, B.C.Syrett, S.S.Wing & R.D.Caligiuri, 'The accelerated corrosion of Cu-Ni Alloys in Sulphide-Polluted Seawater: Mechanism No.2', Corrosion Science, 1983, 23, 223.

[118] T.S.Lee, E.W.Thiele & J.H.Waldorf, 'The Effect of Seawater Velocity on Corrosion Potentials of Materials', Materials Performance, National Association of Corrosion Engineers, 1984, 23, (11), 44-46.

[119] D.B.Anderson and K.D.Efird, 'Cu-Ni resists recirculated seawater', Power, February 1974, 72.

[120] L. Knutsson, E.Mattsson & B.E.Ramberg, 'Erosion-corrosion in copper water tubing', Brit.Corros.J., Vol.7, (1972), 208.

[121] Barry C.Syrett, 'Erosion-Corrosion of Copper-Nickel Alloys in Seawater and Other Aqueous Environments – A Literature Review', Corrosion NACE, Vol.32, No.6, June 1976, 242-252.

[122] C.F.Schrieber, O.Osborn & F.H.Coley, 'Corrosion of metals in desalination environments' Mater.Prot., 1968, 7, (10), 20.

[123] J.F.Bates & J.M.Popplewell, 'Corrosion of condenser tube alloys in sulfide contaminated brine', Corrosion, 1975, 31, 269.

[124] Anna Maria Beccaria, Gildo Poggi, Pierluigi Traverso & Maura Ghiazza, Corrosion Science, Vol.32, No.11, 1991, 1263-1275.

[125] J.N.Al-Hajji & M.R.Reda, 'The Corrosion of Copper-Nickel Alloys in Sulphide-Polluted Seawater: The effect of Sulphide Concentration', Corrosion Science, Vol.34, No.1, 1993, 163-177.

[126] J.P. Gudas & H.P.Hack, 'Sulphide induced corrosion of copper nickel alloys', Corrosion-NACE, Vol.35, No.2, 1979, 67-73.

[127] D.B.Anderson & F.A.Badia, 'Chromium modified copper-nickel alloys for improved seawater impingement resistance' J.Eng.Power, 95, April 1973, 132-135.

[128] D.D.MacDonald, B.C.Syrett and S.S.Wing, 'Corrosion of Copper-Nickel Alloys in Sea Water Polluted with sulfide and Sulfide Oxidation Products', Corrosion-NACE, Vol.35, No.9, September 1979, 409-421.

[129] D.D.MacDonald, B.C.Syrett and S.S.Wing, 'The Corrosion of Copper-Nickel Alloys 706 and 715 in Flowing Water. II – Effect of Dissolved Sulfide', Corrosion-NACE, Vol.35, No.8, August 1979, 367-377.

[130] R. Francis, 'The Effect of Chlorine and Sulphide on the Corrosion of Copper Alloy Heat Exchanger Tubes', Proc. Conf. 'Copper Alloys in Marine Environments', Birmingham, 1985, Copper Development Association, Paper 9.

[131] Mahmoud R.Reda & Jamal N.Alhajji, 'Comparison of Current Reversal Chronopotentiometry (CRC) and Small Amplitude Cyclic Voltammetry (SACV) Method To Determine the Long-Term Corrosion Tendency of Copper-Nickel Alloys in Polluted and Unpolluted Seawater Under Jet-Impingement Conditions', Corrosion Testing in Natural Waters, 1997.

[132] M.R.Reda & J.N.Alhajji, 'Deleterious Role of Complexing Agents in Corrosion of Copper-Nickel Alloys in Sulphide Polluted Seawater', British Corrosion Journal, 1995, Vol.30, No.1, 56-61.

[133] P.T.Gilbert & F.L.Laque, 'Jet Impingement Tests', Journal of Electrochemical Society', September 1954, 448-455.

[134] K.D. Efird, 'The Inter-Relation of Corrosion and Fouling for Metals in Seawater', Materials Performance, 1976, 15(4), 16-25.

[135] A.M.Beccaria & J.Crousier, 'Dealloying of Cu-Ni in Natural Seawater', Br.Corros.J., 1989, Vol.24, No.1, 49-52.

[136] F.Mansfeld, G.Liu, H.Xiao, C.H.Tsai & B.J.Little, 'The Corrosion behaviour of Copper Alloys, Stainless Steels and Titanium in Seawater', Corrosion Science, Vol.36, No.12, 1994, 2063-2095.

[137] T.W.Bostwick, Corrosion, 1961, 17,12-15.

[138] P.T.Gilbert, 'Use of Ferous Sulphate Treatment For Combating Condenser Tube Corrosion', Supplement to Chemistry and Industry, 1977.

[139] R.F.North & M.J.Pryor, Corrosion Science, Vol.8, 1968, 149-157.

[140] D.B.Anderson & B.R.Richards, 'Chlorination of Seawater C effects on Fouling and Corrosion', Presented before ASME Research Committee on Condenser Tubes, Chicago, IL, Nov. 1965.

[141] Kirk, Lee, and Lewis, 'Corrosion and Marine Fouling Characteristics of Copper Nickel Alloys', CDA Conference Copper in Marine Environments, paper 16.

[142] R.Francis, 'The Effect of Sulphides on the Corrosion of Copper Alloy Material Performance', 1981, 22, (8), 44.

[143] E.Heitz, 'Chemo-Mechanical Effects of Flow on Corrosion', Corrosion, Vol.47, No.2, 135-145.

[144] K.C.Goretta, R.C.Arroyo, C.T.Wu & J.L.Routbort, 'Erosion of Work-Hardened Copper, Nickel and 304 Stainless Steel', Wear, 147, (1991), 145-154.

[145] S.Sato and K.Nagata, 'Factors affecting corrosion of condenser tubes of copper alloys and titanium', Corrosion 77, NACE, Toronto, 1977.

[146] B.Little, J.Jacobus & L.Janus, 'Evaluation of Microbiologically Induced corrosion in an estuary', Estuaries, Vol.12, Sept.1989, 138-141.

[147] C.A.Clark, S.Driscoll and P.Guha, 'Development of a new fastener alloy resistant to hydrogen embrittlement', British Corrosion Journal, 1992, Vol.27, No.2, 157.

[148] C.D.S.Tuck, Z.Xianghua and D.E.J. Talbot, 'Hydrogen embrittlement resistance of ultralight strength cupronickel alloy: effects of exposure to gaseous hydrogen environment on fatigue resistance', British Corrosion Journal, 1994, Vol.29, No.1.

[149] C.A Clark and P.Guha, 'High strength cupro-nickel for marine service', British Corrosion Journal, 1982, Vol. 17, No.4.

[150] W.O.Alexander and D.J.Hanson, J. Inst. Met., 1937, 61, 83.

[151] Carol A. Powell, 'Copper-nickel alloys – Resistance to corrosion and biofouling', http://marine.copper.org/1-intro.html.

[152] U.Lotz, 'Effects in flow induced corrosion', Corrosion, Vol. 27, 1990.

[153] G.Bianchi, G.Fiori, P.Longhi and F.Mazza, '"Horse Shoe"-Corrosion of copper alloys in flowing sea water: Mechanism, and possibility of cathodic protection of condenser tubes in power stations', Corrosion-NACE, 1978.

[154] G.Kear, D.Barker, F.C.Walsh and KStrokes, 'The rotating disc electrode as a tool for the determination of nickel aluminium bronze and copper corrosion rates in chloride media', Corrosion Odyssey 2001, Institute of Corrosion, Edinburgh, Session 8, Paper 6.

[155] P.A.Lush and M.J.Carr, 'Copper dissolution in sea water under mixed activation and diffusion control', Corrosion science, Vol.19, 1979, 1079-1088.

[156] R.E.Melchers, 'Temperature effect on seawater immersion corrosion of 90:10 copper-nickel alloy', Corrosion, May 2001, 440-451.

[157] B.C.Syrett and D.D.MacDonald, 'The validity of electrochemical methods for measuring corrosion rates of copper-nickel alloys in sea water', Corrosion, Vol.35, No.11, November 1979.

[158] J.Venzcel, L.Knutsson und G.Wranglen, 'Korrosionsgeschwindgkeit und stoffkrauspoch in stromender NaCl-Losung', Corrosion Science, Vol.4, 1964, 1-15.

[159] V.Wang and J.Postlethwaite, 'The application of low Reynolds numbers k-ε turbulence model to corrosion modelling in the mass transfer region', Corrosion Science, Vol.39, No.7, 1997, 1265-1283.

[160] B.Poulson, 'Predicting the occurrence of erosion-corrosion', Plant corrosion prediction of materials performance, Institution of corrosion science and technology, Editors: J.E.Strutt and J.R.Nickolls, 1987.

[161] S.R. de Sanchez and D.J.Schiffrin, 'The use of high speed rotating disc electrodes for the study of erosion-corrosion of copper base alloys in sea water',

[162] S.Shrestha, Ph.D. Thesis, University of Glasgow, 2000.

[163] J.W.Oldfield, 'Electrochemical theory of galvanic corrosion', Galvanic Corrosion, ASTM STP 978, H. P. Hack, Ed., American Society for Testing and Materials, Philadelphia, 1988, 5-22.